NAVAL POSTGRADUATE SCHOOL

MONTEREY, CALIFORNIA

THESIS

THE PATTERN AND DYNAMICS OF THE MERIDIONAL OVERTURNING CIRCULATION IN THE UPPER OCEAN

by

Erick Lee Edwards

September 2008

Thesis Advisor:	Timour Radko
Second Reader:	Jeffrey Haferman

Approved for public release; distribution is unlimited

THIS PAGE INTENTIONALLY LEFT BLANK

REPORT DOCUMENTATION PAGE			Form Approved OMB No. 0704-0188
Public reporting burden for this collection of information is estimated to average 1 hour per response, including the time for reviewing instruction, searching existing data sources, gathering and maintaining the data needed, and completing and reviewing the collection of information. Send comments regarding this burden estimate or any other aspect of this collection of information, including suggestions for reducing this burden, to Washington headquarters Services, Directorate for Information Operations and Reports, 1215 Jefferson Davis Highway, Suite 1204, Arlington, VA 22202-4302, and to the Office of Management and Budget, Paperwork Reduction Project (0704-0188) Washington DC 20503.			
1. AGENCY USE ONLY *(Leave blank)*	**2. REPORT DATE** September 2008	**3. REPORT TYPE AND DATES COVERED** Master's Thesis	
4. TITLE AND SUBTITLE The Pattern and Dynamics of the Meridional Overturning Circulation in the Upper Ocean			**5. FUNDING NUMBERS**
6. AUTHOR(S) Erick Lee Edwards			
7. PERFORMING ORGANIZATION NAME(S) AND ADDRESS(ES) Naval Postgraduate School Monterey, CA 93943-5000			**8. PERFORMING ORGANIZATION REPORT NUMBER**
9. SPONSORING /MONITORING AGENCY NAME(S) AND ADDRESS(ES) N/A			**10. SPONSORING/MONITORING AGENCY REPORT NUMBER**
11. SUPPLEMENTARY NOTES The views expressed in this thesis are those of the author and do not reflect the official policy or position of the Department of Defense or the U.S. Government.			
12a. DISTRIBUTION / AVAILABILITY STATEMENT Approved for public release; distribution is unlimited			**12b. DISTRIBUTION CODE**

13. ABSTRACT (maximum 300 words)

The physics of the Meridional Overturning Circulation (MOC) and interhemispheric heat transport is explored with an emphasis on the upper and central ocean. Sea surface temperature and wind stress are considered in the context of their ability to influence the MOC pattern and their relative significance is quantified. Most calculations in this study use an idealized rectangular basin which makes it easier to identify the key dynamic processes and explain interaction. Volumetric and advective heat transport streamfunctions are used to analyze interhemispheric exchanges of mass and energy. Data concerning the effects of equatorially-asymmetric wind stress and surface heat flux forcing are used to construct expressions which explicitly define the relationships between wind stress, surface heat flux, interhemispheric volume flow, and heat transport. The relative importance of wind stress and surface heat flux to the overall values of transport is discussed in light of climatology.

The meridional overturning circulation in the upper ocean is found to be the dominant factor in interhemispheric heat transport and in the maintenance of the Earth's climate despite its extremely small contribution to total meridional-vertical circulations in the entire ocean basin. This study suggests that the previous emphasis on deep overturning in the abyssal region and small-scale mixing as the dominant factors in the meridional overturning circulation should be reconsidered and the role of wind stress and surface heat fluxes more thoroughly investigated as determining factors of MOC strength and maintenance. This study explores possible mechanisms responsible for climate shift which could result in long-term changes to weather patterns and ocean conditions altering important factors in the Navy's operating environment. Thus, long-term Navy planning must include an appreciation for possible changes in the forcing mechanisms responsible for the meridional overturning circulation.

14. SUBJECT TERMS meridional overturning circulation, thermohaline circulation, thermocline			**15. NUMBER OF PAGES** 121
			16. PRICE CODE
17. SECURITY CLASSIFICATION OF REPORT Unclassified	**18. SECURITY CLASSIFICATION OF THIS PAGE** Unclassified	**19. SECURITY CLASSIFICATION OF ABSTRACT** Unclassified	**20. LIMITATION OF ABSTRACT** UU

NSN 7540-01-280-5500 Standard Form 298 (Rev. 2-89)
Prescribed by ANSI Std. 239-18

THIS PAGE INTENTIONALLY LEFT BLANK

Approved for public release; distribution is unlimited

THE PATTERN AND DYNAMICS OF THE MERIDIONAL OVERTURNING CIRCULATION IN THE UPPER OCEAN

Erick Lee Edwards
Lieutenant Commander, United States Navy
B.S., United States Naval Academy, 1998

Submitted in partial fulfillment of the
requirements for the degree of

MASTER OF SCIENCE IN METEOROLOGY AND PHYSICAL OCEANOGRAPHY

from the

NAVAL POSTGRADUATE SCHOOL
September 2008

Author: Erick Lee Edwards

Approved by: Timour Radko
Thesis Advisor

Jeffrey Haferman
Second Reader

Mary Batteen
Chairman, Department of Oceanography

THIS PAGE INTENTIONALLY LEFT BLANK

ABSTRACT

The physics of the Meridional Overturning Circulation (MOC) and interhemispheric heat transport is explored with an emphasis on the upper and central ocean. Sea surface temperature and wind stress are considered in the context of their ability to influence the MOC pattern and their relative significance is quantified. Most calculations in this study use an idealized rectangular basin which makes it easier to identify the key dynamic processes and explain interaction. Volumetric and advective heat transport streamfunctions are used to analyze interhemispheric exchanges of mass and energy.

Data concerning the effects of equatorially-asymmetric wind stress and surface heat flux forcing are used to construct expressions which explicitly define the relationships between wind stress, surface heat flux, interhemispheric volume flow, and heat transport. The relative importance of wind stress and surface heat flux to the overall values of transport is discussed in light of climatology.

The meridional overturning circulation in the upper ocean is found to be the dominant factor in interhemispheric heat transport and in the maintenance of the Earth's climate despite its extremely small contribution to total meridional-vertical circulations in the entire ocean basin. This study suggests that the previous emphasis on deep overturning in the abyssal region and small-scale mixing as the dominant factors in the meridional overturning circulation should be reconsidered and the role of wind stress and surface heat fluxes more thoroughly investigated as determining factors of MOC strength and maintenance.

This study explores possible mechanisms responsible for climate shift which could result in long-term changes to weather patterns and ocean conditions altering important factors in the Navy's operating environment. Thus, long-term Navy planning must include an appreciation for possible changes in the forcing mechanisms responsible for the meridional overturning circulation.

THIS PAGE INTENTIONALLY LEFT BLANK

TABLE OF CONTENTS

LIST OF FIGURES

THIS PAGE INTENTIONALLY LEFT BLANK

LIST OF TABLES

THIS PAGE INTENTIONALLY LEFT BLANK

ACKNOWLEDGMENTS

I would first like to thank the following people who helped me in significant ways during the course of my research (in alphabetical order): Eric Adint, Evangelina Anderson, Donna Burych, Mike Cook, Francis Giraldo, Arlene Guest, Janis Higginbotham, Gabriele Jost, Igor Kamenkovich, Scott Katz, Pam Silva, and Susana Valeriano.

I also thank Dr. Jeff Haferman for volunteering his time and expertise in helping me with all of the technical aspects of the experiment. Five minutes of his time saved me many hours of searching for solutions and I never could have started my experiments without him.

I can't thank Dr. Timour Radko enough. I am extremely grateful that he accepted me as his thesis student and I am honored to have had the opportunity to work closely with him and directly experience his enthusiasm for oceanography and benefit from his superb mentoring skills. He is an outstanding instructor and thesis advisor.

Finally, I'd like to thank Julia, Lucian, Cezar, and Monkey. I attribute the vast majority of my success at Naval Postgraduate School to the patience and constant encouragement of my family. Their understanding, support, and unwavering belief in me drove me on when times were difficult. As long as they are with me, I will always be successful.

And I would especially like to thank Monkey for being so quiet during the many hours it took to complete this thesis.

THIS PAGE INTENTIONALLY LEFT BLANK

I. INTRODUCTION

A. THE IMPORTANCE OF THE MERIDIONAL OVERTURNING CIRCULATION

The world ocean is one of the main constituents of the Earth's climate system. Most of the Earth is covered by the world ocean, so a significant portion of the solar radiation that reaches the planet's surface is received by the ocean. Surface waters are warmed by this radiation. The heat capacity of the ocean, along with the presence of ocean currents, allows the ocean to store and redistribute heat energy before it is lost to the atmosphere or space. The ability of the ocean to transfer heat energy from warmer areas of the planet's surface to cooler areas is a significant factor in maintaining the climatic state of the Earth.

Large-scale ocean circulation in the ocean is caused by a variety of factors. Wind-driven currents affect the upper parts of the ocean. Currents driven by density changes in water masses at the sea surface caused by fluxes of heat and freshwater interact with interior mixing caused by temperature and salinity differences. These interactions result in what is known as thermohaline circulation (THC) and this circulation is thought to be an important factor in maintaining the current climate of the Earth.

However, recent work has called into question the forcing mechanisms previously thought responsible for the thermohaline circulation. Also, new factors possibly affecting the stability of the THC in the Atlantic have been identified. Understanding the forcing mechanisms behind the thermohaline circulation is crucial if oceanographers are to make predictions concerning changes in the THC which could likely lead to climatic changes. This would signal a historic shift in the focus of physical oceanography from a primarily observational science to a predictive one.

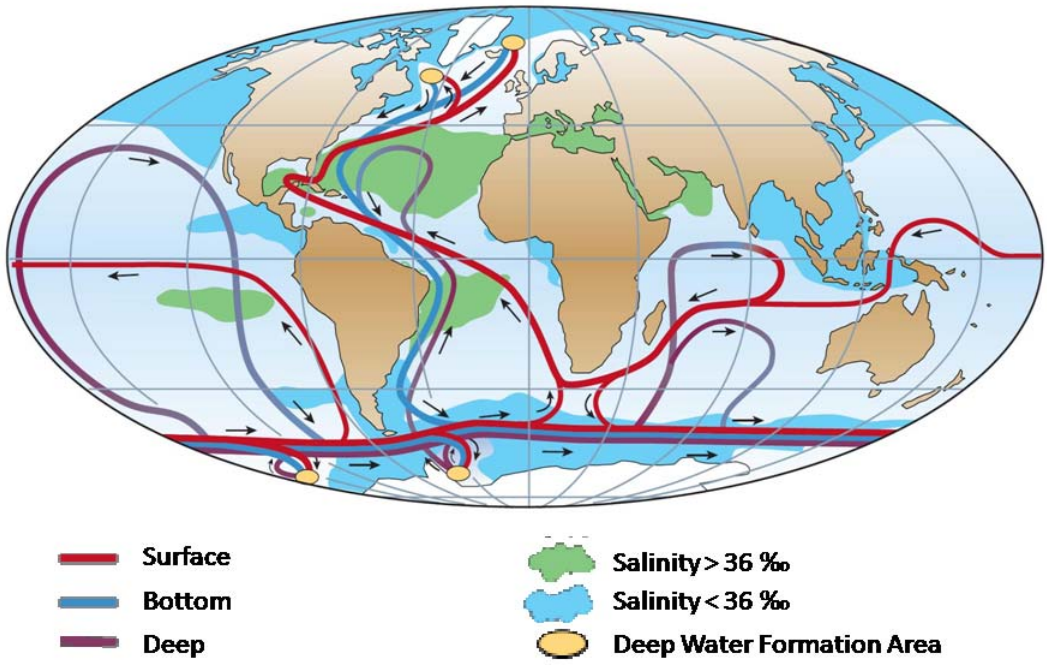

FIGURE 1. Meridional Overturning Circulation in the World Ocean

In this paper, the term "meridional overturning circulation" (MOC) will be used to mean a circulation of ocean water as viewed on a meridional-vertical plane. It is a descriptive, mechanism-neutral, term meaning that this particular type large-scale circulation of the ocean can be described while the exact mechanisms leading to this motion are not specified. By contrast, the term "thermohaline circulation" generally is used to refer to the same phenomenon, with the assumption that the meridional overturning circulation is maintained by the forcing mechanisms of density fluxes at the ocean surface and diffusion in the ocean interior. Since the point of this paper is to reconsider the limitations of classical conceptions of the forcing mechanisms responsible for ocean circulation along meridional-vertical planes, the term MOC will be used throughout.

B. THE CENTRAL PROBLEM

A fundamental problem in physical oceanography and climate science concerns the mechanism, magnitude, and stability of the MOC in the Atlantic. The modern theory of the MOC identifies at least two distinct dynamic components of the MOC – shallow overturning cells in the main thermocline and deep circulation in the abyssal ocean. Historically, development of the MOC theory has been biased towards understanding of the deep abyssal circulation. However, new and emerging evidence suggests that meridional heat transport, the "heat engine" of the Earth's climate, is controlled by the processes operating in the upper ocean.

Unfortunately, the dynamics of the upper cell of the MOC are still poorly understood. What is even more disturbing, the mechanisms for the establishment and maintenance of the upper and lower cells are likely to be substantially different. This casts doubt on the ability of the classical thermodynamically driven Stommel-type models to articulate the conceptual view on the mechanisms of the MOC. For instance, vertical diffusivity – the primary agent for abyssal overturning – is very weak in the central thermocline ($\sim 10^{-5}\, m^2/s$). It is less, by an order of magnitude, than the values required to reproduce realistic MOC via purely diffusive mechanisms. Unlike the abyssal ocean, the thermocline is directly exposed to the surface forcing by winds and air-sea buoyancy fluxes which may provide the energy for meridional overturning. These distinct features call for new approaches and new insights into the dynamics of the MOC.

C. CLASSICAL THEORIES OF MERIDIONAL OVERTURNING CIRCULATION

The classical view of the thermohaline circulation is provided by Stommel and Arons (1960a,b). In this view, deep circulation is described as a source and sink driven circulation. Deep circulation is assumed to be steady and is driven by idealized sources in an ocean with no bottom topography. The sources of deep water are balanced by a uniform upwelling occurring throughout the basin.

Later, Stommel (1961) introduced a two-box model to explain meridional flow. In this model, heat flux into the southern box results in surface flow to the northern box. Heat flux out of the northern box (i.e., cooling) causes the surface water of that box to become more dense, which then sinks to the bottom, and returns along the bottom to the southern box. The strength of the circulation is proportional to the density difference between the two boxes. He also postulated that there are three equilibrium states for thermohaline circulation. Two are controlled by temperature changes (one stable, the other unstable) and one by salinity changes.

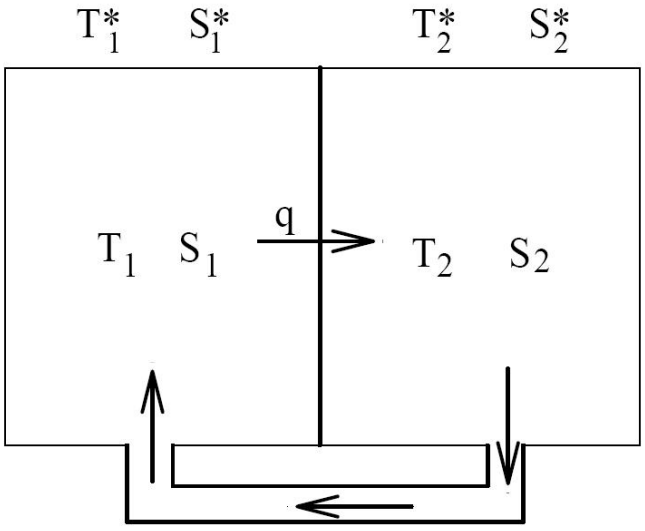

FIGURE 2. Stommel's Two-Box Model

The same year that Stommel offered his two-box model, Wyrtki (1961) developed a model of meridional circulation representing four processes: surface heating of the ocean in the low latitudes resulting in poleward flow at the surface, surface cooling at the high latitudes resulting in sinking, equatorward flow in the deep layer, and rising through the thermocline back to the surface. In Wyrtki's model, the circulation is dominated by changes in density by air-sea heat flux at the surface; no internal mixing is required. However, Wyrtki's model does not take into account the potential for wind stress to contribute to overall meridional circulation and thus describes this circulation in terms of purely thermohaline mechanisms. Figure 3 is a diagram detailing this model (adapted from Wyrtki, 1961).

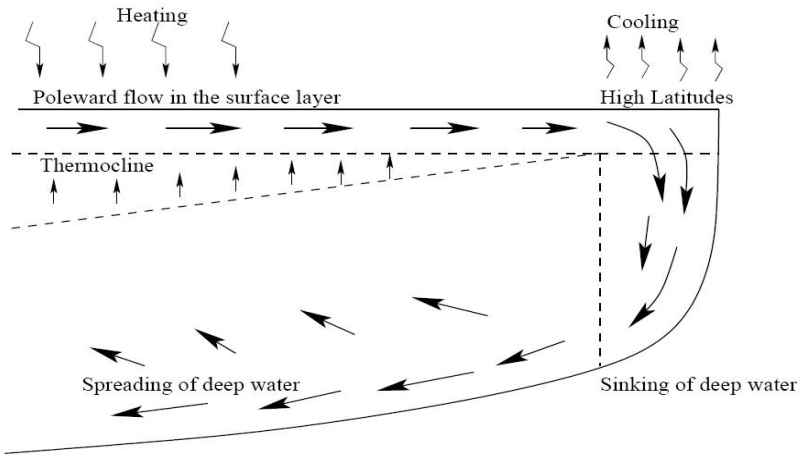

FIGURE 3. Wyrtki's Thermohaline Circulation Model

Munk (1966) also provided a similar model, with diapycnal mixing in the ocean interior replacing surface layer mixing. Upwelling is balanced by downward heat diffusion. The poleward flow of the surface layer is driven by the pressure gradient of the MOC, not by wind stress and as such, is a true THC model.

For 20 years, these simple theories seemed to offer an adequate explanation of deep circulation. However, the uniform poleward flow implied by the early theories could not be verified, and by the 1980's, researchers realized that the simplifications inherent to the classical theories had to be replaced with more realistic assumptions. During this time, as demand for a greater understanding of the mechanisms influencing the Earth's climate came to the fore, Stommel's 1961 theory detailing multiple equilibria in thermohaline circulation became more appreciated by physical oceanographers seeking to understand climate change.

Stommel's two-box model offered an explanation of thermohaline circulation for one hemisphere. Rooth (1982) expanded this model to include three boxes representing the two hemispheres and an equatorial region. This model describes four possible modes of circulation, two of which were unstable. Rooth's work was important in that it explored the possibility of transitions between stable states of meridional overturning circulation.

Bryan (1986) found that introducing a large freshwater flux at the northern boundary of a circulation model caused a collapse in the thermohaline circulation (commonly referred to as the "halocline catastrophe"). Since Bryan's work, understanding the mechanisms responsible for the maintenance of the meridional overturning circulation has become a very important research area in physical oceanography due to the dramatic climate implications of such a finding.

D. RECENT CONTRIBUTIONS TO THE UNDERSTANDING OF THE MOC

Since the 1980s, the physical oceanography community's interest in the MOC has increased significantly. What follows is a brief survey of some important contributions in this area of research.

Marotzke and Willebrand (1991) investigated the effects of freshwater forcing on transitions between global THC equilibrium states using an idealized basin with equatorially-symmetric wind stress and temperature forcing. They concluded that four different stable steady states were found under identical boundary conditions (one of which mirrored today's "conveyor belt" pattern) and that relatively small changes in freshwater flux could lead to a transition between states.

Weaver et al. (1993) used an idealized single-hemisphere ocean basin with prescribed wind, temperature, and freshwater flux forcing to determine the dominant factors on the stability and internal variability of the thermohaline circulation. They found that surface freshwater forcing was the dominant factor in detemining the model's stability and internal variability.

Marotzke and Stone (1995) improved upon Stommel's thermohaline circulation theory by offering a single-hemisphere theoretical analysis of the interactions between atmospheric meridional transports and the thermohaline circulation using a four-box ocean-atmosphere model. They determined that the range of stable solutions with high-latitude sinking was smaller than in related uncoupled box models due to the dependence of freshwater flux on the temperature gradient.

Noticing that different convection patterns were stable under the same surface boundary conditions, Rahmstorf (1995) investigated how multiple steady states arise in an ocean general circulation model using two alternative boundary conditions: classical mixed boundary conditions and a diffusive atmospheric heat balance with fixed salt fluxes. These experiments showed that under the classical mixed-boundary conditions overturning rates of deep water were dependent on the convection site. Under the energy balance atmosphere condition, different convection patterns were found to be associated with very different climatic states. Heat transport of the deep circulation seemed to be dependent on the actual location of convection leading to the conclusion that climate variability in the North Atlantic depended on the location of convection in the high latitudes. This conclusion was further discussed in Rahmstorf (2002) and three distinct circulation modes were detailed: the stadial mode, the interstadial mode, and the Heinrich mode. The significant difference between the first two modes was in the location of North Atlantic Deep Water (NADW) formation. In the Heinrich mode, there was no NADW formation and water of Antarctic origin fills the deep Atlantic basin.

In Rahmstorf and Willebrand (1995), circulation states were compared using traditional mixed boundary conditions and a new thermal boundary condition allowing for an oceanic feedback effect on atmospheric temperatures. This approach allowed for surface temperature forcing that varied with time, taking into account the ocean's effect on atmospheric temperatures. Armed with this new approach, Rahmstorf and Willebrand showed that a temperature feedback involving horizontal heat transport regulated the overturning rate of the "conveyor belt" circulation while a second feedback involving vertical convection stabilized the conveyor belt when freshwater anomalies were introduced into the North Atlantic. Thus, ocean-to-air temperature feedback mitigated the effects of large positive freshwater fluxes in the North Atlantic making the halocline catastrophe postulated by Bryan (1986) much more difficult to effect.

Marotzke (1997) implemented boundary mixing in an ocean general circulation model with no wind forcing and a nearly fixed surface density to investigate the three-dimensional dynamics of thermohaline circulation. The vertical mixing coefficient was

nonzero only near side boundaries and in convective regions. Overturning strength and meridional heat transports were found to be dependent on the vertical mixing coefficient.

Rahmstorf and England (1997) used an atmospheric-ocean hybrid model along with an ocean-only model to study the sensitivity of deep overturning circulation to Southern Hemisphere winds. This study found that the influence of Southern Ocean winds on NADW flow was only moderate. However, the formation rate of Antarctic Bottom Water was found to be strongly dependent on winds over the Southern Ocean.

Rahmstorf and Ganopolski (1999) offered a theory to explain climatic drift previously found in general circulation model experiments. They showed how model initialization with unsuitable relaxation boundary conditions could result in unstable solutions producing unrealistic predictions of changes in thermohaline circulation. This paper emphasized the need to initialize models properly so that model runs do not start off on unstable solution branches.

Expanding on Rooth's three-box model, Scott et al. (1999) examined interhemispheric thermohaline circulation and compared their results with those from single-hemisphere box models. They found that when northern freshwater forcing was made weaker than southern freshwater forcing, ocean salinity feedback became negative whereas ocean salinity feedback can only be positive in single-hemisphere models.

Kamenkovich, Marotzke, and Stone (2000) investigated which physical factors determined meridional heat transport in a global ocean general circulation model with idealized geometry, wind stress, and moisture fluxes. Causes for the underestimation of heat transport in many models were found to be: overly large horizontal viscosities, large resolutions near boundaries, and the lack of interbasin mixing.

Marotzke and Klinger (2000) looked at the three-dimensional dynamics of equatorially asymmetric thermohaline flow with no wind forcing and a nearly fixed surface density. Their results indicated that NADW export rate from the North Atlantic is controlled by mixing and upwelling in the rest of the world ocean.

Scott and Marotzke (2002) explored the large-scale consequences of diapycnal mixing location using a three-dimensional model of buoyancy-forced flow in a single

hemisphere. In contast to previous theories, they illustrated that enhanced boundary mixing in the thermocline, rather than abyssal mixing, can maintain the meridional overturning circulation.

Marshall and Radko (2003) applied a residual-mean theory to the Antarctic Circumpolar Current and found that the interaction of geostrophic eddies with winds and buoyancy fluxes determined the depth and stratification of the thermocline and influenced the pattern of the MOC.

Klinger et al. (2004) examined the importance of zonal periodicity and other factors in setting the sensitivity of the MOC to the wind stress and concluded that the zonal wind stress over the Southern Ocean was responsible for a significant fraction of the MOC associated with NADW.

Timmermann and Goosse (2004) found that neglecting wind stress in a global coupled atmosphere-ocean model led to a complete shutdown of the meridional overturning circulation thus proving that wind forcing plays a substantial role in the maintenance of large-scale MOC in the Atlantic.

Boccaletti et al. (2005) showed that surface circulation dominates the heat transport in global ocean models making it likely that ocean heat fluxes will respond to changes in atmospheric winds rather than to changes in abyssal mixing. This indicates that a decrease in deep overturning circulation does not necessarily imply a significant change in global oceanic heat transport, suggesting that variability in the global heat budget transport may be decadal rather than centennial or longer.

Radko and Marshall (2006) developed a theory for the large-scale three-dimensional structure of the Antarctic Circumpolar Current and the upper cell of its overturning circulation. When compared to observations, their prognostic model had the ability to predict the amplitude and distribution of air-sea buoyancy fluxes. Model predictions of the thermocline were consistent with the hydrography of the Southern Ocean.

Hirschi and Marotzke (2007) found that numerical models could be used to reproduce the variability of the MOC using only boundary densities and wind stress. On

seasonal timescales, MOC variability was found to be due mostly to wind stress. Boundary density was the leading cause of interannual MOC variability.

Radko (2007) offered a two-dimensional analytical residual-mean model of the MOC in the upper ocean to illustrate the dynamics of interhemispheric interaction. Symmetric wind stress and air-sea buoyancy forcing leads a solution with little interhemispheric flow exchange or heat transfer. This configuration was shown to be unstable, leading to one or two possible stable regimes, one with high-latitude sinking in the north, the other with sinking in the south. In contrast to earlier studies investigating the role of salt advection, this study showed that the positive feedback between atmospheric winds and oceanic meridional circulation could also lead to spontaneous symmetry breaking.

E. CRITICISMS OF THE EARLY THEORIES

With few exceptions, all previous research into the meridional overturning circulation has emphasized two processes: deep overturning circulation in the abyssal region and small-scale vertical mixing throughout the ocean basin. Focusing only on these two aspects of meridional overturning circulation may not be appropriate in light of Boccaletti et al. (2005) and Radko (2007). Boccaletti et al. stipulate that advective meridional heat transport is dominated by processes occurring in the thermocline while Radko postulates that interhemispheric transports occur mostly in the upper ocean due to equatorially asymmetric forcing.

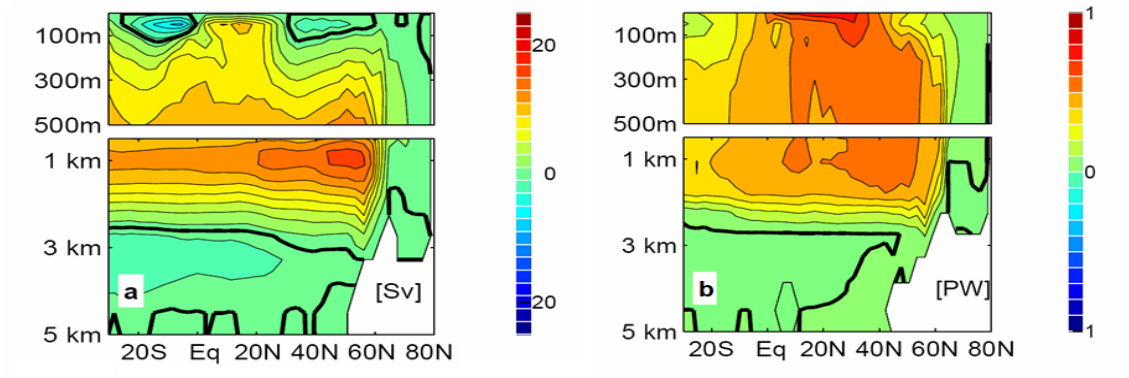

FIGURE 4. Streamfunction and Heatfunction for the North Atlantic

Figure 4 from Boccaletti et al. (2005) offers interesting insights into the locations of maximum volume and heat transports in the North Atlantic. Figure 4a shows that the center of meridional overturning circulation occurs at a level of about one kilometer. Circulation is weak at the upper-most levels. In contrast, the center of maximum heat transport circulation occurs at these upper-most levels (Figure 4b) where the volumetric transport streamfunction is the weakest. A simple conceptual diagram illustrates why this may be the case. The thermocline has a smaller volume transport when compared to the abyssal region. However, the temperature gradient in the thermocline is much larger. Even though the amount of volumetric transport in the abyssal cells dwarfs that of the thermocline cells, heat transport in the abyssal cells is very small. At these levels, cold water is being exchanged with water only slightly warmer. In the thermocline, with its large temperature differences, a much smaller volume of transport can effectively advect a vastly greater amount of heat. This would seem to indicate that overturning in the thermocline, not in the deep layers, is more critical for interhemispheric heat transport and a more important factor in influencing the world climate.

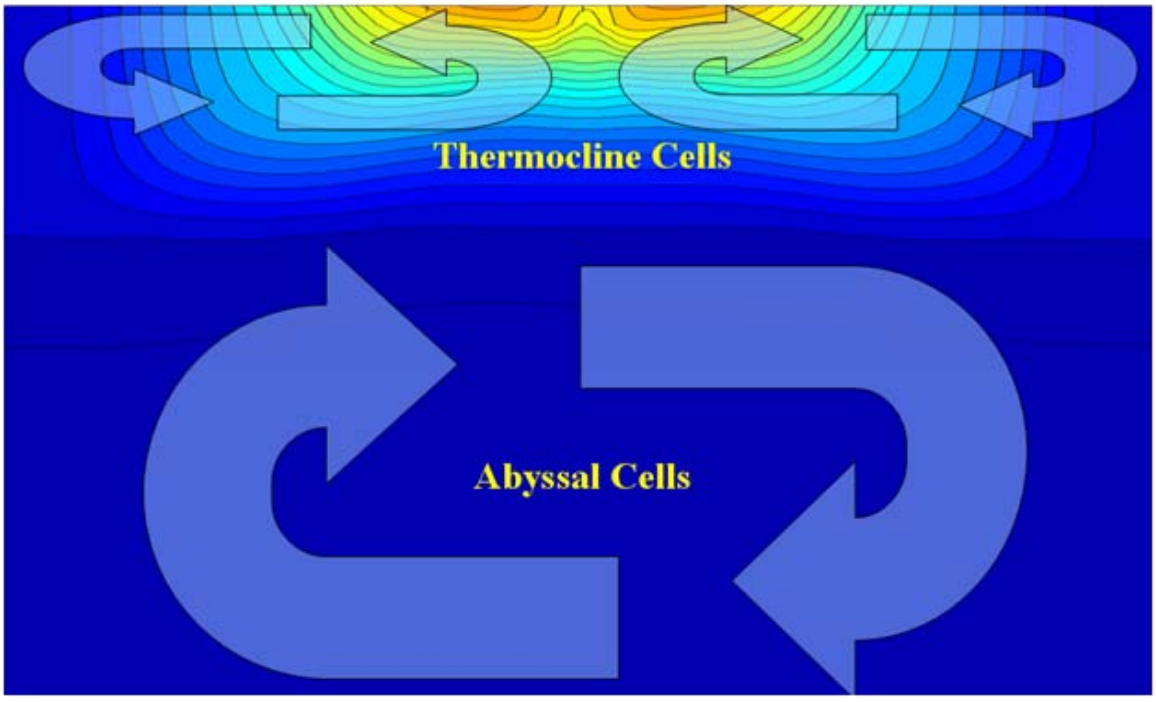

FIGURE 5. Thermocline and Abyssal Cells

If the thermocline plays a vastly more important role in maintaining climate, then physical oceanographers need to reconsider the concept of meridional overturning cells. Previously, when the research focus was on abyssal overturning, wind stress and surface heat fluxes were neglected as possible mechanisms affecting the strength and maintenance of meridional overturning circulation. However, wind stress and density fluxes do affect circulation at the surface, therefore it follows that these mechanisms could indeed be important factors in determining the strength and character of the MOC.

F. THIS PAPER'S CONTRIBUTION TO THE UNDERSTANDING OF THE MERIDIONAL OVERTURNING CIRCULATION

The major objective of this thesis is to understand the dynamics of the upper branch of the MOC in the Atlantic basin. Specific inquiries will address a number of issues. The relative contribution of sea surface forcing in shaping the pattern of the MOC and interhemispheric heat transport in the upper ocean will be determined. The effectiveness of mechanical forcing by winds and that of thermodynamic forcing by air-sea buoyancy fluxes will be investigated. The possibility of predicting the strength of the MOC and meridional heat transport based on surface forcing mechanisms will be explored as well as the role of interhemispheric surface forcing asymmetries.

It is the emphasis on the upper ocean that distinguishes this paper from earlier theoretical and modeling studies of the MOC. Process-oriented numerical simulations are used to address these problems. Model output will be used to identify the zero order physics and dynamics at play, while recording and explaining the sensitivity of the MOC to the form and magnitude of surface forcing. Independent analysis of wind stress and surface heat flux forcing coupled with a highly-idealized geometry makes for a well-defined problem where the effects of asymmetric forcing on the magnitude of the MOC and interhemispheric heat transport can be easily isolated.

II. METHODS

A. APPROACH

Numerical modeling is the most ideal tool to address the dynamics of the MOC on a quantitative level. While most of the numerical experiments are of an idealized process-oriented character, these simulations were guided and supplemented by the analysis of the relevant sea-surface data and comprehensive general circulation models.

For this study, the Massachusetts Institute of Technology General Circulation Model (MITgcm) was employed. The intensity and distribution of sea surface forcing (sea surface temperature and wind stress) were systematically varied while the response of the upper MOC cell was recorded. The focus of the analysis was on the meridional transport of heat and volume. The numerical results were then compared to previous studies and rationalized by developing illustrative theoretical models.

An idealized model of intermediate complexity was chosen to investigate the mechanisms of wind stress and surface heat flux forcing on the MOC and interhemispheric heat transport. Simple box models are very useful in articulating initial conceptual frameworks and motivating further research, but can be inconclusive concerning actual physics at play. On the other hand, comprehensive general circulation models are effective in giving extremely detailed data but a loss of transparency concerning general physical concepts can occur as the particulars of the real world are introduced into the model. A model of intermediate complexity mitigates the disadvantages of simple and complex models by idealizing real-world parameters so that useful insights can be gained into the mechanisms responsible for phenomena found in nature.

To understand the effects of wind stress and heat flux on the MOC, the MITgcm was used in conjunction with an idealized single-basin geometry. Four types of cases were explored. The first type involved equatorially symmetric wind stress and surface temperature forcing. This type will be called the Symmetric case. Two additional types

of model runs introduced either equatorially asymmetric wind stress or temperature forcing (referred to as Asymmetric Wind or Asymmetric Temperature cases, respectively). The final type combined both equatorially asymmetric wind stress and temperature forcing (Dual-Asymmetric cases).

B. THE NUMERICAL MODEL

1. MITgcm

The MITgcm is a numerical model designed for the study of the atmosphere, ocean, and climate. It can be used to model both atmospheric and oceanic circulation and has non-hydrostatic capability which allows it to be used to study both small and large-scale processes. It uses the finite volume method to solve oceanographic equations, providing support for the treatment of irregular geometries using orthogonal curvilinear grids and shaved cells. Tangent linear and adjoint code are maintained alongside the forward model, permitting sensitivity and optimization studies. MITgcm supports a wide variety of physical parameterizations and was developed to perform efficiently on a wide variety of platforms.

2. The Idealized Basin

The idealized basin is a Cartesian box measuring 6,660 km in the zonal direction and 13,320 km in the meridional direction with a constant depth of 4005 m. It covers 120° of latitude and 60° of longitude. The northern and southern hemispheres each cover 60° of latitude. There are 100 grid points along the x-direction and 200 grid points along the y-direction giving a model resolution of 0.6° in both horizontal directions.

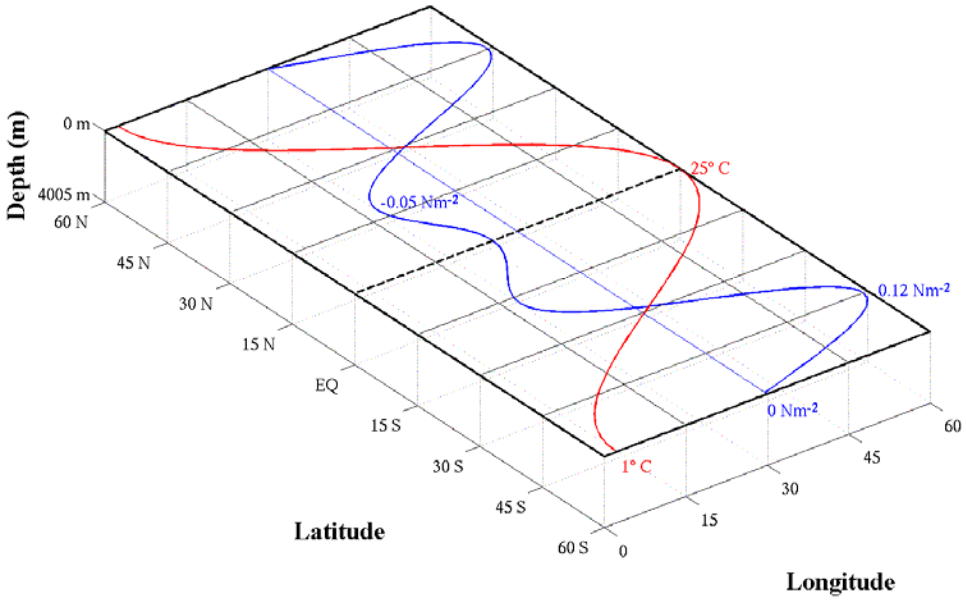

FIGURE 6. The Idealized Basin

The idealized basin is shown above as Figure 6. The surface boundaries are in bold while the dashed line represents the equator. Forcing curves for the symmetric case are superimposed on the surface as examples. The red curve shows symmetric temperature forcing by latitude. The blue curve indicates symmetric wind stress forcing by latitude. Representative values are included for both curves.

The idealized basin has 20 vertical levels. Vertical resolution varies exponentially from 22 meters at the surface to 678 meters at the deepest level. The resolution ($\mathbf{\Delta Z}$) at each vertical level is given by the following equation:

$$\Delta \mathbf{Z}(\mathbf{l}) = \mathbf{C}\left[\exp(\alpha \mathbf{l}) - \exp(\alpha(\mathbf{l}-1))\right] \quad (1)$$

Where $\mathbf{C}$ = 112.5 m, α=0.18, and $\mathbf{l}$ = the vertical level (ranging from one to 20).

This particular set of dimensions allows a large enough volume to adequately represent an ocean basin to examine the effects of changing wind stress and surface heat flux forcing on meridional overturning circulation. An exponential vertical resolution scheme is employed to capture greater detail at the upper levels of the ocean, the focus of this study.

3. Surface Forcing Parameters

a. Wind Stress

Zonal wind stress forcing is considered in this study, which varies only in the meridional direction. To clearly separate the equatorially symmetric and asymmetric processes – the focus of this study – total wind stress magnitude is composed of symmetric and asymmetric components. The wind stress equation is:

$$\tau = \tau_{\mathbf{sym}} - \mathbf{A}\tau_{\mathbf{asym}}. \tag{2}$$

The coefficient, **A**, is the only variable altered between runs and is used to determine the magnitude of the wind stress asymmetry between the hemispheres of the idealized basin.

The symmetric portion of the wind stress equation is given by:

$$\tau_{\mathbf{sym}} = \tfrac{3}{4}\tau_0\left[\tfrac{3}{4}\cos\left(5\pi\phi\right) - \cos\left(3\pi\phi\right)\right], \tag{3}$$

where $\tau_0 = 0.1\,N/m^2$, $\phi = \frac{3}{2\pi}\theta$, and θ is the latitude. Thus, ϕ is equal to $\frac{1}{2}$ at 60° N, $-\frac{1}{2}$ at 60° S, and zero at the equator.

The asymmetric portion of wind stress is given by:

$$\tau_{\mathbf{asym}} = \tfrac{1}{144}\tau_0\left[-\tfrac{2}{3}\sin\left(2\pi\phi\right) + \tfrac{11}{24}\sin\left(4\pi\phi\right) - \tfrac{1}{12}\sin\left(6\pi\phi\right)\right]. \tag{4}$$

The asymmetric part of the equation was written so as to reduce the asymmetry near the equator while emphasizing a mid-latitude asymmetry. Figure 7 illustrates an example of a wind stress forcing curve with its symmetric and asymmetric components.

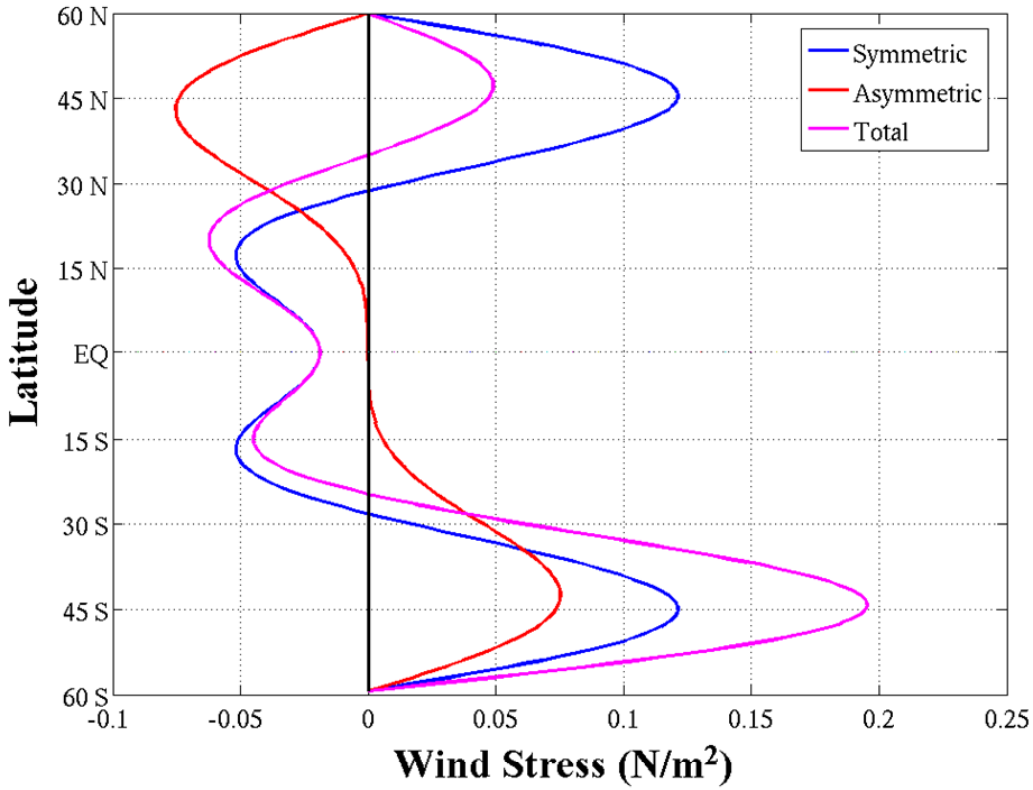

FIGURE 7. Components of the Wind Stress Forcing Curve

The value of A controls the magnitude of the peak wind stress and the overall mean wind stress found in both hemispheres. When A = 0, the wind stress curve is symmetric about the equator. When A > 0, the magnitude of westerly peak wind stress and mean hemispheric wind stress is higher in the northern hemisphere, while A < 0 causes a higher peak magnitude and mean hemispheric wind stress to occur in the southern hemisphere. In this study, values of A that produce mid-latitude peak wind stress ratios and interhemispheric mean wind stress differences representative of the current climate are used. Table 1 summarizes the values of A that were used in this experiment along with other measures of the wind stress asymmetry.

TABLE 1. Wind Stress Ratios, Peaks, and Locations

Value of A	Ratio of Wind Stress	Wind Stress Difference (Nm^{-2})	Peak Wind Stress (Nm^{-2})		Peak Wind Stress Location	
			Southern Hemisphere	Northern Hemisphere	Southern Hemisphere	Northern Hemisphere
0	1:1	0.000	0.121	0.121	45.3° S	45.3° N
-36	3:2	0.022	0.146	0.097	44.7° S	45.6° N
-60	2:1	0.037	0.163	0.081	44.7° S	45.9° N
-90	3:1	0.055	0.183	0.061	44.7° S	46.5° N
-108	4:1	0.066	0.195	0.049	44.4° S	47.1° N

In the table above, the first column gives the southern-to-northern ratio of the magnitudes of peak westerly wind stresses found in the mid-latitudes of both hemispheres. The second column shows the difference in the mean wind stresses between the hemispheres. The actual value of the peak westerly wind stress is given for both hemispheres in the following two columns. The latitude where the peak westerly wind stress occurs for both hemispheres is given in the last two columns. In all cases above, the southern hemisphere was given the stronger wind stress, which corresponds to negative values of A.

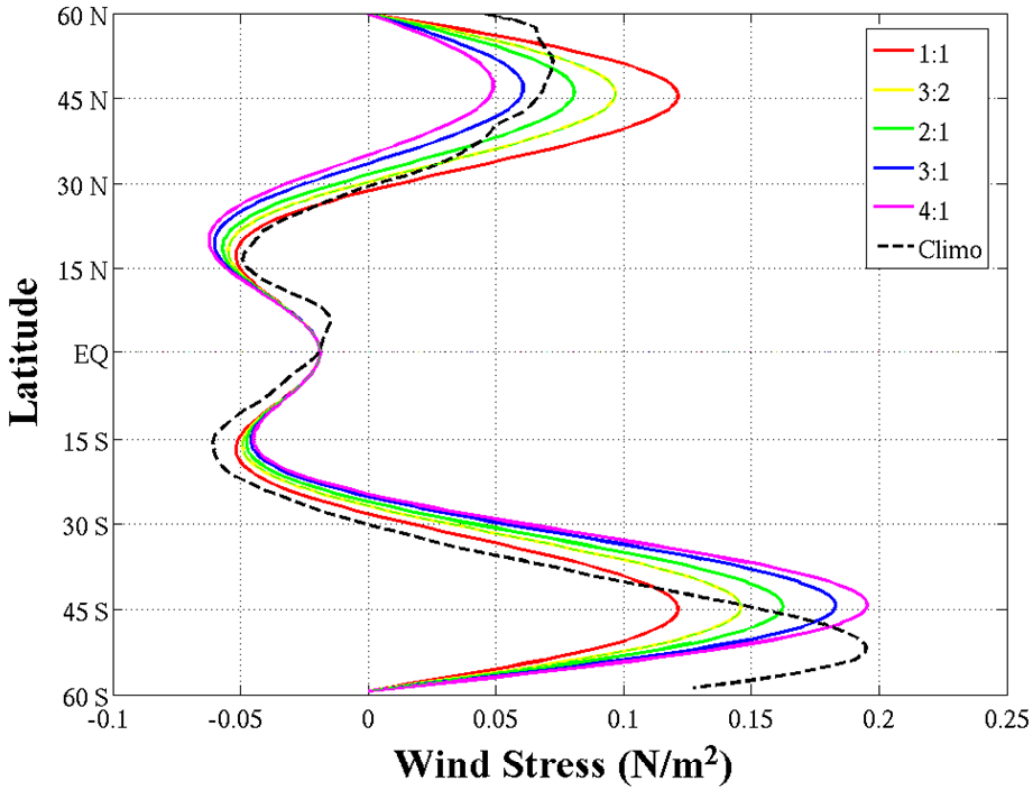

FIGURE 8. Zonal Wind Stress Forcing

Figure 8 shows all wind stress forcing curves used in this study. The climatology curve is the annual and zonal mean derived from NOGAPS wind stress data from 1990-1997.

b. Sea Surface Temperature

As with wind stress, sea surface temperature forcing is varied only in the meridional direction. The sea surface temperature forcing consists of symmetric and asymmetric components, as well. The temperature forcing equation is:

$$\mathbf{T} = \mathbf{T}_{sym} - \mathbf{B}\mathbf{T}_{asym}, \tag{5}$$

where the coefficient, **B**, is the only variable altered between runs and is used to determine the value of the maximum temperature and the meridional location of that maximum.

The symmetric portion of the temperature forcing equation is given by:

$$\mathbf{T_{sym}} = \mathbf{T_{mid}} + \mathbf{T_{add}} \cos\left(2\pi\phi\right), \tag{6}$$

where T_{mid} = 13 °C, T_{add} = 12 °C, and $\phi = \frac{3}{2\pi}\theta$ with θ equal to the latitude. Thus, the symmetric temperature equation gives a temperature range of 1 °C to 25 °C, with the maximum temperature located along the equator.

The asymmetric portion of the temperature equation is given by:

$$\mathbf{T_{asym}} = \frac{1}{3}\sin\left(2\pi\phi\right) - \frac{1}{3}\sin\left(4\pi\phi\right) + \frac{1}{6}\sin\left(6\pi\phi\right) \tag{7}$$

The asymmetric part of the equation emphasizes an interhemispheric asymmetry with a maximum sea surface temperature in the equatorial band, while minimizing asymmetry at the northern and southern limits to ensure that sea surface temperature remained close to 1 °C at those locations. Figure 9 shows an example of a sea surface temperature forcing curve with its symmetric and asymmetric components.

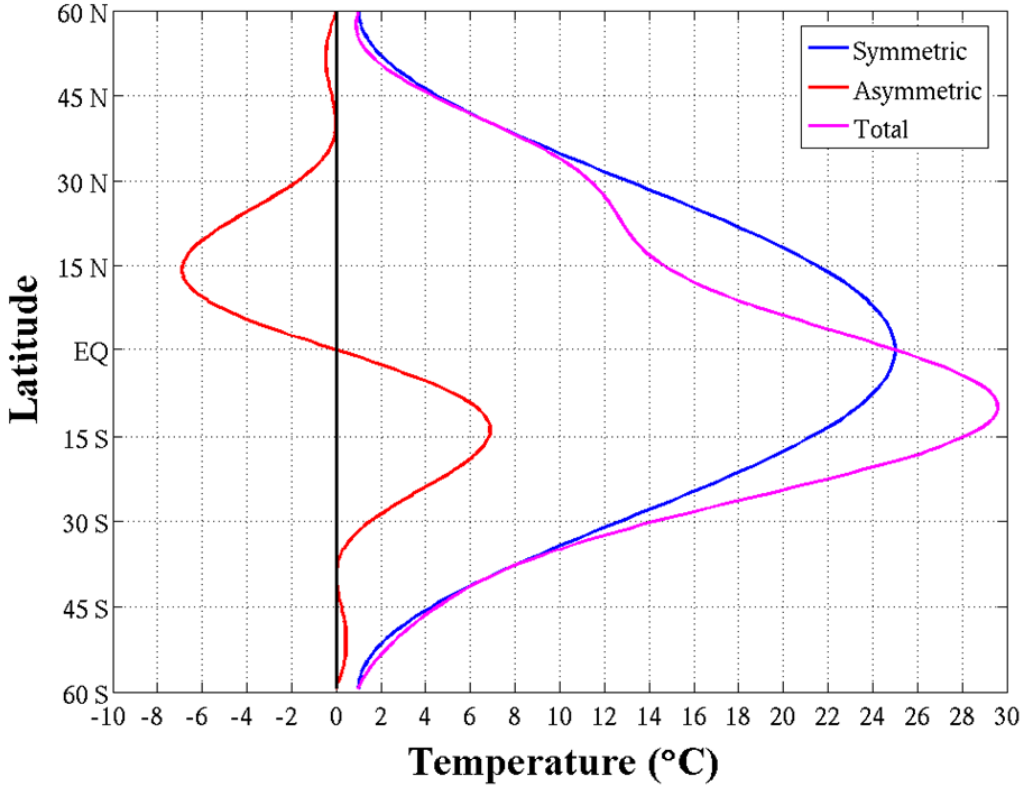

FIGURE 9. Components of the Temperature Forcing Curve

The coefficient, B, allows for easily manipulation of the temperature forcing in successive model runs. When B = 0, the temperature forcing curve is purely symmetric. For B > 0, the maximum temperature is found in the northern hemisphere while B < 0 places the peak temperature in the southern hemisphere. The absolute value of B determines the magnitude of the temperature peak. Table 2 gives all values of B that were used in this study along with corresponding values dependent on the magnitude of B. The second column shows the highest value of temperature forcing for that particular value of B, while the third column gives the latitude where this maximum is found during the model run. There is little change in the latitude of peak temperature between successive model runs with asymmetric temperature forcing; all peak temperatures remain within two degrees of one another. The last column gives the difference in mean sea surface temperature between the northern and southern hemispheres. All values of B

used in this experiment were negative, making the peak location and mean sea surface temperatures higher in the southern hemisphere for every model run.

TABLE 2. Temperature Peaks and Mean Sea Surface Temperature Differences

Value of B	Peak Temperature (°C)	Peak Temperature Location	Mean Sea Surface Temperature Difference (°C)
0.0	25.0	Equator	0.00
-5.0	26.7	7.8° S	2.46
-7.5	28.1	9.0° S	3.70
-10.0	29.6	9.9° S	4.93

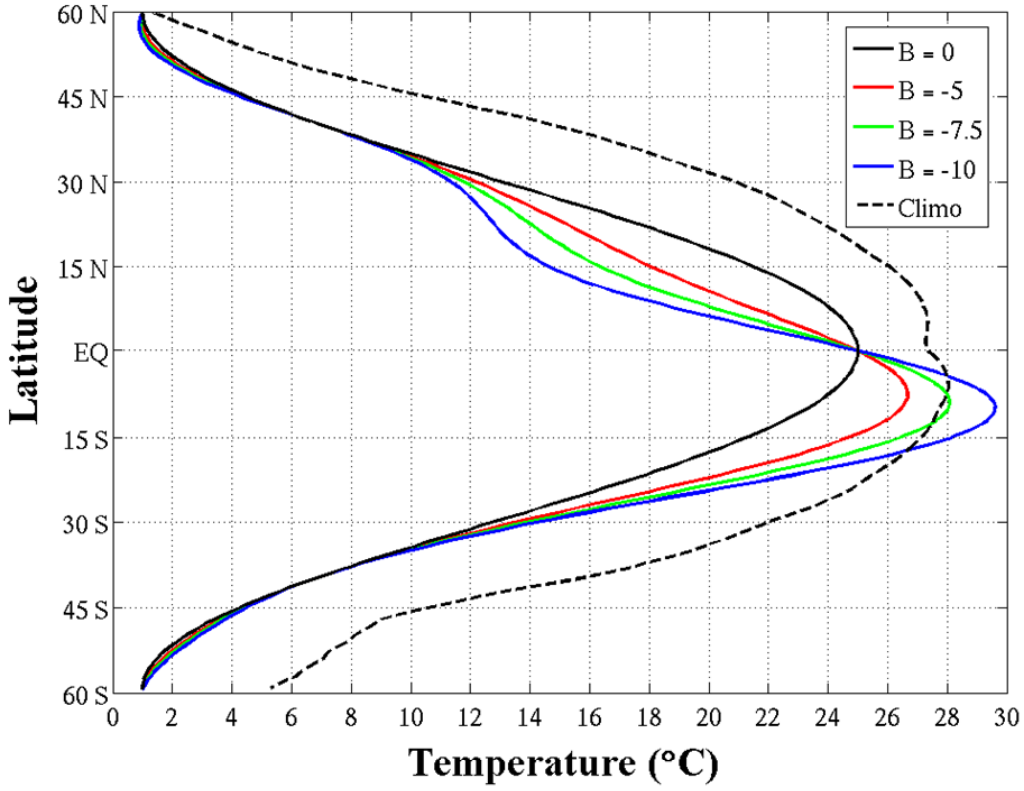

FIGURE 10. Zonal Temperature Forcing

Figure 10 gives all sea surface temperature forcing curves used in this study. The climatology curve is derived from NCEP reanalysis data for years 1984 to 2004.

4. Inputs into MITgcm

Table 3 is a summary of variable input parameters used for all model runs in this experiment. As discussed previously, the idealized Cartesian basin had meridional and zonal extents of 120° and 60° while depth was kept constant throughout the basin at 4,005 meters. The diffusivity and viscosity values fell within ranges used in previous, similar, experiments. The temperature restoring time scale was two months and the model was integrated forward at 10-minute intervals.

The mid-latitude beta plane approximation was used to calculate the Coriolis parameter for each latitude represented by the model. All model runs used the Gent-McWilliams parameterization to represent the effect of mesoscale eddies on isopycnals (Gent and McWilliams, 1990). It is important to note that no attempt was made to realistically simulate deep overturning cells since the purpose of this experiment is to determine the dynamics and contributions to volume and heat transport in the thermocline cells.

TABLE 3. Summary of Numerical Parameters

Parameter(s)	Value(s)
Basin width, length	60°, 120°
Basin depth	4005 m
Horizontal, vertical diffusivity	2×10^{3} m^2 s^{-1}, 5×10^{-5} m^2 s^{-1}
Horizontal, vertical viscosity	5×10^{4} m^2 s^{-1}, 5×10^{-5} m^2 s^{-1}
Longitude, latitude grid spacing	0.6°, 0.6°
Number of vertical levels, grid spacing	20 levels varied exponentially from 22 to 678 m
Temperature restoring timescale	60 days
Time step, momentum	10 min
Time step, tracers	10 min

5. Model Runs

Twenty cases were run using the MITgcm in this study. Table 4 summarizes these cases, giving the values of A and B that were used in the wind stress and temperature forcing equations, respectively. Differences in mean wind stress and sea surface temperature between the southern and northern hemispheres are listed next to the corresponding values of A and B that produce those differences. Case A was the only dual-symmetric case, having both equatorially-symmetric wind stress and temperature forcing. Cases C, K, and L were run with symmetric wind stress forcing and asymmetric sea surface temperature forcing. In Cases Q, I, J, and B, temperature forcing was kept symmetric while wind stress forcing was made sequentially more asymmetric. All other cases were dual-asymmetric.

TABLE 4. Model Run Summary

	$\Delta\tau$ (Nm^{-2})	0	0.022	0.0367	0.055	0.066
ΔT (°C)	Coefficients	A = 0	A = -36	A = -60	A = -90	A = -108
4.93	B = -10	L	T	G	H	P
3.70	B = -7.5	K	S	E	F	O
2.46	B = -5	C	R	M	N	D
0	B = 0	A	Q	I	J	B

The MITgcm was set to record data files every year during model runs. Four output fields were used in this study: temperature, zonal velocity, meridional velocity, and vertical velocity.

All model runs were integrated until equilibrium had been reached. Equilibrium was considered to have been reached when the ratio of the hemispheric net surface heat flux difference and heat transport across the equatorial plane came to within 1% of its discernible final asymptotic value. Figure 11 shows the equilibrium curve for Case R and is provided as an example. Equilibrium for this particular case was reached at 44 years and all other cases reached equilibrium in similar amounts of time.

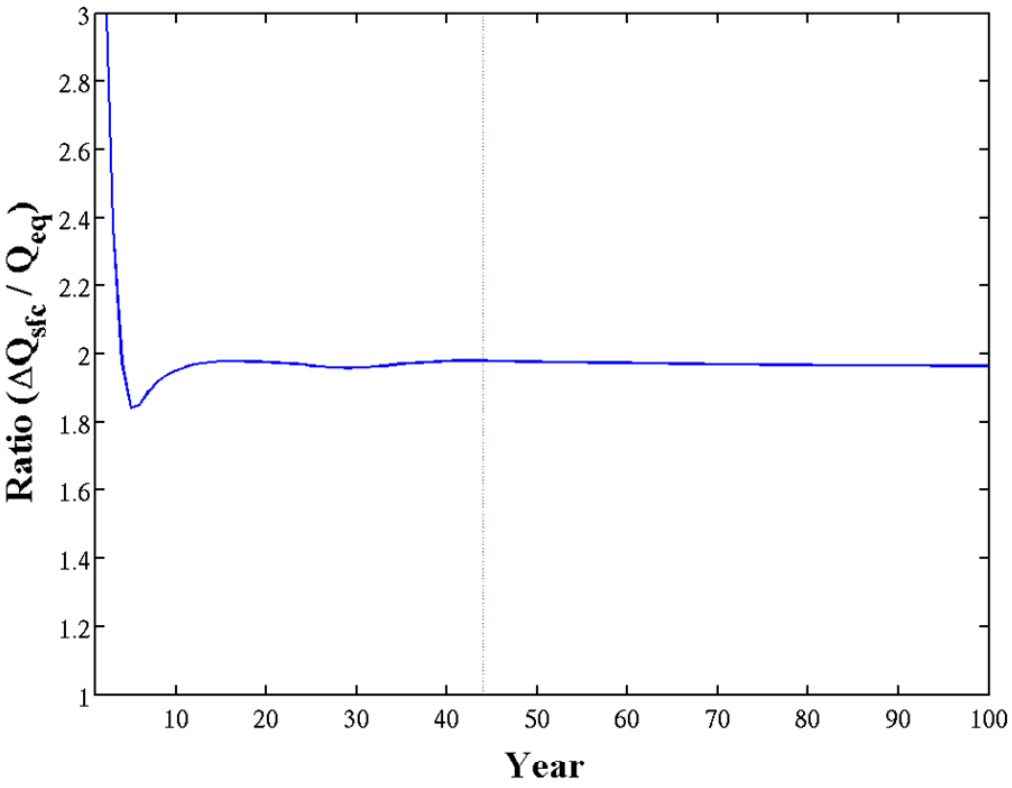

FIGURE 11. Equilibrium Curve for Case R

C. QUANTIFYING THE MOC

1. Volume Streamfunction

The simplest way to define the MOC is in terms of volume transport along a meridional-vertical plane. The focus of this study is on interhemispheric exchanges, therefore it is natural to express the cross-equatorial volume transport in terms of a volume transport streamfunction at the equatorial plane as follows.

Our starting point is the continuity equation:

$$\frac{\partial \mathbf{u}}{\partial \mathbf{x}} + \frac{\partial \mathbf{v}}{\partial \mathbf{y}} + \frac{\partial \mathbf{w}}{\partial \mathbf{z}} = 0 . \tag{8}$$

Integrating (8) zonally, results in:

$$\frac{\partial \langle \mathbf{v} \rangle}{\partial \mathbf{y}} + \frac{\partial \langle \mathbf{w} \rangle}{\partial \mathbf{z}} = 0 , \tag{9}$$

where $\langle\ \rangle$ denotes the zonal coast-to-coast averages. Since the zonally-integrated flow is non-divergent along a meridional-vertical plane, Equation (9) can be expressed in terms of a streamfunction:

$$\langle \mathbf{v} \rangle = \frac{\partial \Psi}{\partial \mathbf{z}}, \tag{10}$$

and

$$\langle \mathbf{w} \rangle = -\frac{\partial \Psi}{\partial \mathbf{y}}, \tag{11}$$

with velocities averaged over all years of the model run.

Using Equation (10), the streamfunction of meridional volumetric transport is expressed as:

$$\Psi(\mathbf{y}, \mathbf{z}) = \int_{-\mathbf{H}}^{\mathbf{z}} \langle \mathbf{v}(\mathbf{y}, \mathbf{z}) \rangle \, \mathbf{dz}, \tag{12}$$

where $\langle \mathbf{v}(\mathbf{y}, \mathbf{z}) \rangle$ is the time-averaged and zonally-integrated meridional velocity for a given latitude-depth combination. Equation (12) gives the streamfunction value for every grid point along the meridional-vertical extent of the basin. To analyze interhemispheric volume exchanges, the focus is on the streamfunction values at the equator, therefore a useful measure interhemispheric volume transport (as a proxy of meridional overturning circulation) is given as:

$$\Psi_{\mathbf{Eq}} = \max\left(\Psi|_{\mathbf{y}=0} \right). \tag{13}$$

Thus, the meridional volumetric transport across the equator is calculated by integrating the transport from the bottom of the basin up to the level of maximum volumetric transport. This definition gives the total volumetric transport across the equator at the lower levels. Continuity dictates that the net volumetric transport at all levels above the level of maximum transport be of the same magnitude, but opposite in direction. Maximum streamfunction at the equator, calculated for each model run, is an indicator of the strength of the MOC. For the dual-symmetric model run, it is expected that meridional transport will be very nearly zero, as all wind and temperature forcing is symmetric about the equator. For all other model runs, volumetric transport should be to

the north at upper levels, and to the south at levels closer to the bottom. This is due to the chosen pattern of asymmetries in wind stress and/or temperature forcing with stronger forcing in the southern hemisphere.

2. Heat Streamfunction

It has been shown how a streamfunction can be used to analyze interhemispheric volume transport. The exchange of heat between hemispheres can also be analyzed in a similar manner. Advective heat transport is the primary mechanism of heat exchange at the upper levels of the ocean and this transport can be expressed in terms of a "heatfunction" (Boccaletti et al., 2005).

We start with the advective-diffusion equation for temperature:

$$\frac{\partial \mathbf{T}}{\partial \mathbf{t}} + \frac{\partial (\mathbf{uT})}{\partial \mathbf{x}} + \frac{\partial (\mathbf{vT})}{\partial \mathbf{y}} + \frac{\partial (\mathbf{wT})}{\partial \mathbf{z}} = \mathbf{K_H} \nabla_{\mathbf{H}}^2 \mathbf{T} + \mathbf{K_V} \frac{\partial^2 \mathbf{T}}{\partial \mathbf{z}^2}. \tag{14}$$

Neglecting the interior diffusion in the central thermocline and applying time averaging and zonal integration, Equation (14) reduces to:

$$\frac{\partial \langle \mathbf{vT} \rangle}{\partial \mathbf{y}} + \frac{\partial \langle \mathbf{wT} \rangle}{\partial \mathbf{z}} = 0. \tag{15}$$

In the steady state, divergence is zero because there are no internal heat sources or sinks in the thermocline interior, and therefore, Equation (15) can be expressed in terms of a "heatfunction," Ψ_Q, as follows:

$$\mathbf{c_p} \rho_0 \langle \mathbf{vT} \rangle = \frac{\partial \Psi_\mathbf{Q}}{\partial \mathbf{z}}, \tag{16}$$

and

$$\mathbf{c_p} \rho_0 \langle \mathbf{wT} \rangle = -\frac{\partial \Psi_\mathbf{Q}}{\partial \mathbf{y}}, \tag{17}$$

where $\rho_0 = 1025$ kg/m^3 and $\mathbf{c_p} = 3850$ J/kg°C, with $\mathbf{c_p}$ and ρ_0 being the sea water density and heat capacity. Equation (16) can be formulated to calculate heat transport in the meridional-vertical plane:

$$\Psi_\mathbf{Q} = \mathbf{c_p} \rho_0 \int_{-\mathbf{H}}^{\mathbf{z}} \langle \mathbf{v}(\mathbf{y},\mathbf{z}) \mathbf{T}(\mathbf{y},\mathbf{z}) \rangle \, \mathbf{dz}, \tag{18}$$

where $\langle \mathbf{v}(\mathbf{y},\mathbf{z})\mathbf{T}(\mathbf{y},\mathbf{z}) \rangle$ is the time-averaged and zonally-integrated product of meridional velocity and temperature for a given latitude-depth combination. To analyze interhemispheric heat exchanges, the focus is on the heatfunction values of the at the equator, therefore a useful measure interhemispheric heat transport is given by:

$$\Psi_{Q_{Eq}} = \max\left(\Psi_{Q}\big|_{y=0}\right) \tag{19}$$

Thus, the interhemispheric heat transport is expressed as the maximum value of the heatfunction along the equator. For the dual-symmetric model run, it is expected that this heat transport will be very nearly zero, as all wind and temperature forcing is symmetric about the equator. For all other model runs, heat transport should be to the north at upper levels, and to the south at levels closer to the bottom.

III. RESULTS

A. DESCRIPTION OF THE MODEL OUTPUT

Qualitative observations gleaned from yearly output data indicated that each model run offered a reasonable description of an idealized two-hemisphere ocean. The pattern and magnitudes of steady-state horizontal currents, sea surface temperatures, net surface fluxes, vertical temperature stratification, and other measurable parameters were qualitatively consistent with climatological data. A few examples are provided below.

Figure 12 shows the annual mean net heat flux into the ocean derived from ECMWF climatology data. Figure 13 shows net heat flux into the ocean for Case B at equilibrium. The model case is characterized by an equatorial band of positive heat flux much like that found in the Atlantic and Pacific oceans in climatology. Also, the western boundary currents are well-represented in the model as areas of net heat flux from the ocean to the atmosphere and space.

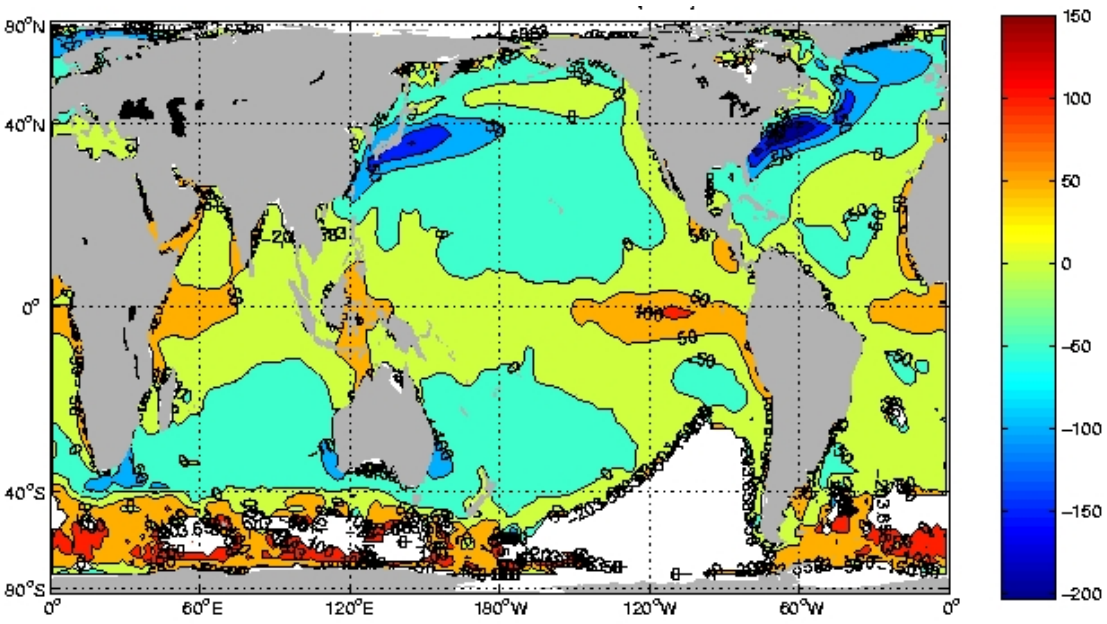

FIGURE 12. Annual Mean Net Heat Flux into the Ocean

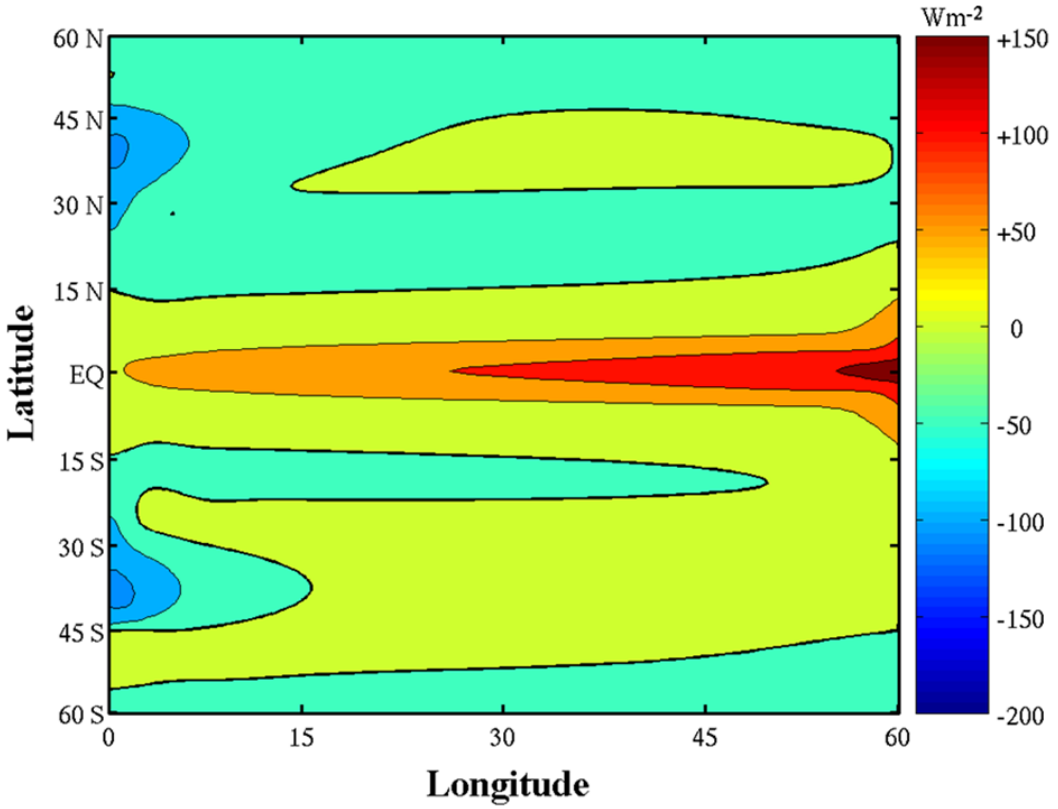

FIGURE 13. Net Heat Flux into the Ocean for Case B

Likewise, Figure 14 illustrates typical temperature stratification patterns found in model runs. The upper levels have been exaggerated to display finer detail in the thermocline. The left plot (a) shows a meridional-vertical cross-section while the right (b) gives a zonal-vertical cross-section.

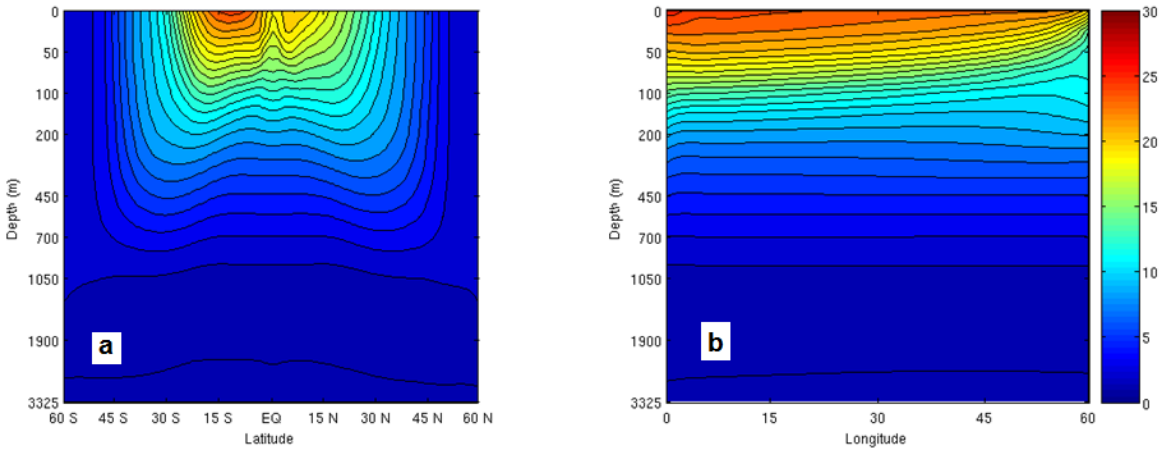

FIGURE 14. Typical Temperature Stratification Patterns, (a) a zonally-averaged meridional cross-section, (b) a zonal cross-section at the equator

Table 5 summarizes several global characteristics of the interhemispheric transport obtained from each model run. The first column lists the cases in the order they were run. A letter designation was given to each case. The next two columns give the values of the coefficients for the forcing equations. Wind Stress Difference gives the difference in the mean wind stress between the southern and northern hemispheres. Likewise, SST Difference gives the difference between the mean sea surface temperatures found in the southern and northern hemispheres. These two differences are dependent on the values chosen for A and B in each case. Following these columns, the total time the model was run is shown.

The final result for equilibrium interhemispheric volume transport is given in the Volume Transport column in Sverdrups. The equilibrium interhemispheric heat transport in terawatts is listed next. Finally, the overall difference in the total sea surface flux found in both hemispheres is given.

TABLE 5. Global Characteristics of the Interhemispheric Transport

Case	Value of A	Value of B	Wind Stress Difference (Nm^{-2})	SST Difference (°C)	Model Run Time (Years)	Volume Transport (Sv)	Heat Transport (TW)	Surface Flux Difference (TW)
A	0	0	0	0	67	0.67	0	43
B	-108	0	0.066	0	55	4.52	223	405
C	0	-5	0	2.46	62	3.27	148	297
D	-108	-5	0.066	2.46	57	4.93	374	752
E	-60	-7.5	0.037	3.70	50	5.14	354	737
F	-90	-7.5	0.055	3.70	54	5.56	416	861
G	-60	-10	0.037	4.93	59	6.43	432	914
H	-90	-10	0.055	4.93	53	6.80	497	1,049
I	-60	0	0.037	0	58	2.47	124	206
J	-90	0	0.055	0	60	3.69	185	328
K	0	-7.5	0	3.70	61	4.55	225	474
L	0	-10	0	4.93	51	5.78	305	661
M	-60	-5	0.037	2.46	56	3.87	275	552
N	-90	-5	0.055	2.46	51	4.38	340	683
O	-108	-7.5	0.066	3.70	60	5.81	450	930
P	-108	-10	0.066	4.93	56	7.05	534	1,121
Q	-36	0	0.022	0	114	1.45	74	106
R	-36	-5	0.022	2.46	100	3.53	225	453
S	-36	-7.5	0.022	3.70	102	4.82	302	632
T	-36	-10	0.022	4.93	104	6.08	382	816

B. PATTERNS OF VOLUME AND HEAT TRANSPORT

A complete summary of the patterns of heat and volume transport in all model runs are relegated to the Appendix. Typical examples of the streamfunction (Figure 15) and heatfunction (Figure 16) fields in the dual-asymmetric runs are shown below. The asymmetric nature of volume and heat transport at the upper levels is the salient feature of both plots.

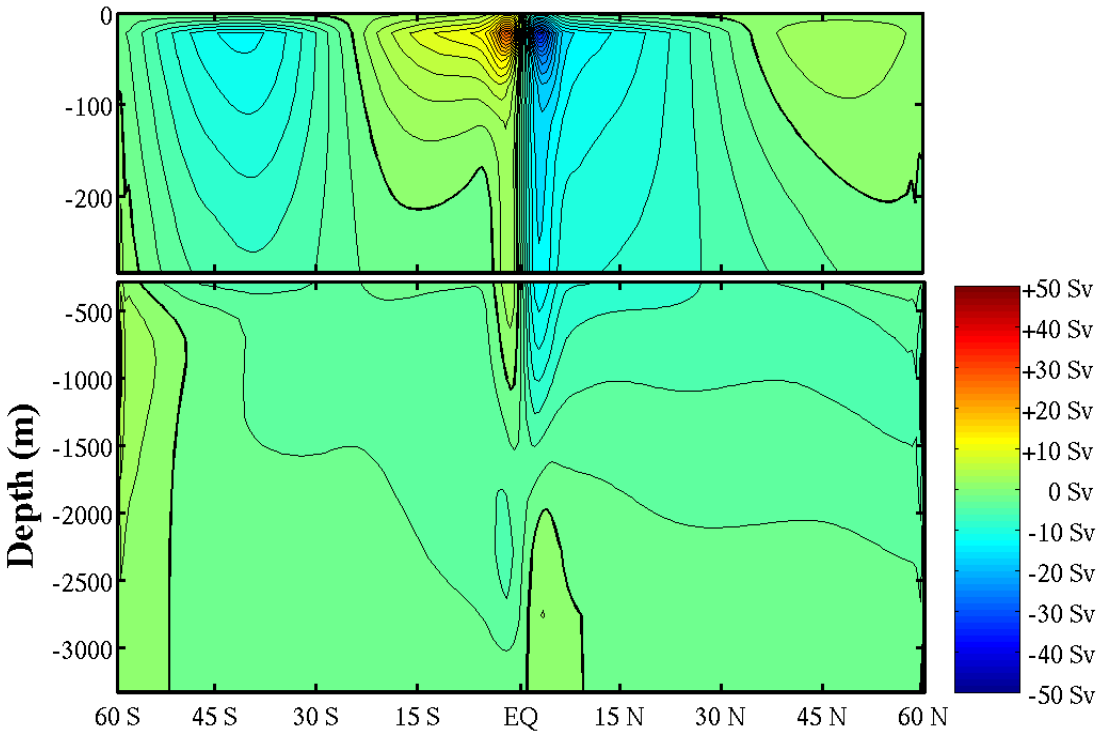

FIGURE 15. Volume Streamfunction for Case P

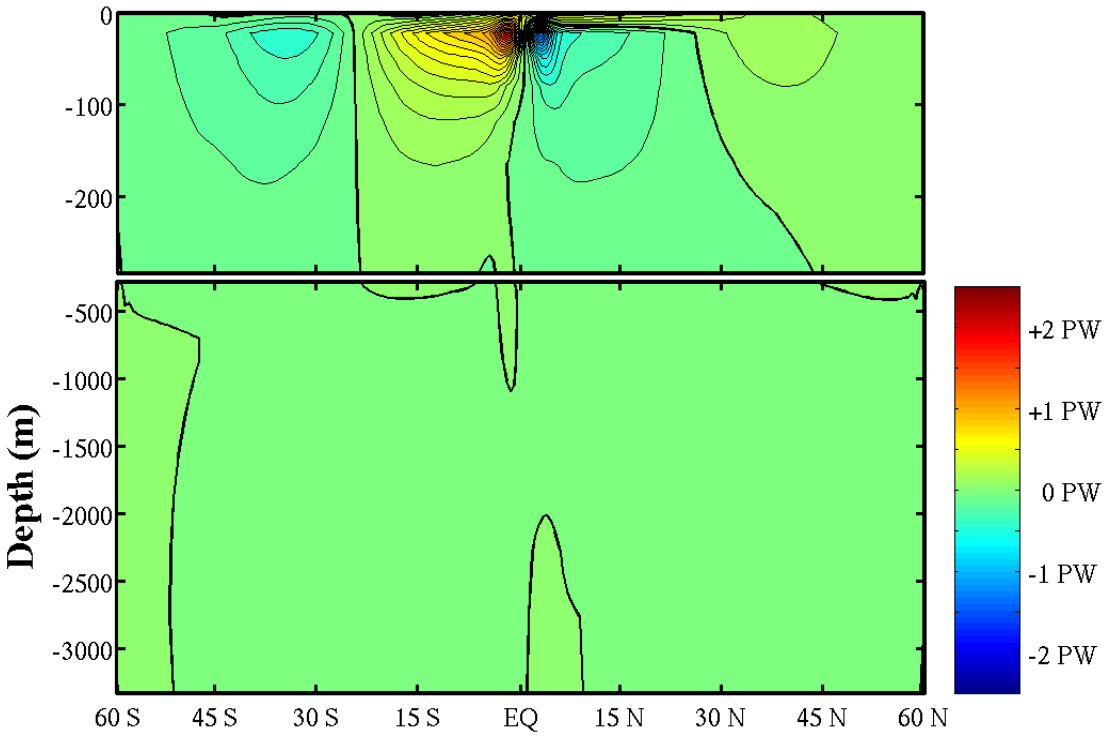

FIGURE 16. Heatfunction for Case P

THIS PAGE INTENTIONALLY LEFT BLANK

IV. INTERPRETATION AND ANALYSIS

A. REGRESSION ANALYSIS

1. Method

In addition to examining raw numerical data and result plots, it is desirable to explicitly express the relationships between equatorially-asymmetric forcing mechanisms and interhemispheric transports. The first step in developing these expressions is to use regression analysis to formulate explicit relationships between mean interhemispheric wind stress difference, mean interhemispheric sea surface temperature differences and corresponding responses on interhemispheric volume and heat transports.

2. Volume Transport

The response of volume transport to forcing asymmetries in wind stress and sea surface temperature is shown in Figure 17 and Figure 18. Regression analysis was used to explain the volume transport response when keeping sea surface temperature asymmetry constant while varying wind stress forcing asymmetry (Figure 17) and also when wind stress forcing is kept constant while varying the sea surface temperature hemispheric asymmetries (Figure 18). All regression curves were resolved as second-order polynomial equations. Figure 19 gives the overall volume transport response to both wind stress and sea surface temperature mean differences between the hemispheres. In all plots, diamonds denote individual model cases.

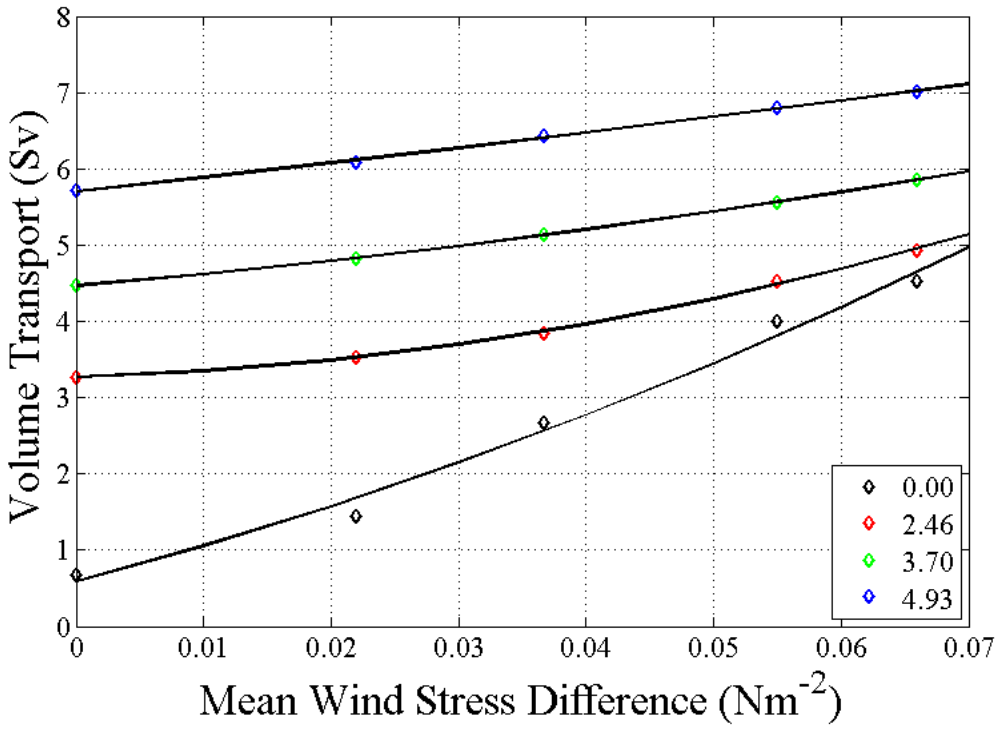

FIGURE 17. Volume Transport Response to Wind Stress Asymmetry

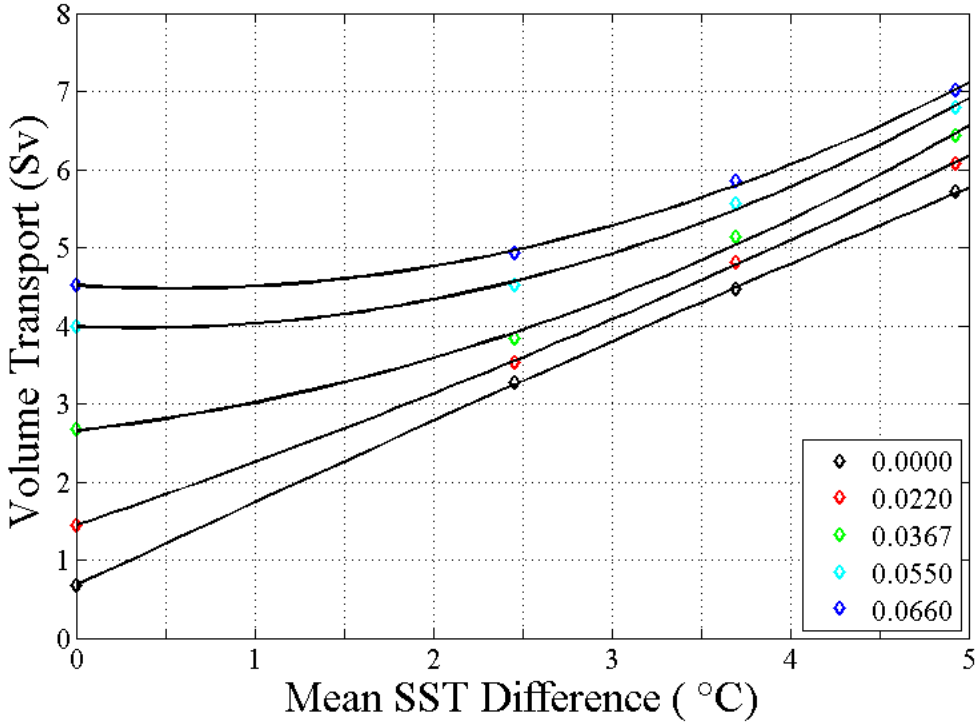

FIGURE 18. Volume Transport Response to Sea Surface Temperature Asymmetry

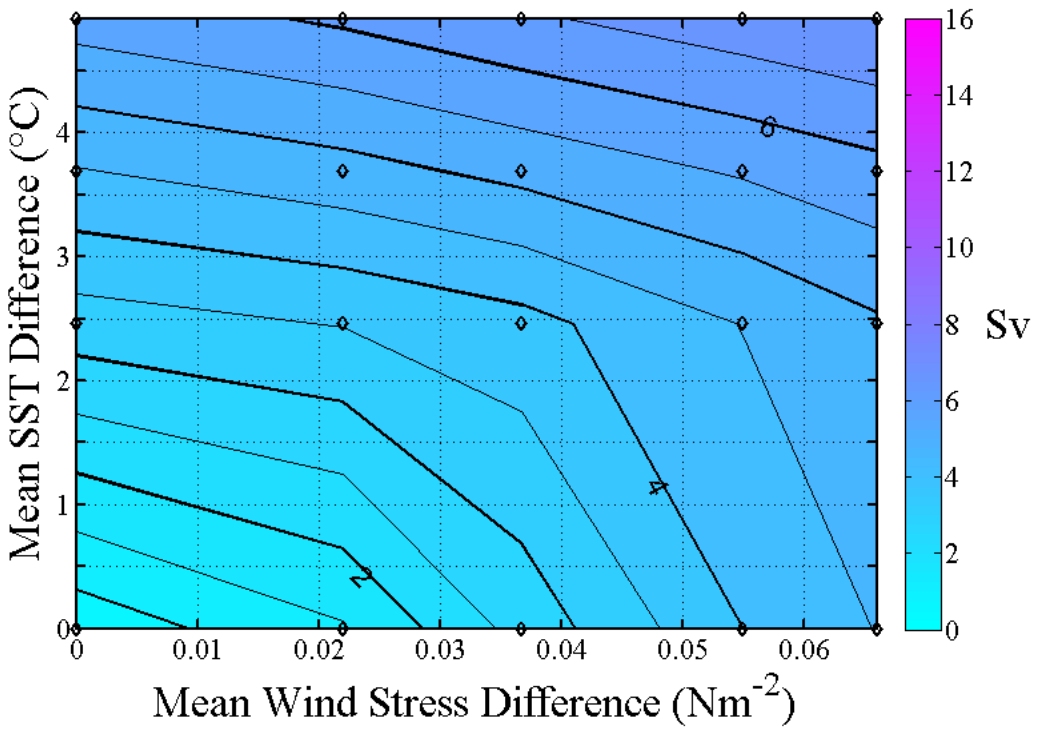

FIGURE 19. Overall Volume Transport Response to Asymmetry

3. Heat Transport

Similarly, regression analysis was used to determine heat transport response to changes in wind stress and sea surface temperature forcing asymmetries. Figure 20 shows the changes in overall interhemispheric heat transport when wind stress forcing asymmetry is increased with constant sea surface temperature forcing asymmetry. In Figure 21, the heat transport increases are linked to increasing asymmetry in hemispheric sea surface temperatures with constant wind stress forcing. Figure 22 displays the overall heat transport response to varied asymmetry in mean hemispheric wind stress and sea surface temperature. As before, diamonds mark the locations of the 20 individual cases of this experiment.

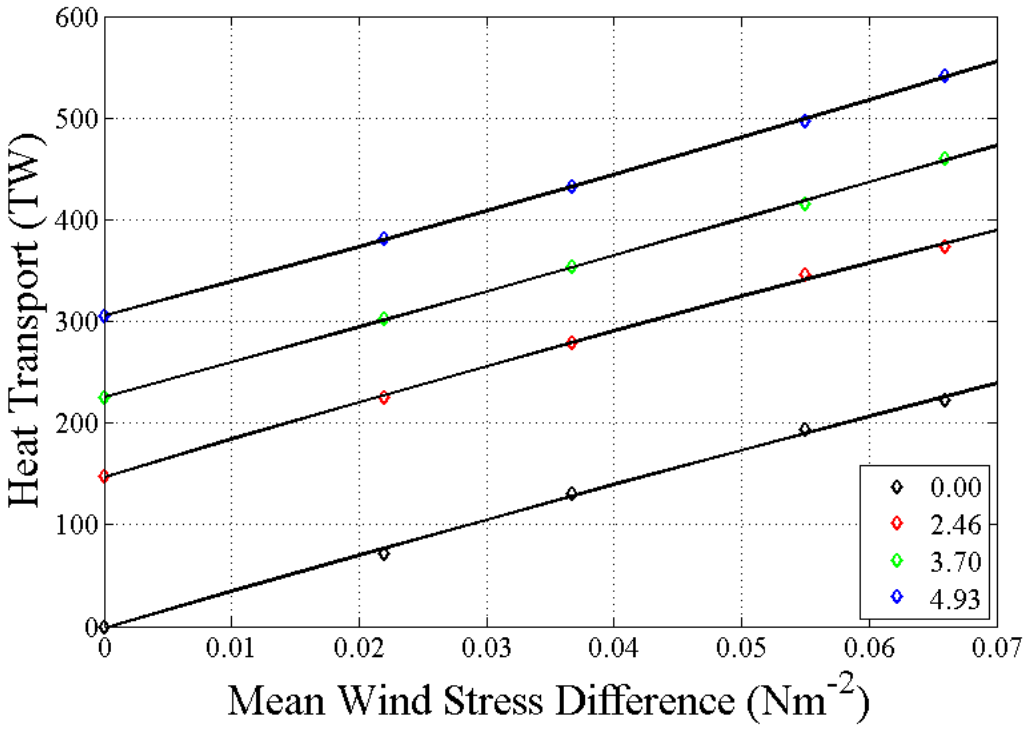

FIGURE 20. Heat Transport Response to Wind Stress Asymmetry

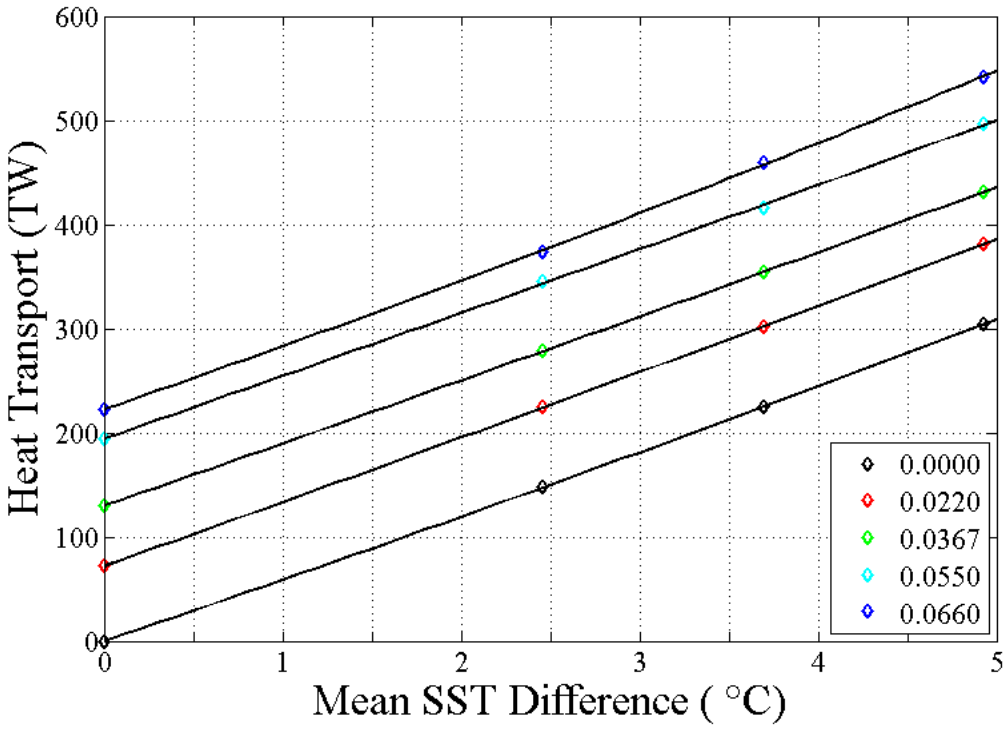

FIGURE 21. Heat Transport Response to Sea Surface Temperature Asymmetry

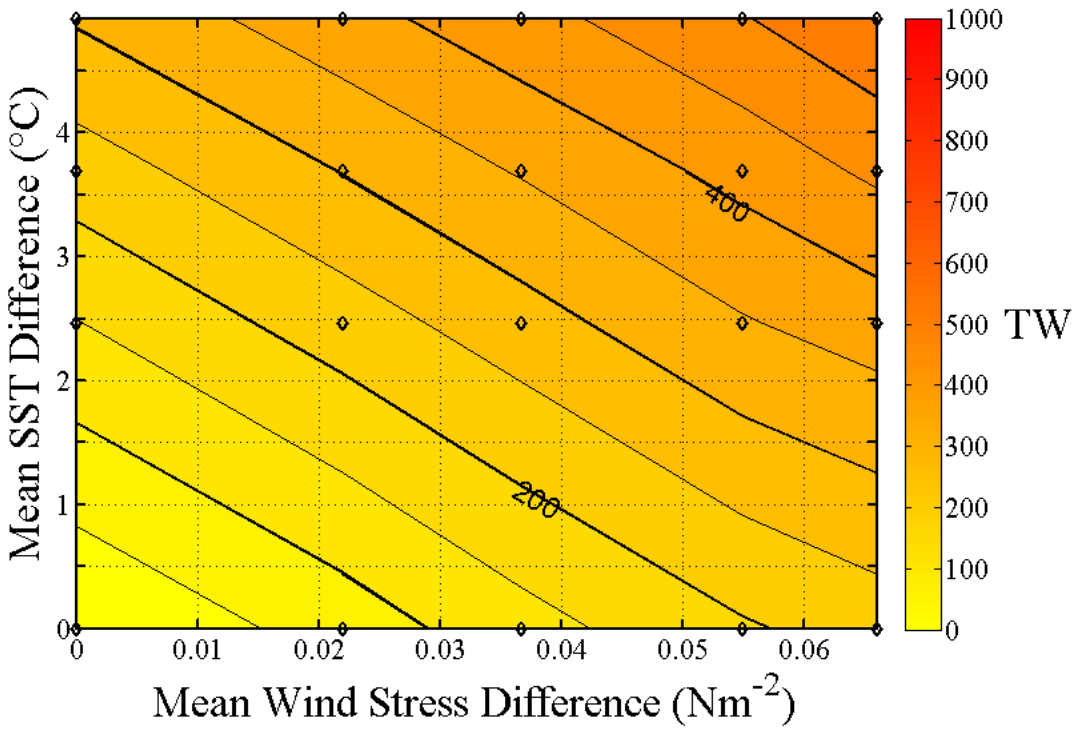

FIGURE 22. Overall Heat Transport Response to Asymmetry

4. Explicit Dependencies

Each plot of transport response to increasing wind stress asymmetry yields four separate equations describing this response. Likewise, each plot of the relationship between interhemispheric transport and mean hemispheric sea surface temperature asymmetries provides five equations. Using the multiple regression function of MATLAB, these 18 equations were used to construct two final equations relating the mean interhemispheric differences in wind stress and sea surface temperature to volume and heat transports.

The solution equation for volume transport (in Sv) is:

$$\mathbf{V} = 0.0795\mathbf{T}^2 + 177.378\boldsymbol{\tau}^2 - 8.740\mathbf{T}\boldsymbol{\tau} + 0.686\mathbf{T} + 44.549\boldsymbol{\tau} + 0.728 \qquad (20)$$

and has an error of ± 0.37 Sv.

The solution equation for heat transport (in TW) is:

$$\mathbf{Q} = 0.562\mathbf{T}^2 - 367.416\boldsymbol{\tau}^2 + 23.379\mathbf{T}\boldsymbol{\tau} + 58.756\mathbf{T} + 3466.598\boldsymbol{\tau} - 0.027 \qquad (21)$$

and has an error of ± 5.37 TW.

In these equations, **T** refers to the difference in the mean sea surface temperature between the hemispheres and is directly related to the value of B in Equation (5). The value of $\boldsymbol{\tau}$ is determined by the value of A in Equation (2) and is the difference in the mean wind stress found in the northern and southern hemispheres.

5. Analysis of the Dominant Trends

Overall volume and heat transports have now been explicitly expressed in terms of the differences in the mean values of wind stress and sea surface temperature in both hemispheres. Although the relative contributions of wind stress and heat flux asymmetries to total transport are dependent on specific difference values, the dominant trends can be inferred by considering the orders of magnitude of **T** and $\boldsymbol{\tau}$ that are consistent with climatology. The annual mean climatological values of the mean hemispheric wind stress difference along with the absolute mean sea surface temperature difference between hemispheres are substituted into the solution equation to determine the relative contributions of wind stress and net surface heat flux to the overall volume and heat exchanges between hemispheres. Table 6 is a climatology summary of these values.

TABLE 6. Climatology Summary

Month	Mean Wind Stress Difference ($\times 10^2$ Nm^{-2})	Absolute Mean SST Difference (°C)
January	1.06	1.78
February	1.50	2.69
March	2.63	2.61
April	3.49	1.51
May	3.74	0.43
June	2.92	2.78
July	3.26	5.05
August	3.53	6.43
September	3.17	6.19
October	2.80	4.64
November	1.96	2.41
December	1.34	0.05
Mean	2.62	3.05

Taking Equations (20) and (21), and substituting the annual mean values gives:

$$\mathbf{V} = 0.0795(3.05)^2 + 177.378(0.0262)^2 - 8.740(3.05)(0.0262) + 0.686(3.05) + 44.549(0.0262) + 0.728 \quad (22)$$

$$\mathbf{V} = 0.74 + 0.12 - 0.70 + 2.09 + 1.17 + 0.73 = 4.15\ \mathbf{Sv} \quad (23)$$

and

$$\mathbf{Q} = 0.562(3.05)^2 - 367.416(0.0262)^2 + 23.379(3.05)(0.0262) + 58.756(3.05) + 3466.598(0.0262) - 0.027 \quad (24)$$

$$\mathbf{Q} = 5.22 - 0.25 + 1.87 + 179.21 + 90.82 - 0.03 = 276.84\ \mathbf{TW} \quad (25)$$

All terms in the volume transport equation are important, being of approximately the same order of magnitude. However, the heat transport equation shows a dependency on the linear terms only, with those terms contributing to 97% of the overall interhemispheric heat transport.

B. ASYMMETRIC FORCING CONTRIBUTIONS TO TRANSPORTS

1. Volume Transport

According to the solution equations and given the current climatic annual mean values, wind stress asymmetry between the northern and southern hemispheres can account for 31% of the interhemispheric volume transport. Differences in net surface heat flux can account for the remaining 69% of volume transport. On average, the interhemispheric volume transport increases by approximately one Sverdrup for every 1°C difference in mean sea surface temperature between hemispheres. There is also, on average, an increase of flow by 0.2 Sv for every increase of 0.01 Nm^{-2} in mean wind stress difference between hemispheres. Because all terms in the volume solution equation are important, the actual increases are highly dependent on the combination of wind stress and sea surface temperature difference. Figure 23 is indicative of the non-linear nature of the relationship between these two variables.

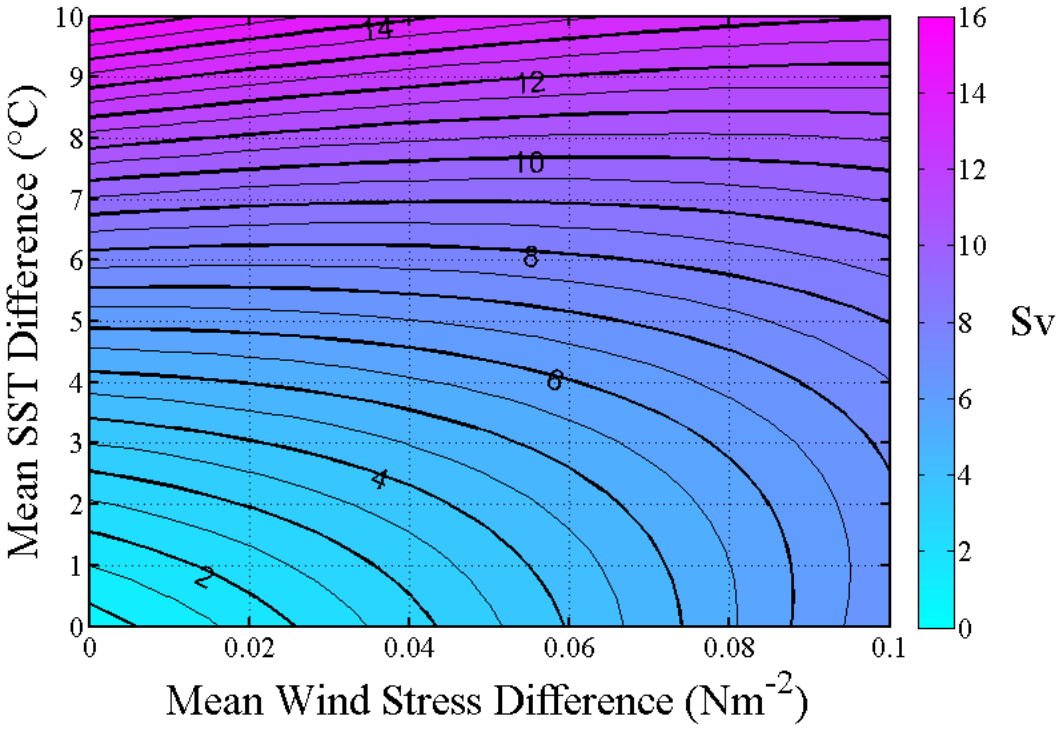

FIGURE 23. Volume Transport Response to Dual-Asymmetry

2. Heat Transport

According to the solution equations and given the current climatic annual mean values, wind stress asymmetry between the northern and southern hemispheres can account for 33% of the interhemispheric volume transport. Differences in net surface heat flux account for the remaining 67% of volume transport. The interhemispheric heat transport increases by approximately 64 TW for every 1°C difference in mean sea surface temperature between hemispheres. There is also an increase of heat transport by 34 TW for every increase of 0.01 Nm^{-2} in mean wind stress difference between hemispheres. Since the linear terms dominate the heat transport solution equation, these relationships between wind stress and heat flux asymmetries with the heat transport are very independent of one another, meaning that total changes in heat transport will be the result of the sum of the changes in heat transport due to changes in the individual terms.

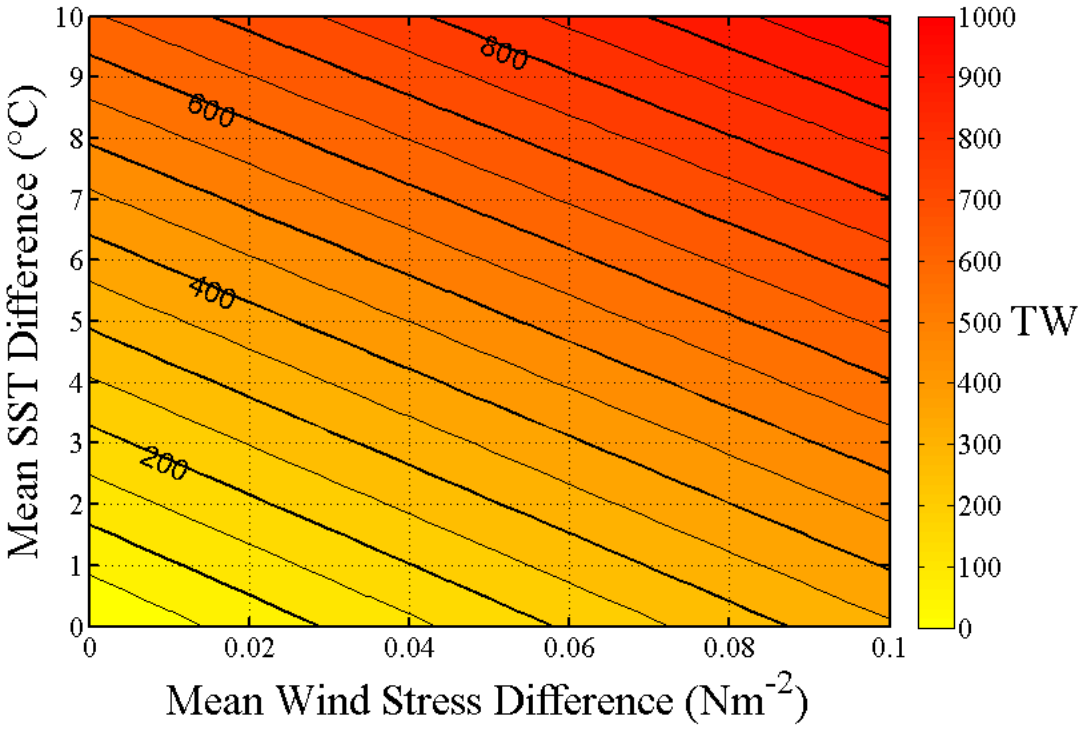

FIGURE 24. Heat Transport Response to Dual-Asymmetry

C. SIGNIFICANCE OF THE THERMOCLINE CELL FOR THE VOLUME AND HEAT TRANSPORTS

Comparing the model determinations of volume transport and heat transport with climatological values reveals the importance of the thermocline as the main conduit of interhemispheric heat flow. Volume transport in the thermocline cell accounts for only 23% of the overall interhemispheric volume transport reported from climatological values (Pickard and Emery, 2003). However, 87% of the overall advective heat transport at the equator (Hsiung et al., 1989) can be accounted for in this smaller percentage of volume transport. Thus, the thermocline meridional overturning circulation cells have a disproportionally larger role in affecting the overall climate of the Earth than mere volumetric flow would suggest.

TABLE 7. Significance of the Thermocline Cell

Interhemispheric Transport of:	Thermocline (model)	Overall (climatology)	Percentage
Volume (Sv)	4.15	18	23%
Heat (TW)	276.84	320	87%

V. CONCLUSIONS

The physics of the Meridional Overturning Circulation (MOC) and interhemispheric heat transport has been explored with an emphasis on the upper and central ocean. It has been shown how a model of intermediate complexity can be used to identify the key dynamic processes and explain interaction. Sea surface temperature and wind stress were considered in the context of their ability to influence the MOC pattern. The relative significance of sea surface heat flux and wind stress was quantified. A model of intermediate complexity was used to identify the key dynamic processes and explain interaction. Volumetric and advective heat transport streamfunctions were used to analyze interhemispheric exchanges of mass and energy.

Expressions were constructed which explicitly defined the relationships between equatorially-asymmetric wind stress and surface heat flux to volume flow and heat transport. The relative importance of wind stress and surface heat flux to the overall values of transport was discussed in light of climatology. Under current climate conditions, equatorially-asymmetric wind stress can account for approximately one-third of the volume and advective heat transport between the northern and southern hemispheres in the upper ocean while the remaining two-thirds can be attributed to interhemispheric sea surface heat flux differences.

The MOC in the upper ocean is the dominant factor in interhemispheric heat transport and in the maintenance of the Earth's climate despite its extremely small contribution to total meridional-vertical circulations in the entire ocean basin. Thus, thermocline overturning cells are more effective in terms of heat transport than abyssal overturning cells. Asymmetries in wind stress and surface heat flux forcing control the strength of interhemispheric transports. This study suggests that the previous emphasis on deep overturning in the abyssal region and small-scale mixing as the dominant factors in the MOC should be reconsidered and the role of wind stress and surface heat fluxes more thoroughly investigated as determining factors of MOC strength and maintenance.

The MOC is an important constituent of the Earth's climate system. Understanding the forcing mechanisms responsible for the strength and maintenance of this circulation is crucial if oceanographers are to make predictions concerning changes in the meridional overturning circulation. Paleoclimatology data indicates that the MOC has undergone many changes throughout Earth's history resulting in climate shifts to new equilibriums (Rahmstorf, 2002). A climate shift similar in magnitude to previous shifts could result in long-term changes to weather patterns and ocean conditions altering important factors in the Navy's operating environment. Thus, long-term Navy planning must include an appreciation for possible changes in the forcing mechanisms responsible for the meridional overturning circulation.

VI. DIRECTIONS FOR FUTURE RESEARCH

A. SUGGESTIONS

To aid in future research in the field of meridional overturning circulation, I offer a hierarchy of models of increasing complexity. Each suggestion below builds on all previous suggestions.

1. Idealized Basin (Open Channel)

A small, but significant, change with the potential to yield better insights into wind stress and heat flux forcing as contributors to the strength of the MOC would be to include a channel in the southern hemisphere of the idealized basin presented in this paper. This channel would represent the Southern Ocean and the larger wind stresses introduced into the southern hemisphere of the basin would induce westerly flow not inhibited by an eastern boundary. The meridional extent of the channel should be closely matched to the actual width of the Drake Passage (approximately 10° of latitude).

2. Idealized Basin (Realistic Geometry)

Another possible improvement upon this experiment would be to use polar coordinates (instead of Cartesian coordinates) while keeping all other factors the same. With this alternation, the zonal extent of the basin would vary with latitude, giving more appropriate basin widths at each latitude. This improvement could be combined with the open channel described above.

3. Realistic Basin (Bathymetry)

The next step after implementing the changes above would be to construct a realistic basin in polar coordinates using bathymetric data available for the Atlantic Ocean. The experiment should be run with idealized wind stress and surface flux forcing. The results of the previous idealized experiments could be compared with the results

from this experiment to confirm previous findings, or to modify previous theories in light of the bathymetric conditions found in the Atlantic.

4. Realistic Basin (Forcing)

Once experiments using idealized forcing and realistic bathymetry for the Atlantic have been completed, a researcher could then use wind stress and surface heat flux data from climatology to compare results with the experiments using idealized forcing inputs. Successive runs after the initial run using climatology as a base would alter wind stresses and surface fluxes using asymmetric forcing curves such as the ones used in this study. Researchers would then be in a position to make accurate claims concerning the effects of long-term changes in wind stress and surface flux forcing on the strength and maintenance of the meridional overturning circulation in the Atlantic Ocean.

5. Global Simulation

The most exciting experiment would be to fully model the world ocean, with realistic bathymetry and climatological forcing mechanisms. Wind stresses and surface fluxes could be varied to reproduce possible scenarios involving long-term changes in these forcing mechanisms. The model could be initialized with unaltered climatology data at some point in the past and allowed to run until present day. If this default scenario produced results that match current ocean conditions, researchers would be in a prime position to use the model to predict changes in the MOC. By varying the forcing parameters, model runs could produce likely scenarios for the near future. This would be an ambitious project and could yield a wealth of information.

6. Other Mechanisms

Of course, possible forcing mechanisms responsible for the strength and maintenance of the meridional overturning circulation in the Atlantic Ocean are not necessarily limited to wind stress and surface heat flux. Other forcing mechanisms could play an important role in the meridional overturning circulation in the thermocline. Changes in seawater density due to freshwater influx, salinity increases, and long-term

precipitation changes could be investigated. Although geothermal heat flux is thought to be an insignificant factor in meridional overturning circulation, an investigation of this forcing parameter may give useful insights, if only to confirm previous assumptions.

Another possible area of investigation is to use paleoclimatology data to investigate the existence or nonexistence of the MOC in the Atlantic during periods of glacial maximums and minimums. Modeling the possible MOC of the past may allow us to more accurately predict possible circulations in the future, as the prediction of future states is the ultimate goal of research in this area.

THIS PAGE INTENTIONALLY LEFT BLANK

APPENDIX. FIGURES

A. MERIDIONAL STREAMFUNCTION

All figures in this section show the streamfunction of volumetric transport. Each plot is a latitude-depth cross-section. The zero contour is in bold and contour lines are spaced at two Sverdrup intervals. Positive (negative) values indicate counterclockwise (clockwise) circulation. The figure is split at a depth of 360 meters so that detail near the surface can be easily viewed.

1. The Symmetric Case

Case A was the only model run with both symmetric wind stress and temperature forcing.

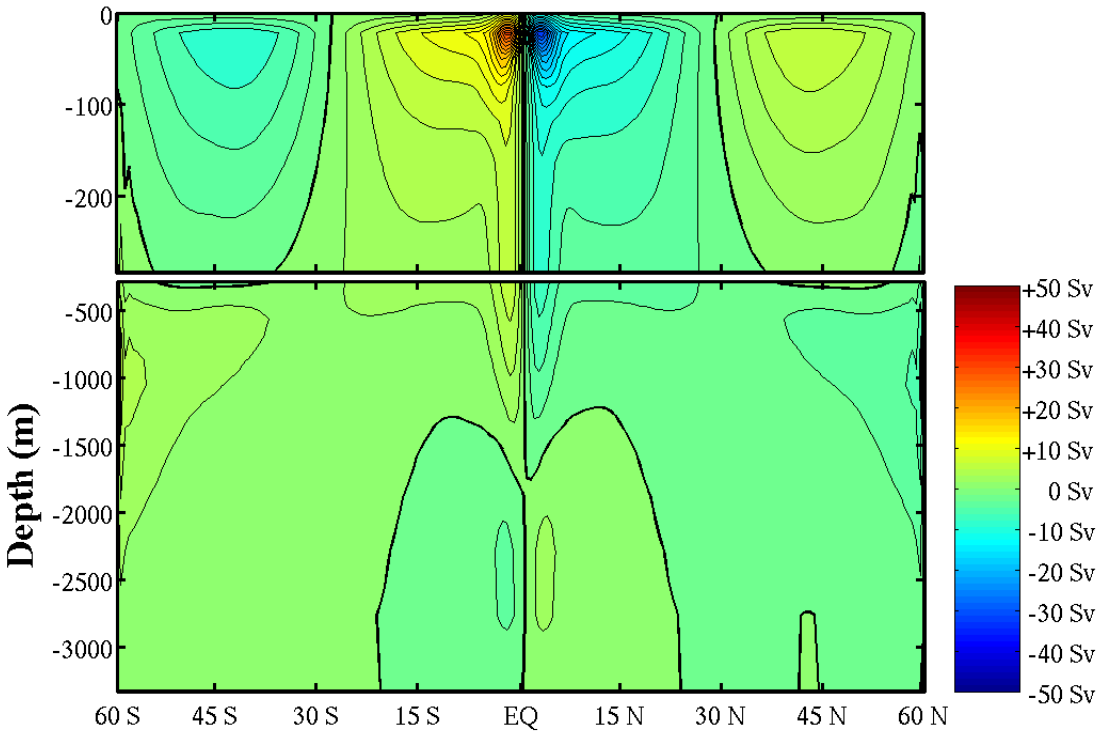

FIGURE 25. Meridional Volume Transport for the Symmetric Case

2. Cases of Wind Stress Asymmetry

The following figures show cases with asymmetric wind forcing and symmetric temperature forcing. The case designation is given after the wind stress ratio.

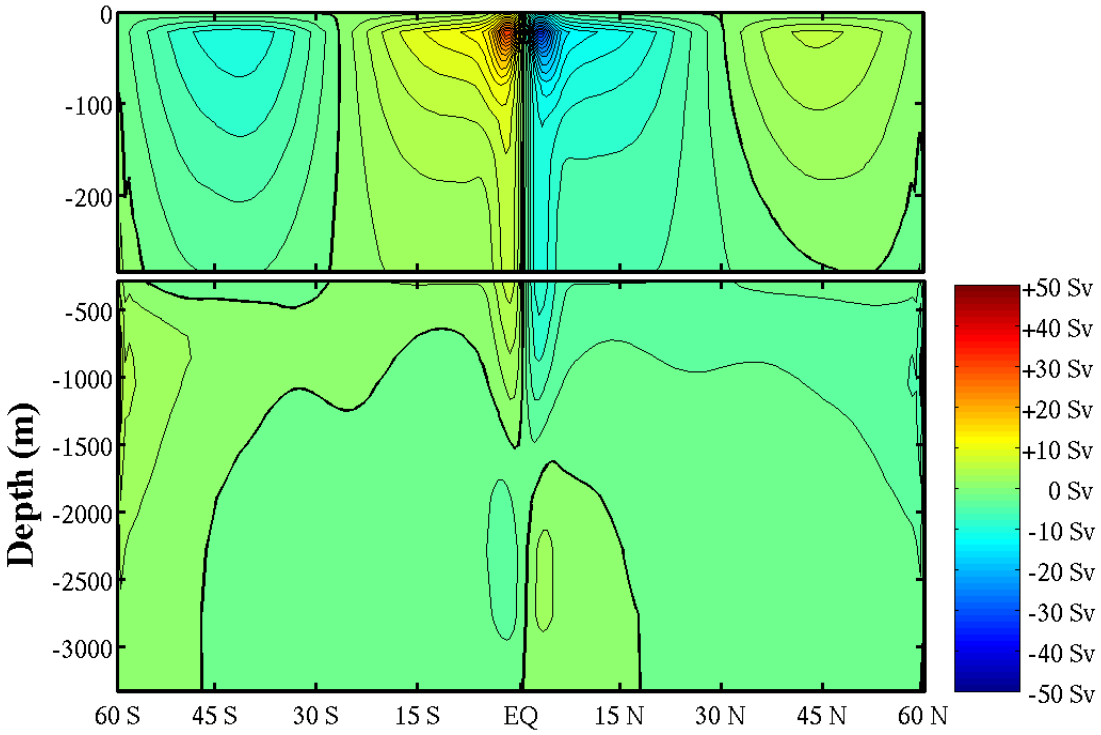

FIGURE 26. Meridional Volume Transport for Ratio 3:2 (Case Q)

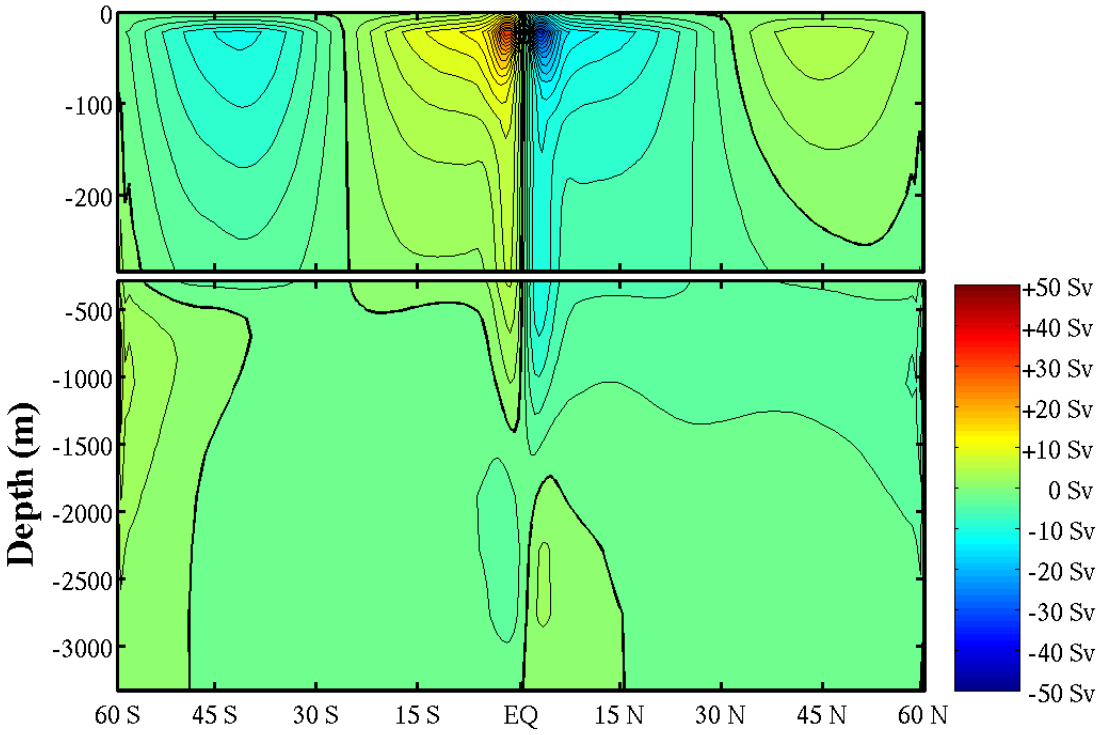

FIGURE 27. Meridional Volume Transport for Ratio 2:1 (Case I)

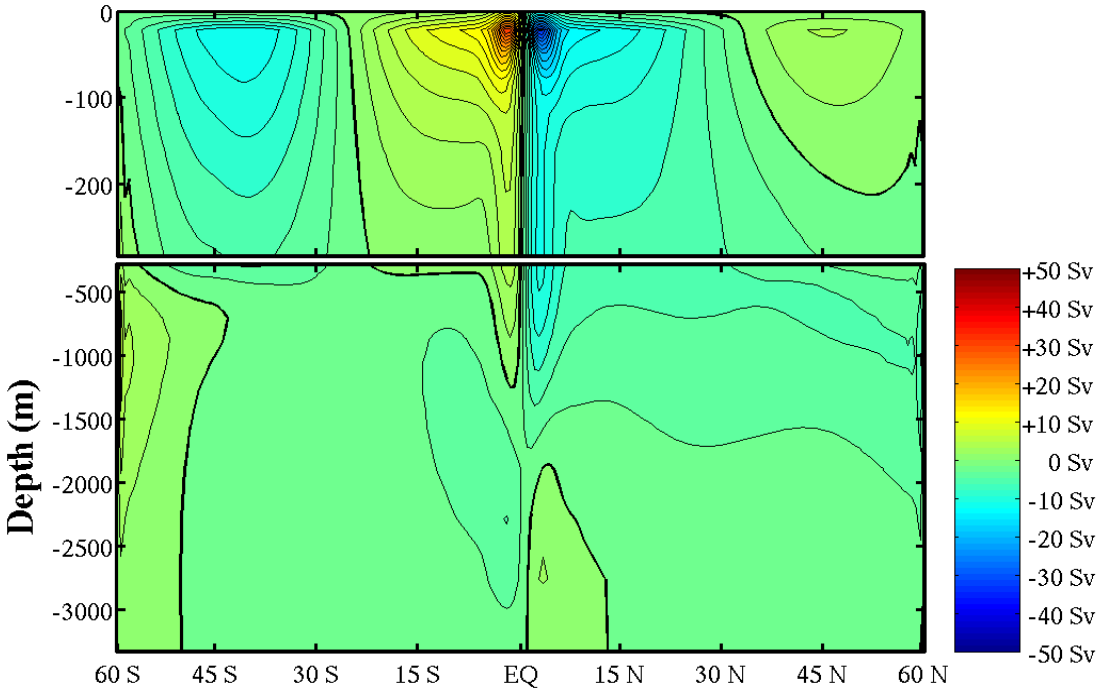

FIGURE 28. Meridional Volume Transport for Ratio 3:1 (Case J)

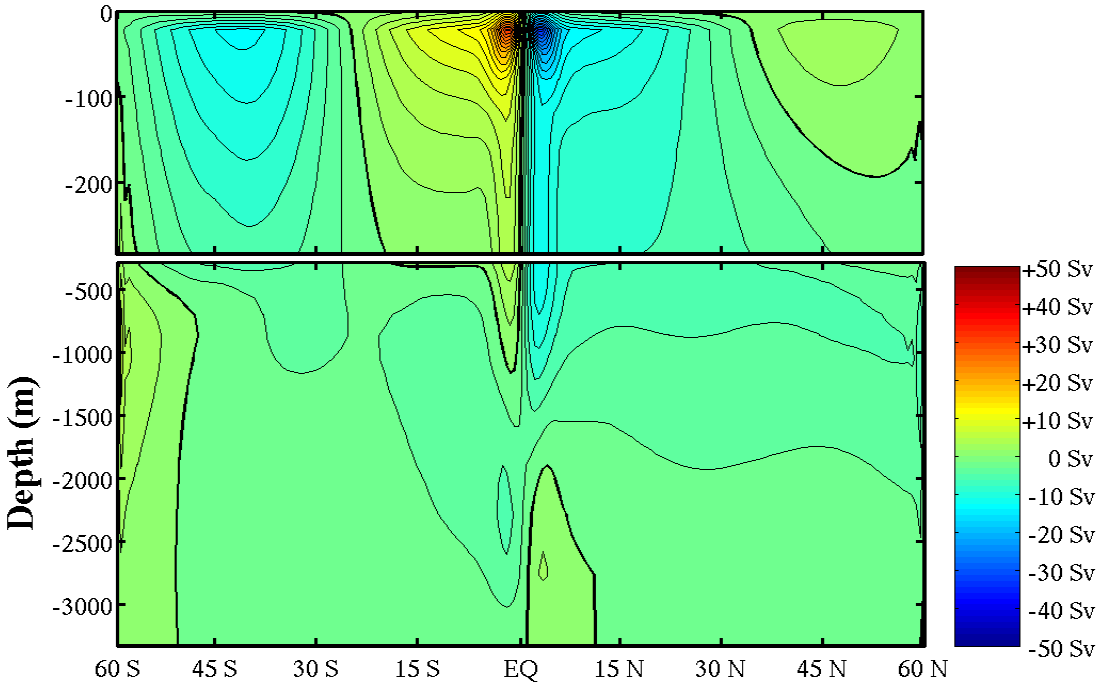

FIGURE 29. Meridional Volume Transport for Ratio 4:1 (Case B)

3. Cases of Temperature Forcing Asymmetry

The next series of figures shows the volume transport for cases of symmetric wind stress and asymmetric temperature forcing. The value of the coefficient B used in Equation (5) is given for each figure. The specific model run follows in parenthesis.

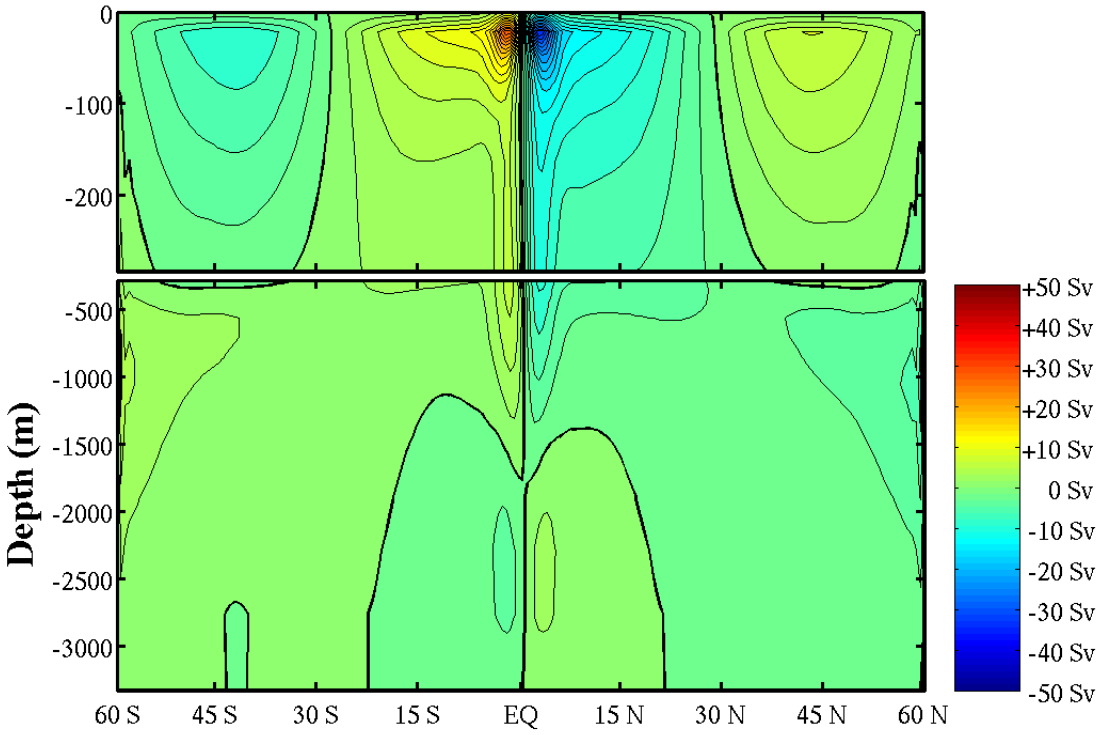

FIGURE 30. Meridional Volume Transport for B = -5 (Case C)

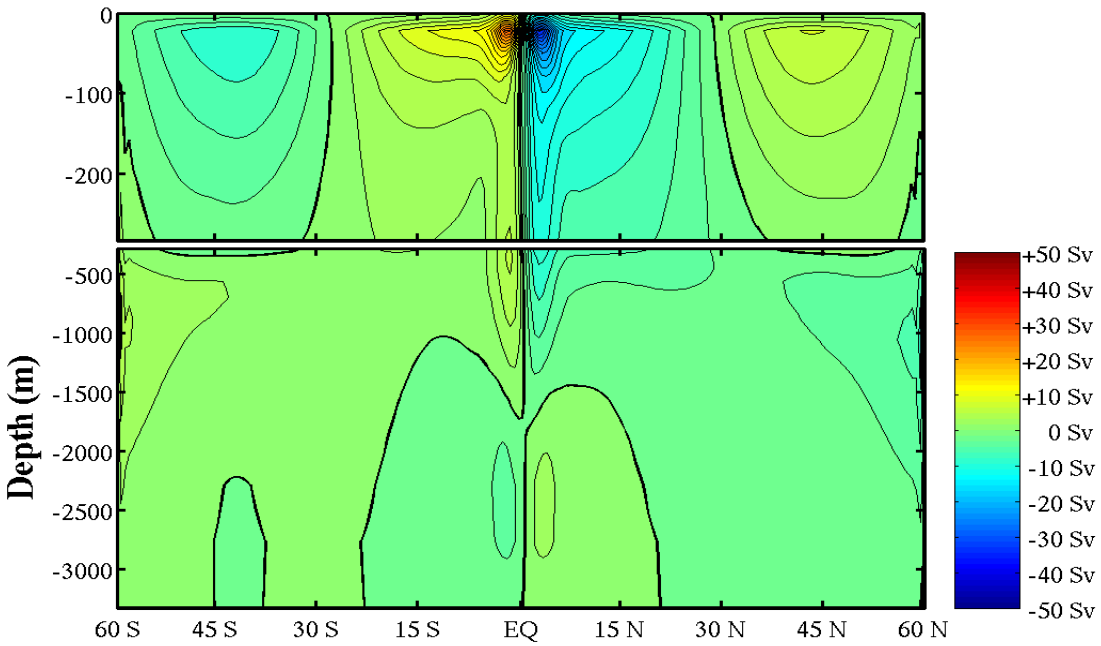

FIGURE 31. Meridional Volume Transport for B = -7.5 (Case K)

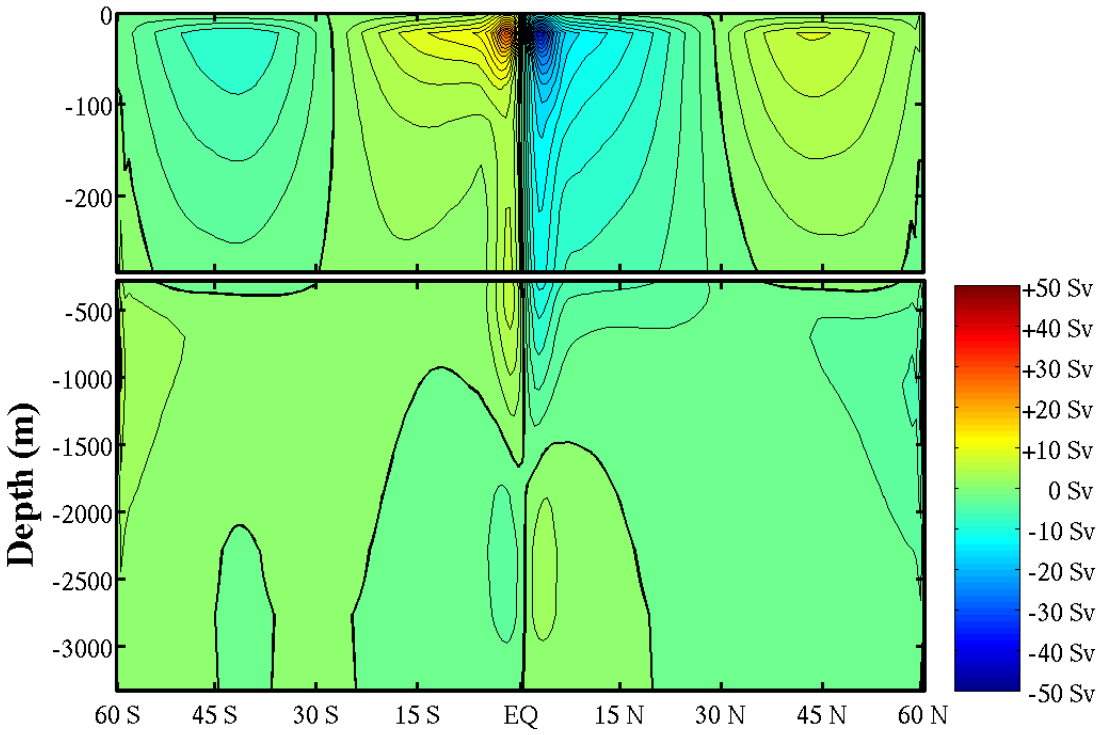

FIGURE 32. Meridional Volume Transport for B = -10 (Case L)

4. Cases of Wind Stress and Temperature Forcing Asymmetry

Most model runs used asymmetric forcing in both wind stress and sea surface temperature. The following figures are labeled with the wind stress amplitude ratio and the value of the coefficient B. The specific case is also listed. These figures are grouped by wind stress peak amplitude ratio and then in order of lower to higher temperature forcing.

a. Dual-Asymmetric Cases with Wind Stress Ratio of 3:2

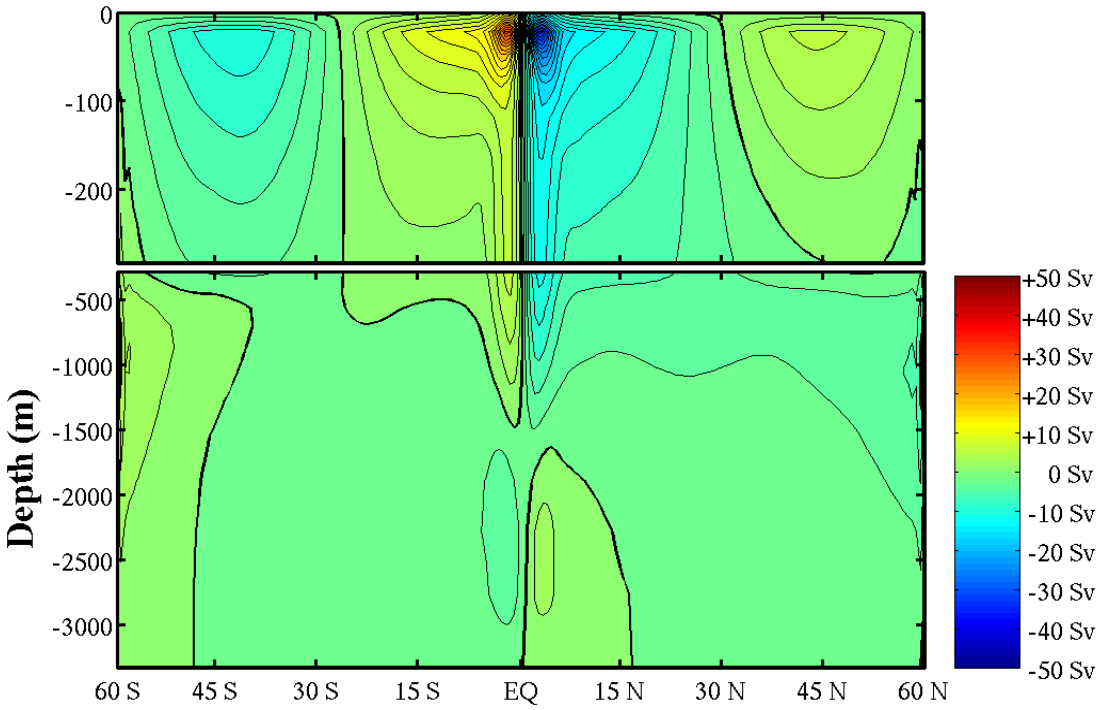

FIGURE 33. Meridional Volume Transport for Ratio 3:2 and B = -5 (Case R)

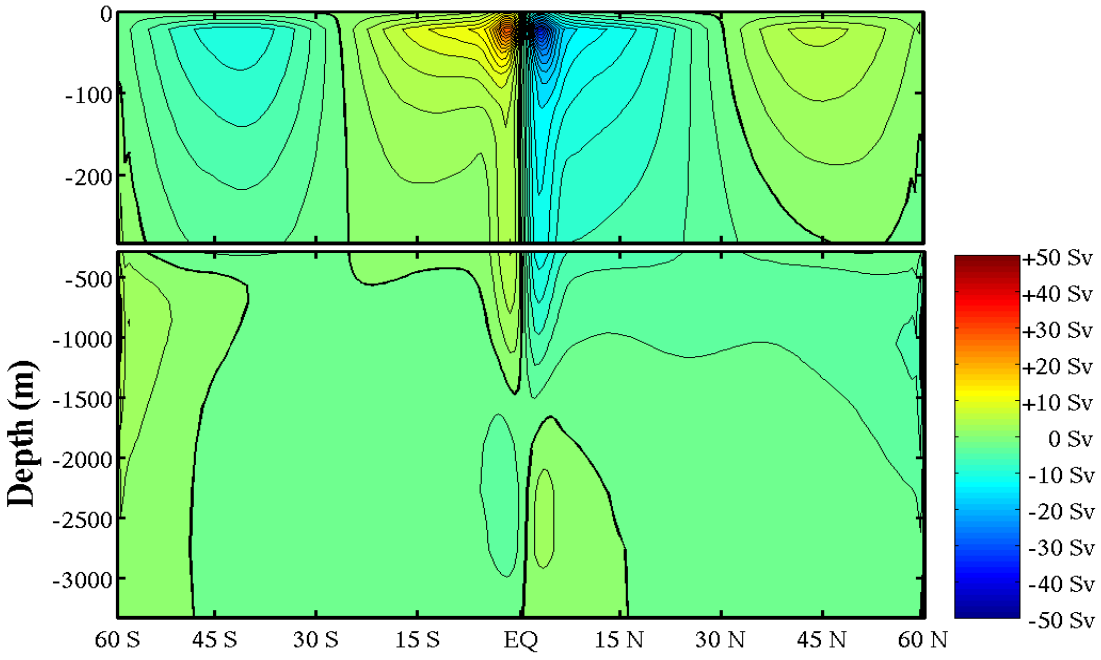

FIGURE 34. As FIGURE 33 except B = -7.5 (Case S)

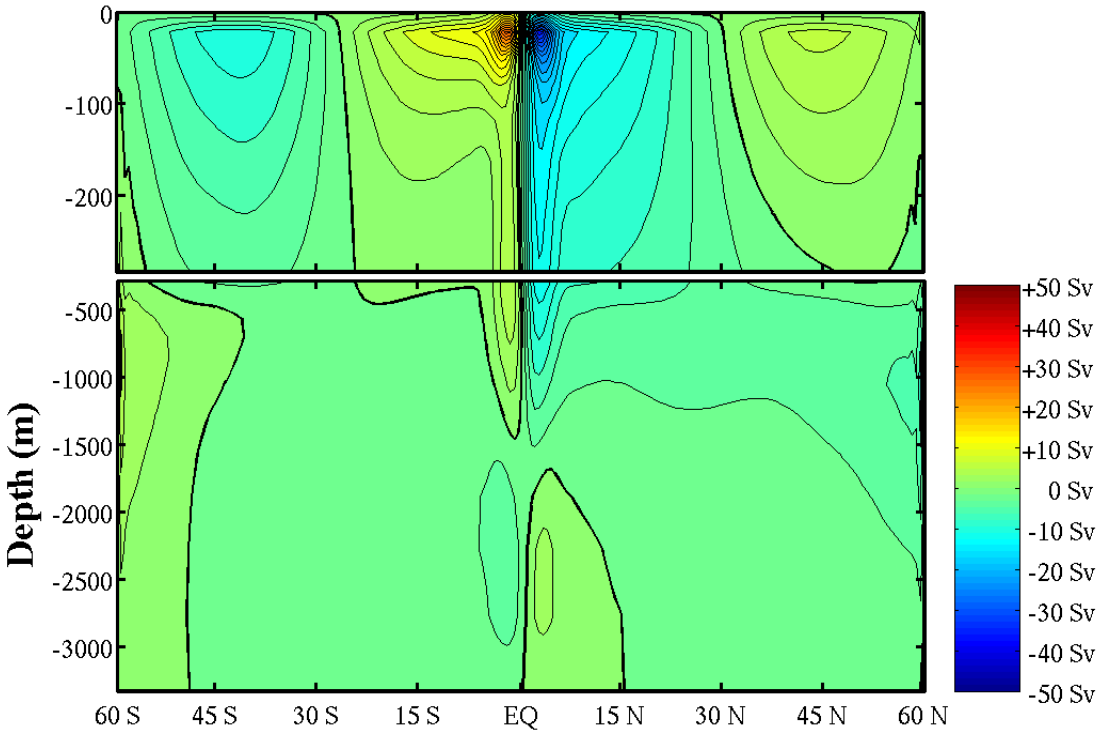

FIGURE 35. As FIGURE 33 except B = -10 (Case T)

b. Dual-Asymmetric Cases with Wind Stress Ratio of 2:1

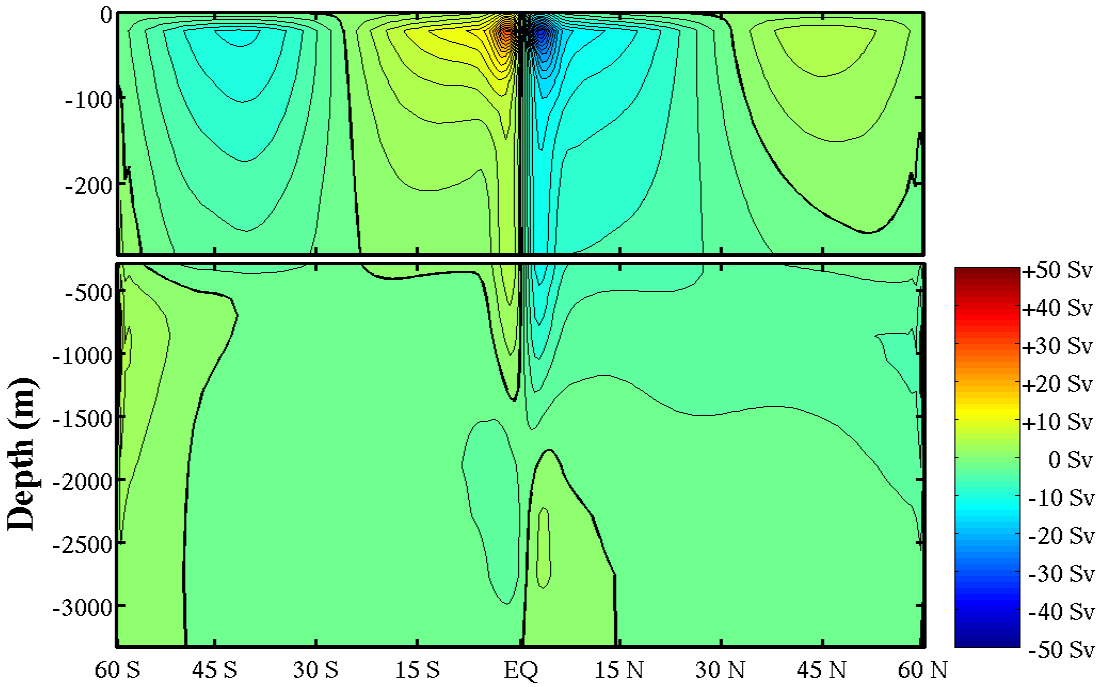

FIGURE 36. Meridional Volume Transport for Ratio 2:1 and B = -5 (Case M)

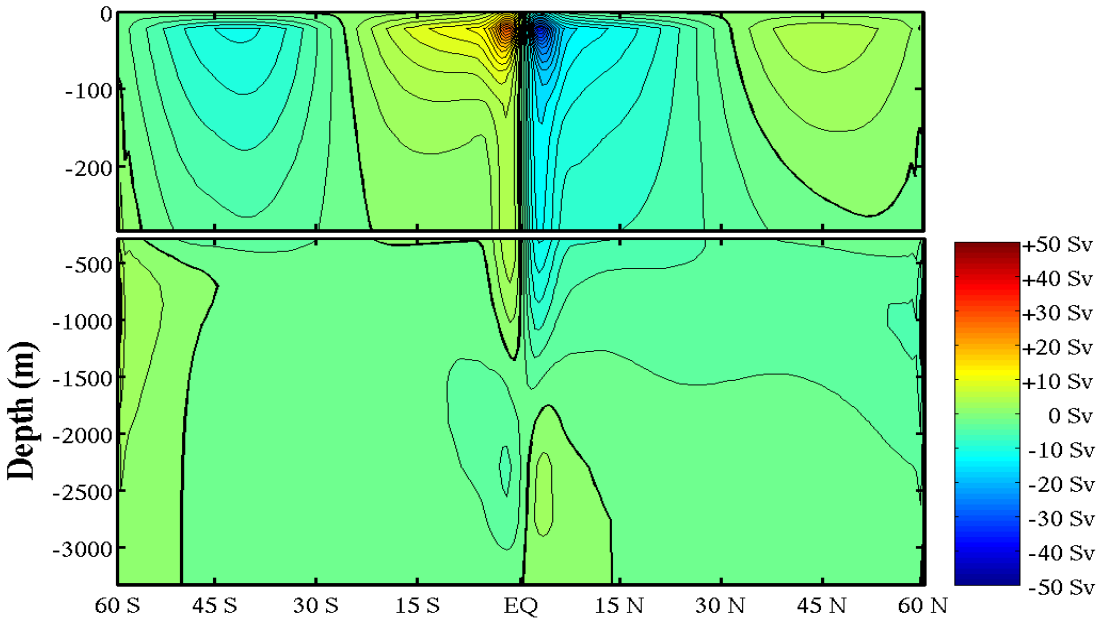

FIGURE 37. As FIGURE 36 except B = -7.5 (Case E)

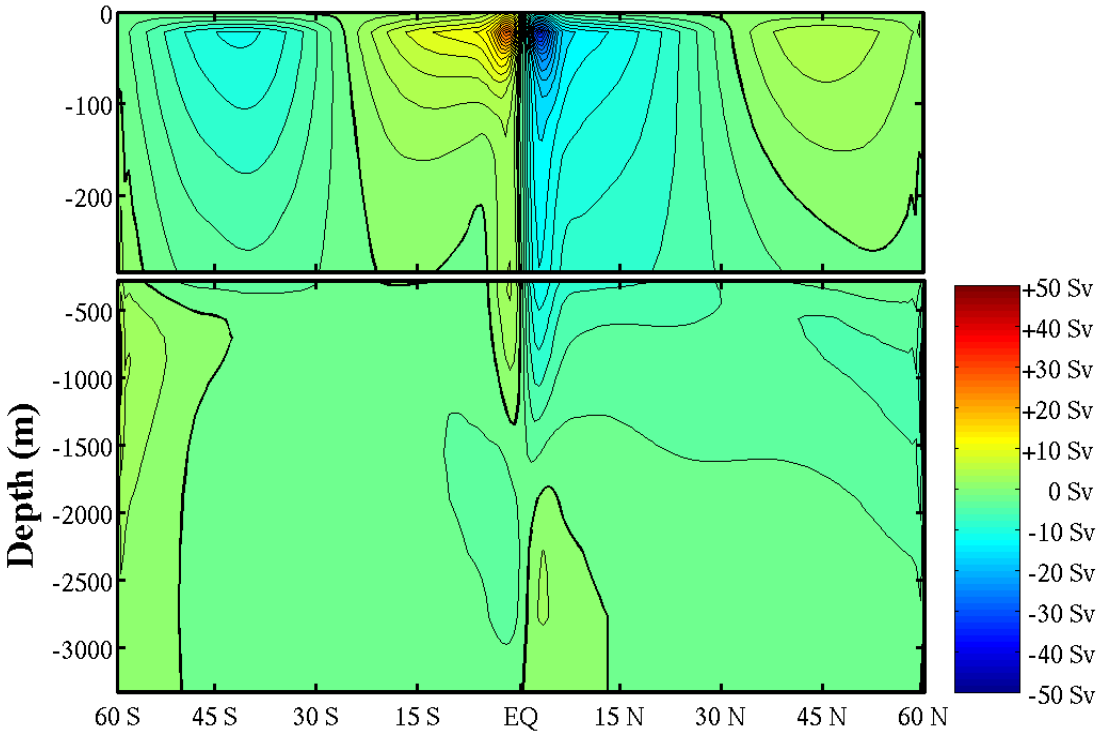

FIGURE 38. As FIGURE 36 except B = -10 (Case G)

c. Dual-Asymmetric Cases with Wind Stress Ratio of 3:1

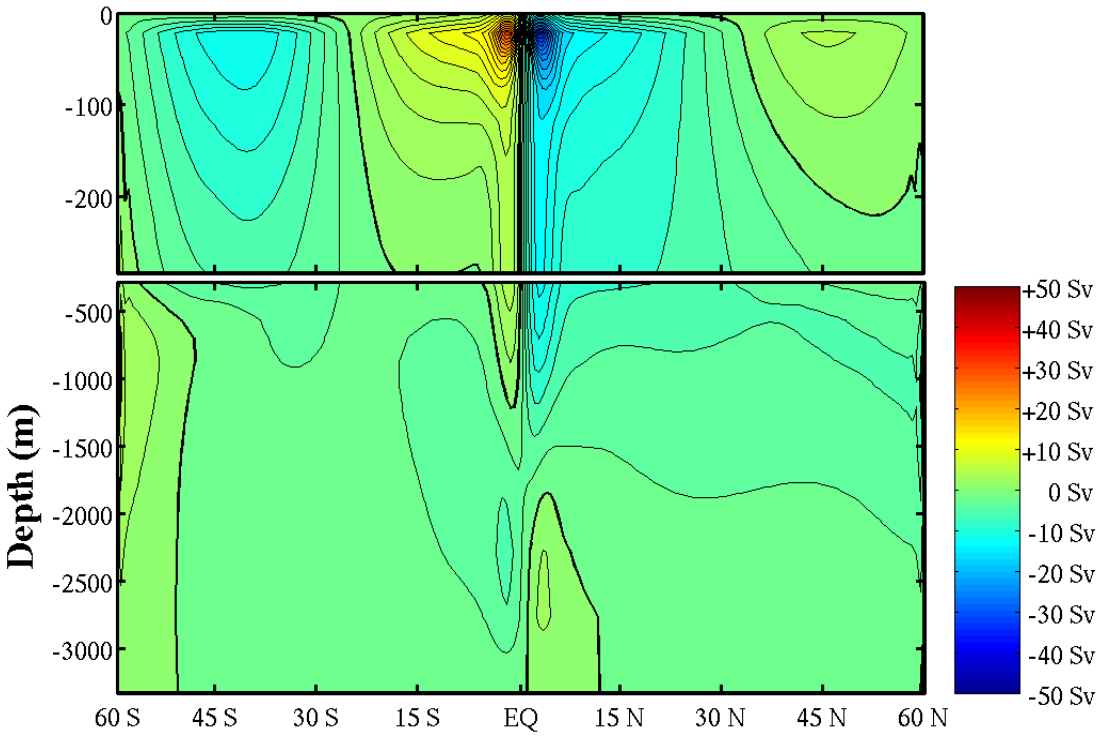

FIGURE 39. Meridional Volume Transport for Ratio 3:1 and B = -5 (Case N)

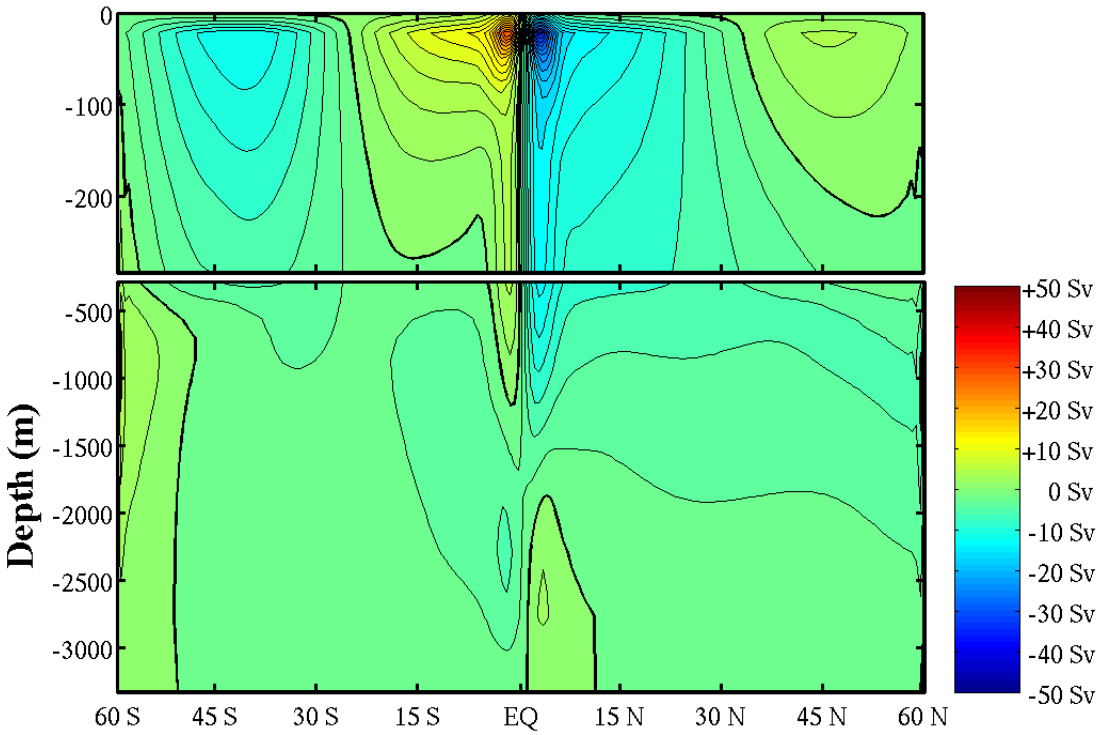

FIGURE 40. As FIGURE 39 except B = -7.5 (Case F)

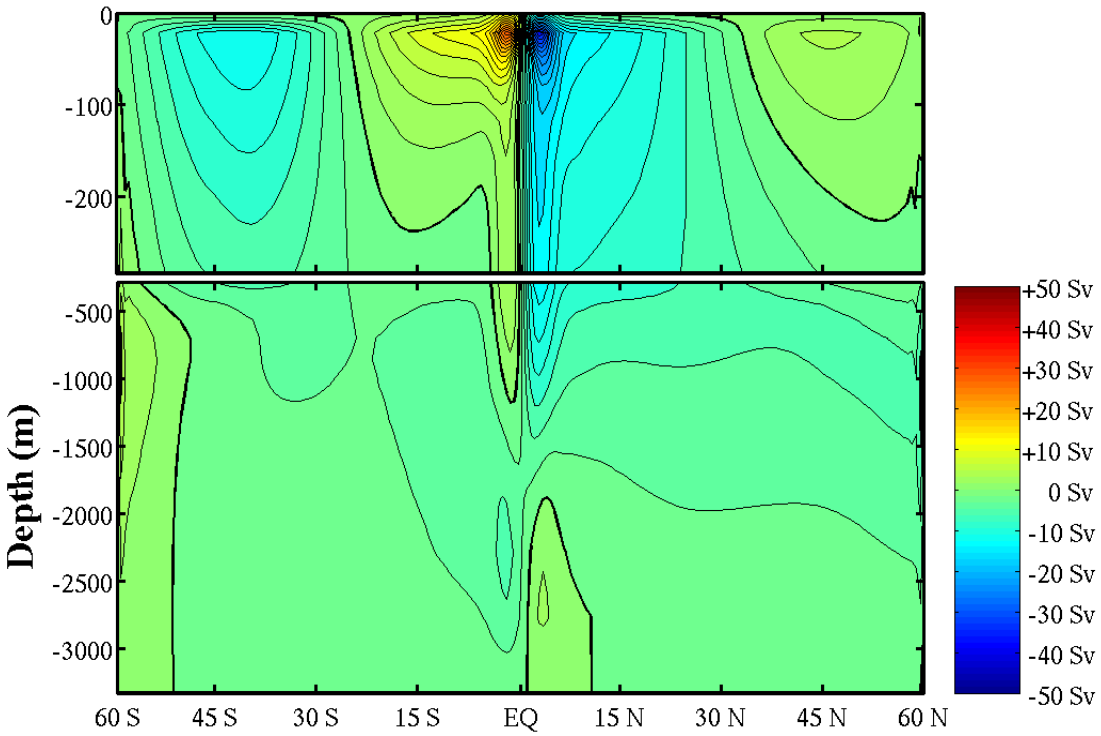

FIGURE 41. As FIGURE 39 except B = -10 (Case H)

d. Dual-Asymmetric Cases with Wind Stress Ratio of 4:1

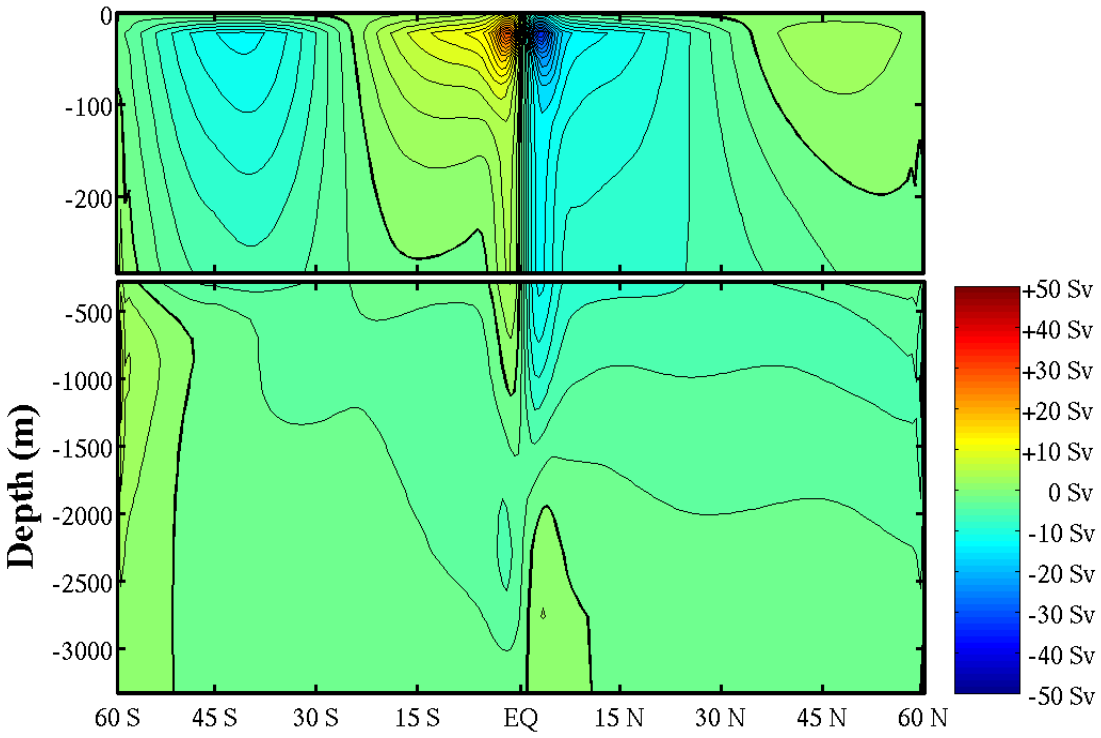

FIGURE 42. Meridional Volume Transport for Ratio 4:1 and B = -5 (Case D)

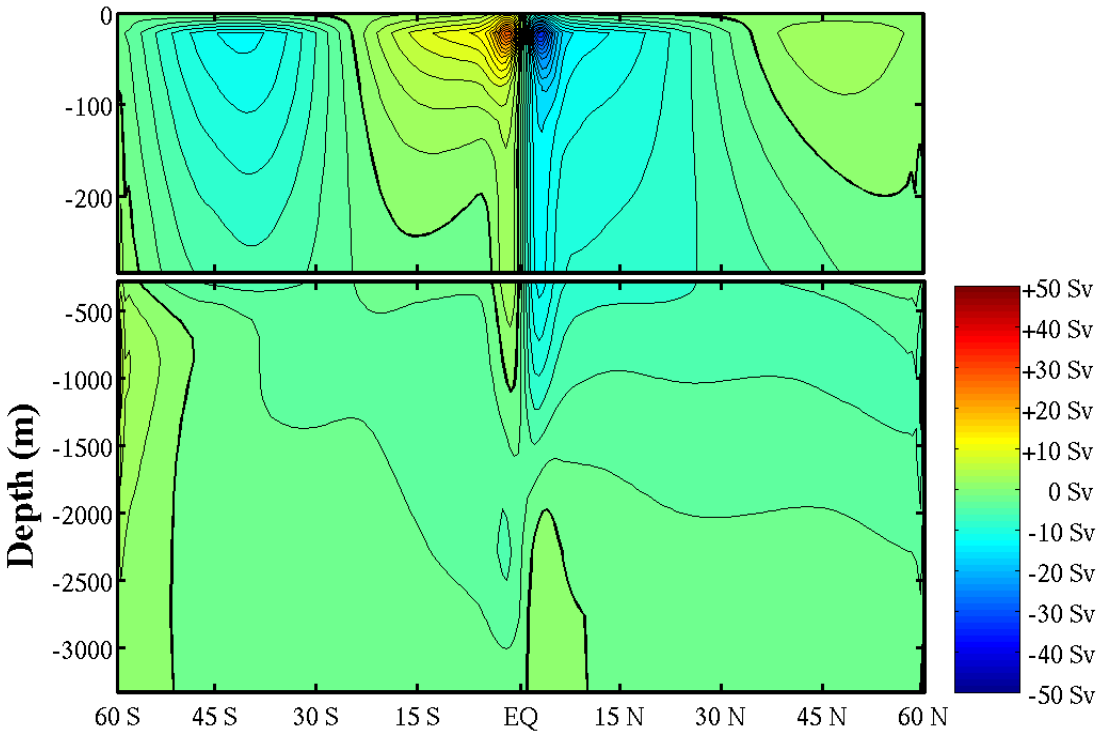

FIGURE 43. As FIGURE 42 except B = -7.5 (Case O)

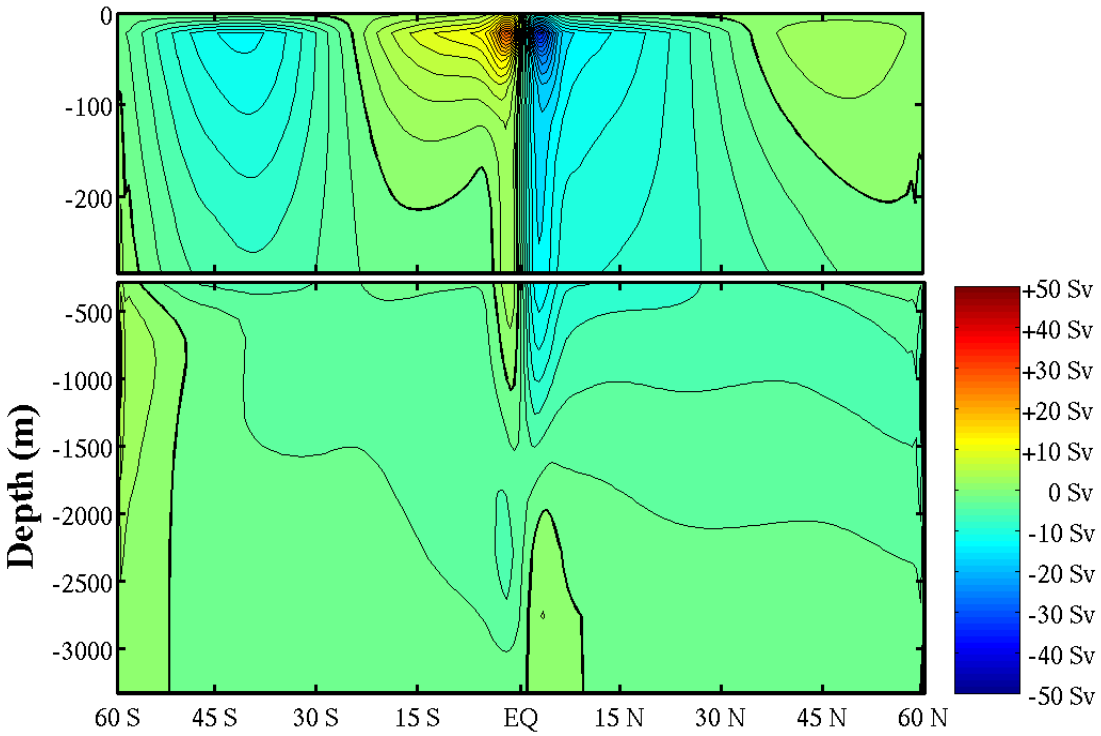

FIGURE 44. As FIGURE 42 except B = -10 (Case P)

B. MERIDIONAL HEAT TRANSPORT

All figures in this section show the streamfunction of heat transport. Each plot is a latitude-depth cross-section. The zero contour is in bold and contour lines are spaced at 0.2 PW intervals. Positive (negative) values indicate counterclockwise (clockwise) circulation. The figure is split at a depth of 360 meters so that detail near the surface can be easily viewed.

1. The Symmetric Case

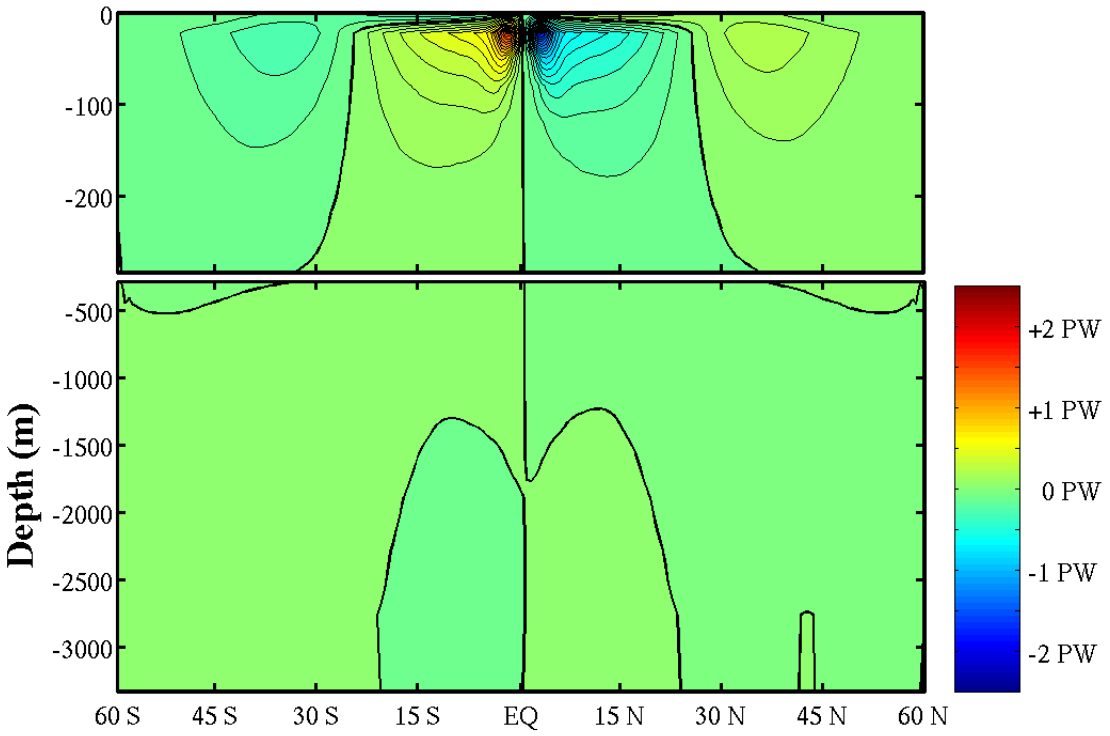

FIGURE 45. Meridional Heat Transport for the Symmetric Case

2. Cases of Wind Stress Asymmetry

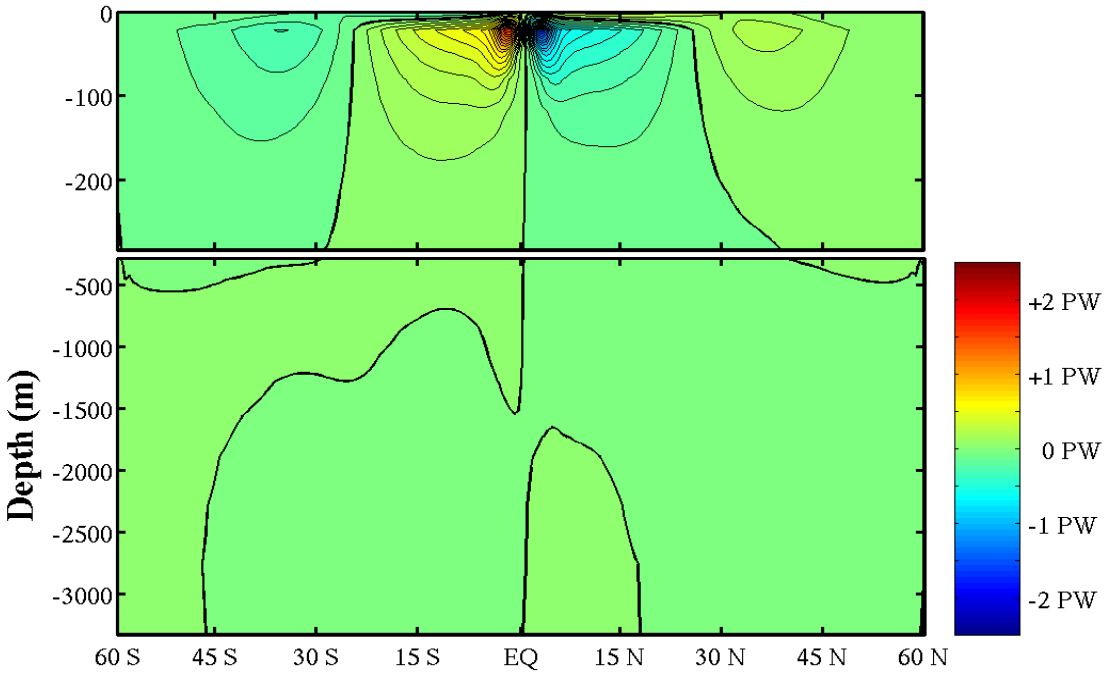

FIGURE 46. Meridional Heat Transport for Ratio 3:2 (Case Q)

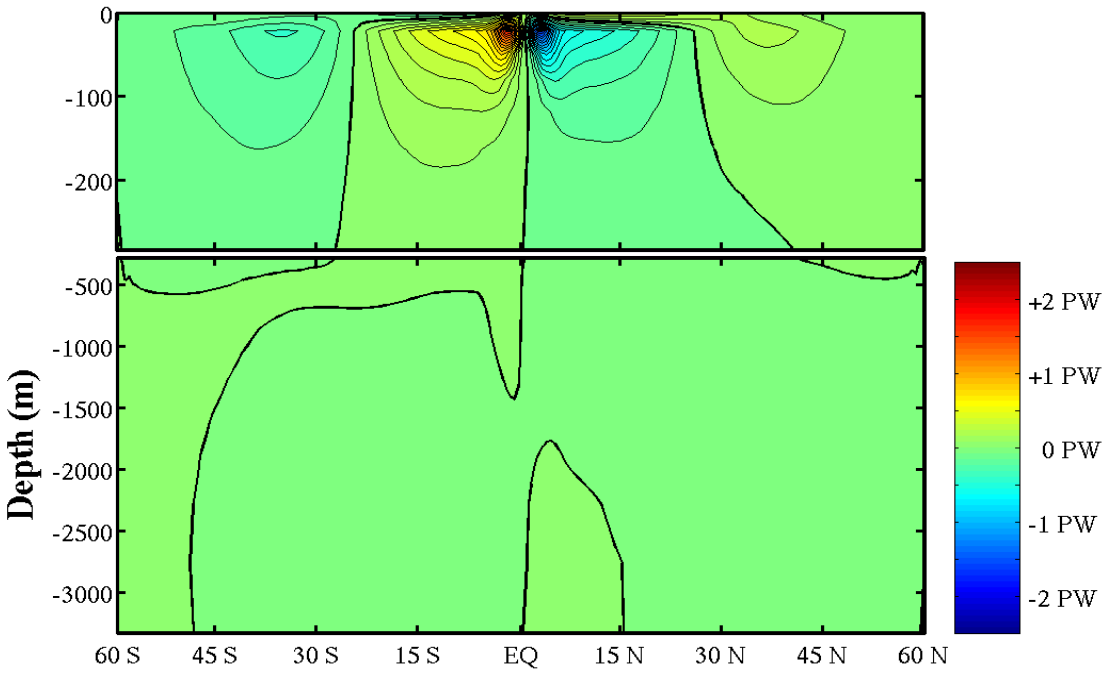

FIGURE 47. Meridional Heat Transport for Ratio 2:1 (Case I)

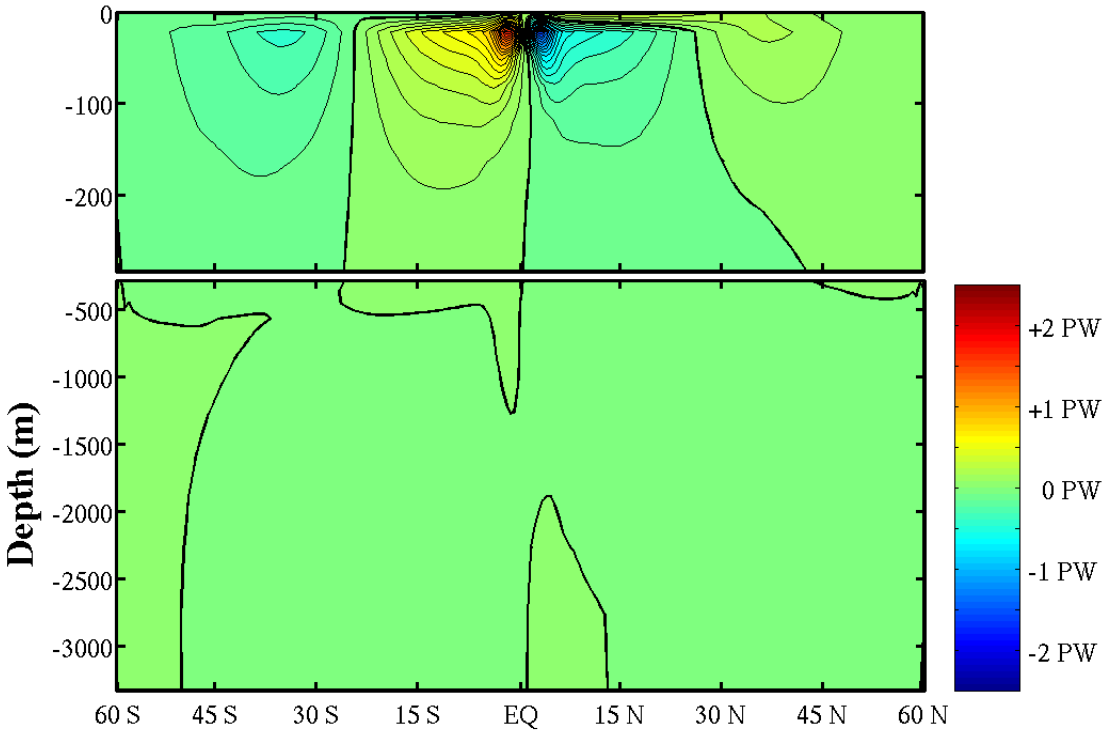

FIGURE 48. Meridional Heat Transport for Ratio 3:1 (Case J)

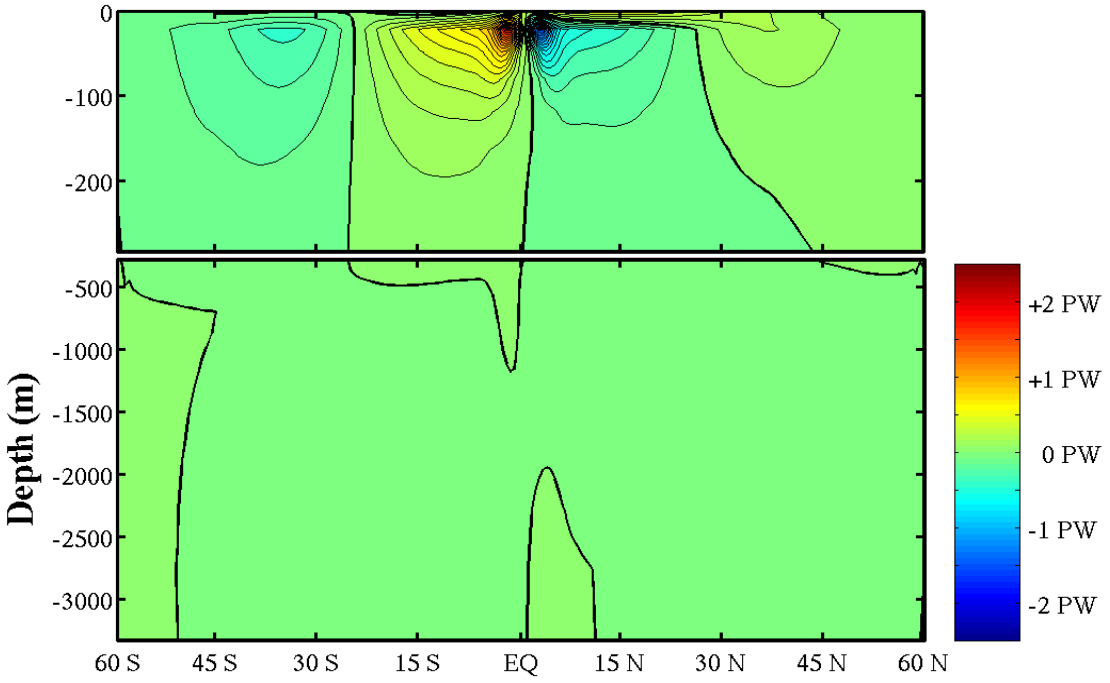

FIGURE 49. Meridional Heat Transport for Ratio 4:1 (Case B)

3. Cases of Temperature Forcing Asymmetry

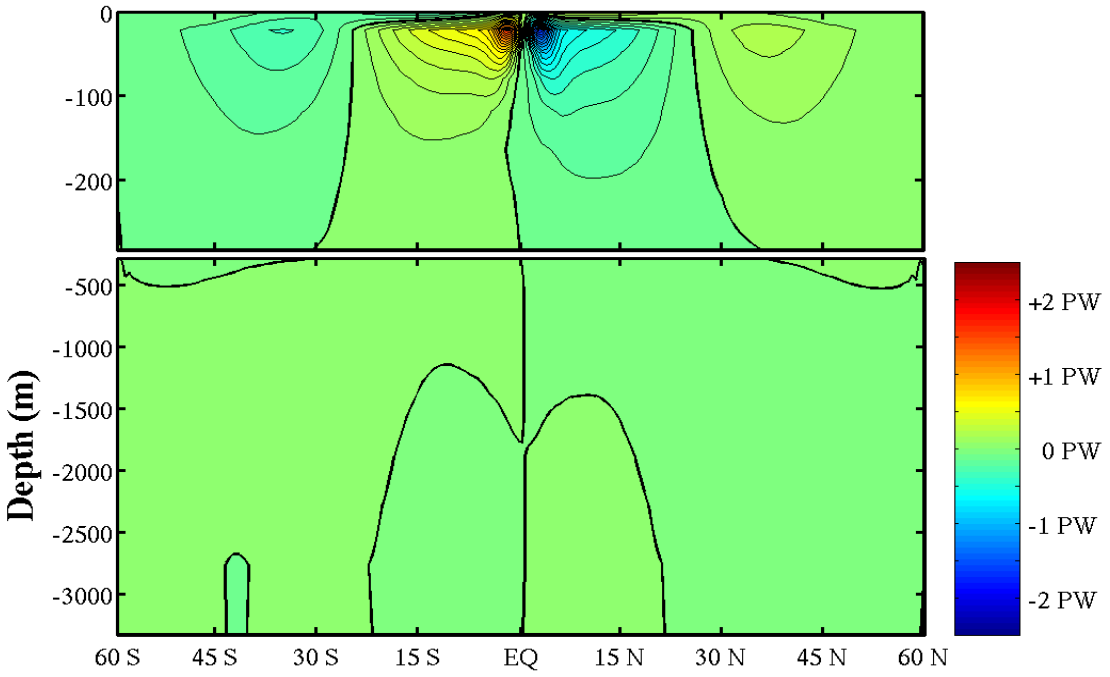

FIGURE 50. Meridional Heat Transport for B = -5 (Case C)

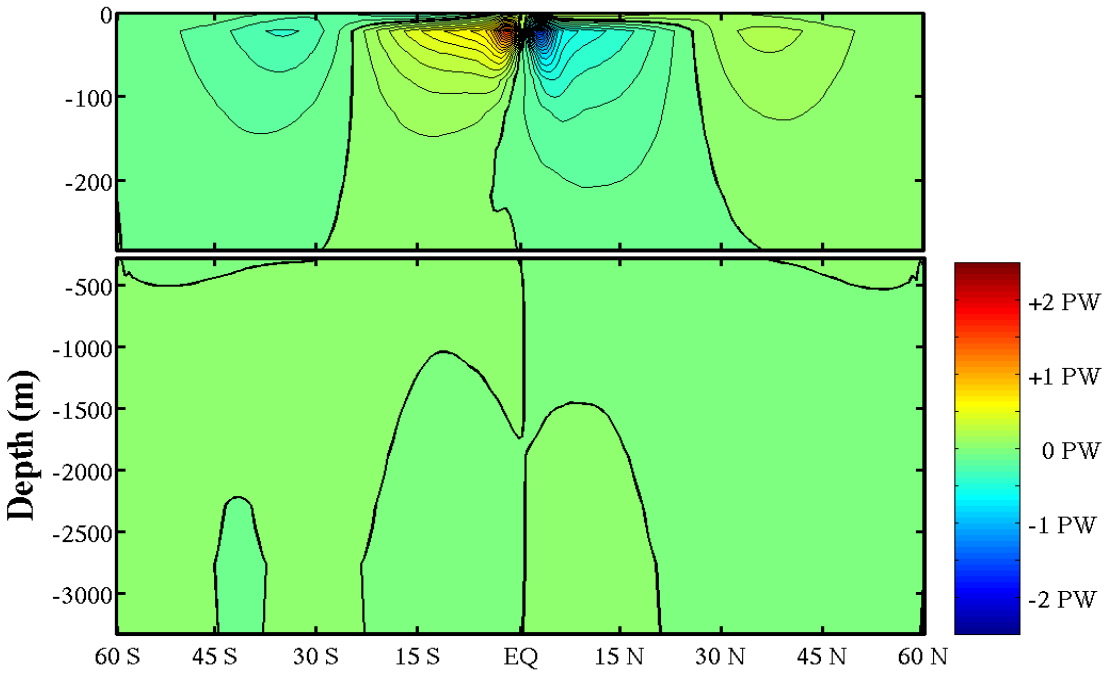

FIGURE 51. Meridional Heat Transport for B = -7.5 (Case K)

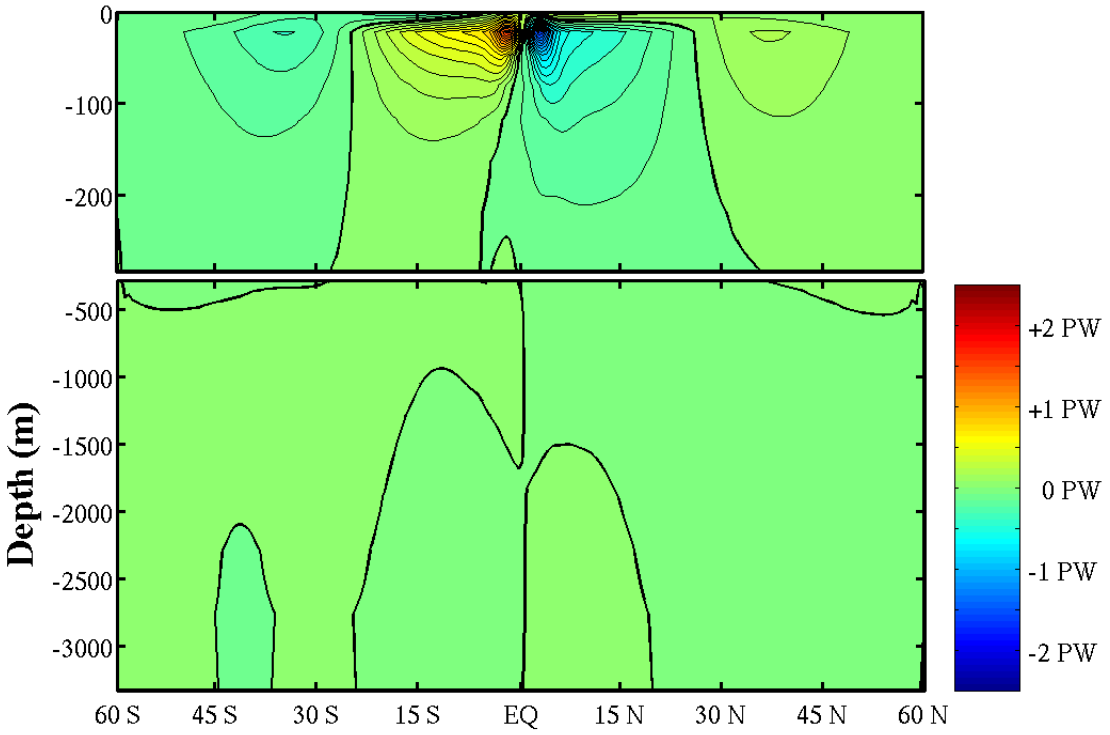

FIGURE 52. Meridional Heat Transport for B = -10 (Case L)

4. Cases of Wind Stress and Temperature Forcing Asymmetry

As mentioned before, nine of the 16 model runs used asymmetric forcing in both wind stress and sea surface temperature. The following figures are labeled with the wind stress amplitude ratio and the value of the coefficient B. The specific case is also listed. These figures are grouped by wind stress peak amplitude ratio and then in order of lower to higher temperature forcing.

a. Dual-Asymmetric Cases of Wind Stress Ratio of 3:2

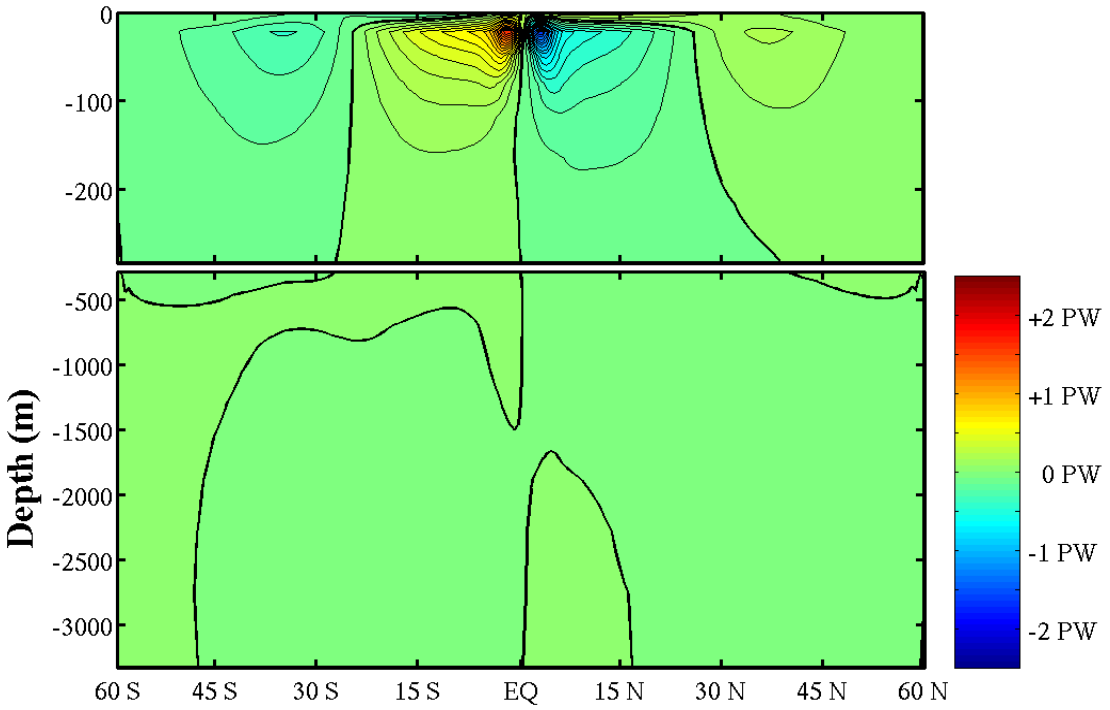

FIGURE 53. Meridional Heat Transport for Ratio 3:2 and B = -5 (Case R)

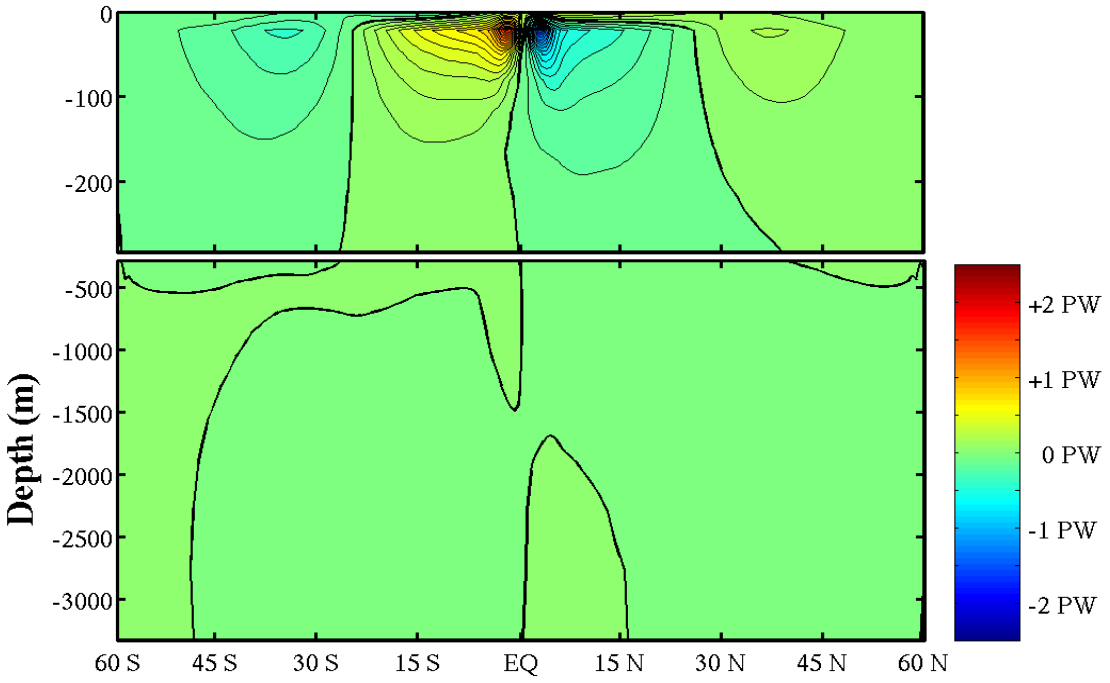

FIGURE 54. As FIGURE 53 except B = -7.5 (Case S)

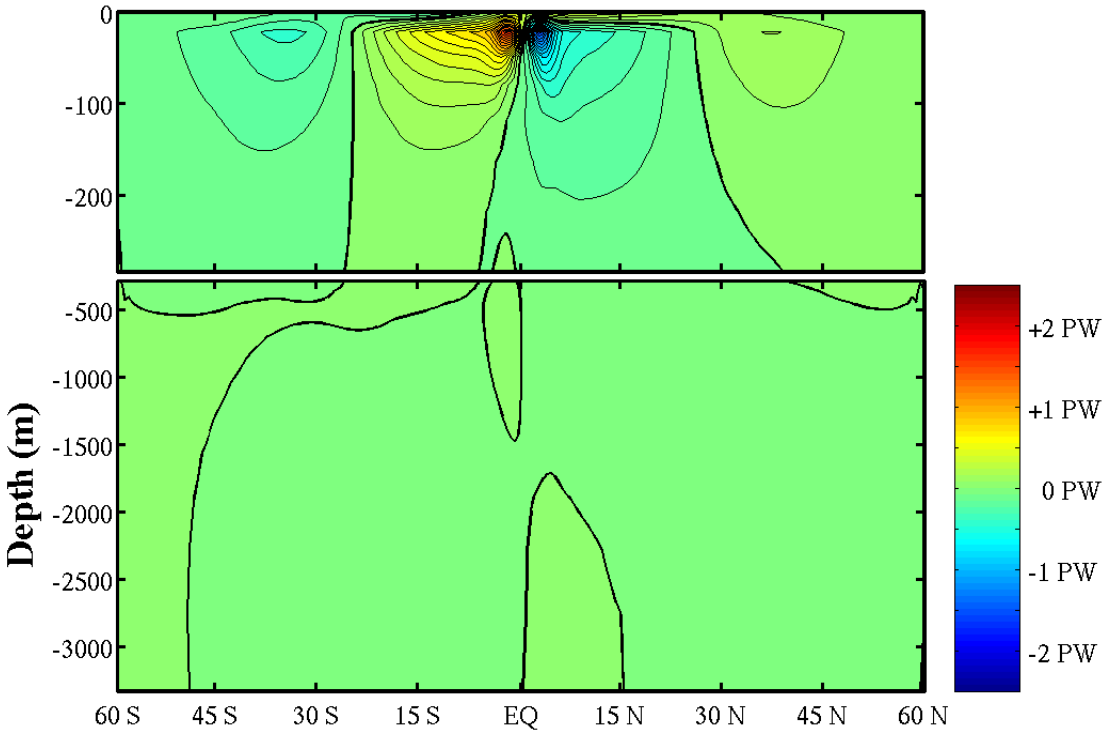

FIGURE 55. As FIGURE 56 except B = -10 (Case S)

b. Dual-Asymmetric Cases of Wind Stress Ratio of 2:1

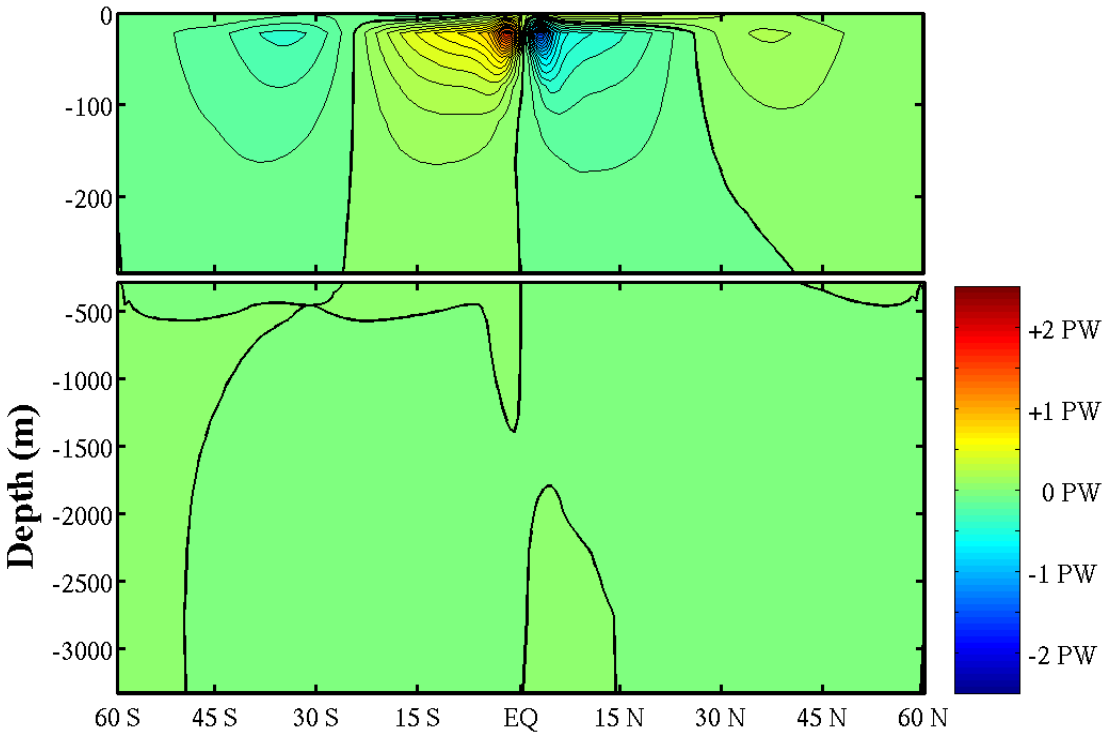

FIGURE 56. Meridional Heat Transport for Ratio 2:1 and B = -5 (Case M)

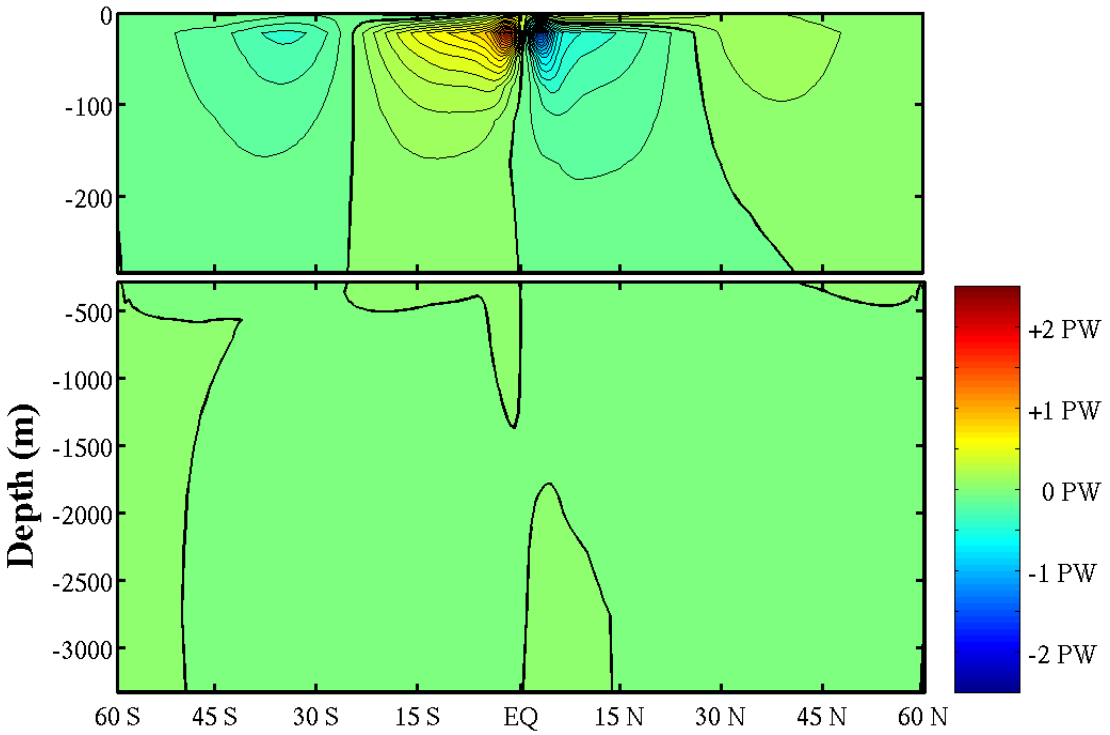

FIGURE 57. As FIGURE 56 except B = -7.5 (Case E)

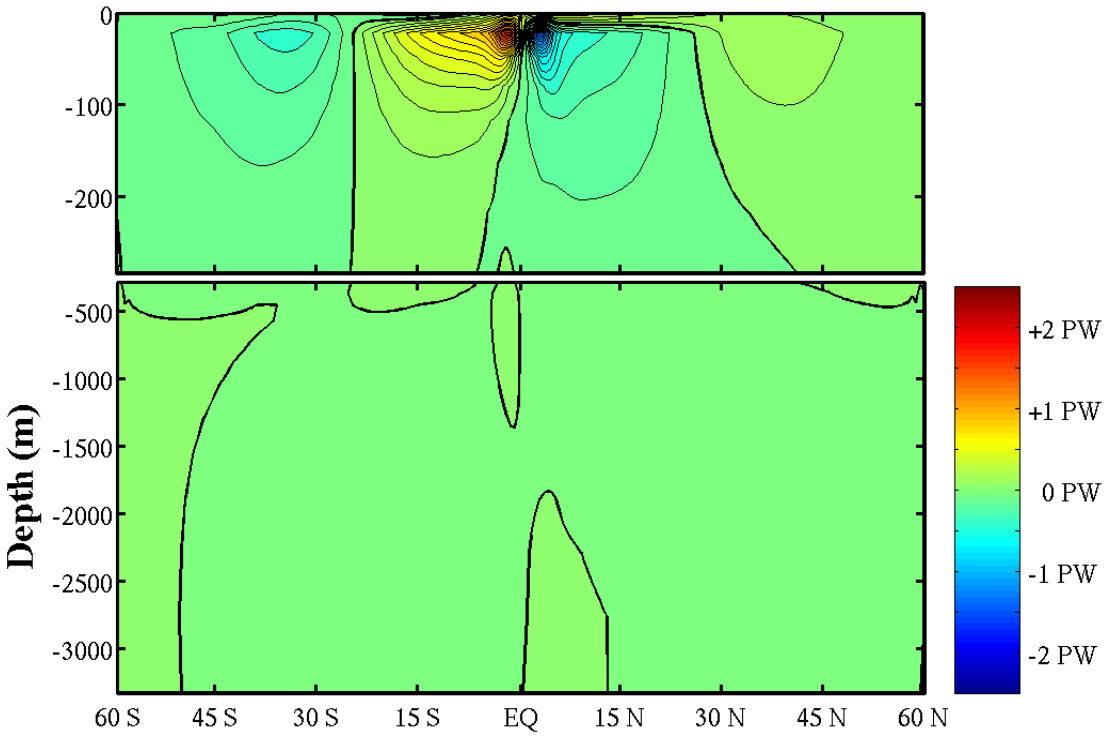

FIGURE 58. As FIGURE 56 except B = -10 (Case G)

c. Dual-Asymmetric Cases for Wind Stress Ratio of 3:1

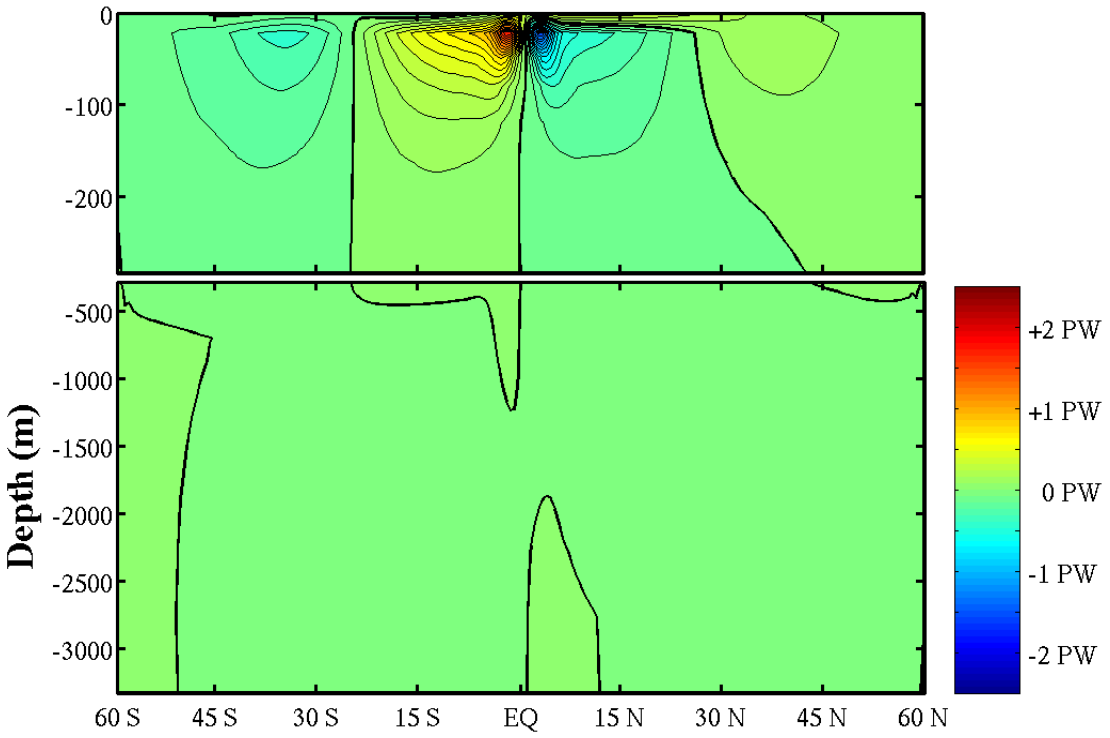

FIGURE 59. Meridional Heat Transport for Ratio 3:1 and B = -5 (Case N)

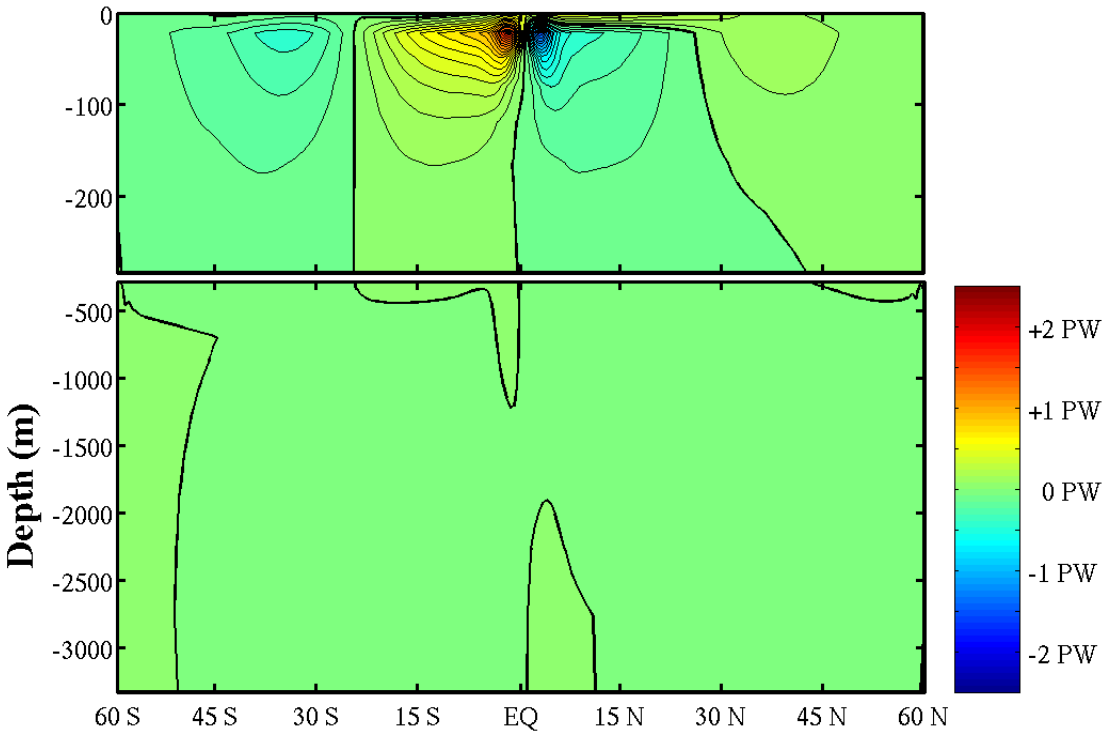

FIGURE 60. As FIGURE 59 except B = -7.5 (Case F)

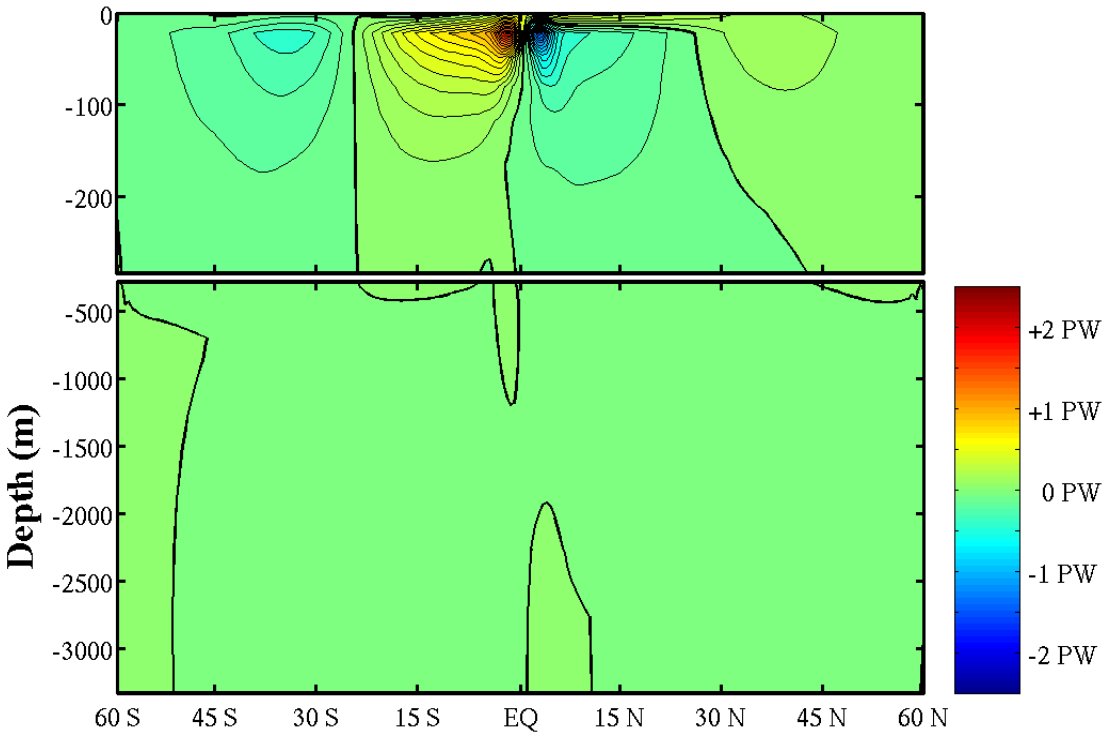

FIGURE 61. As FIGURE 59 except B = -10 (Case H)

d. Dual-Asymmetric Cases for Wind Stress Ratio of 4:1

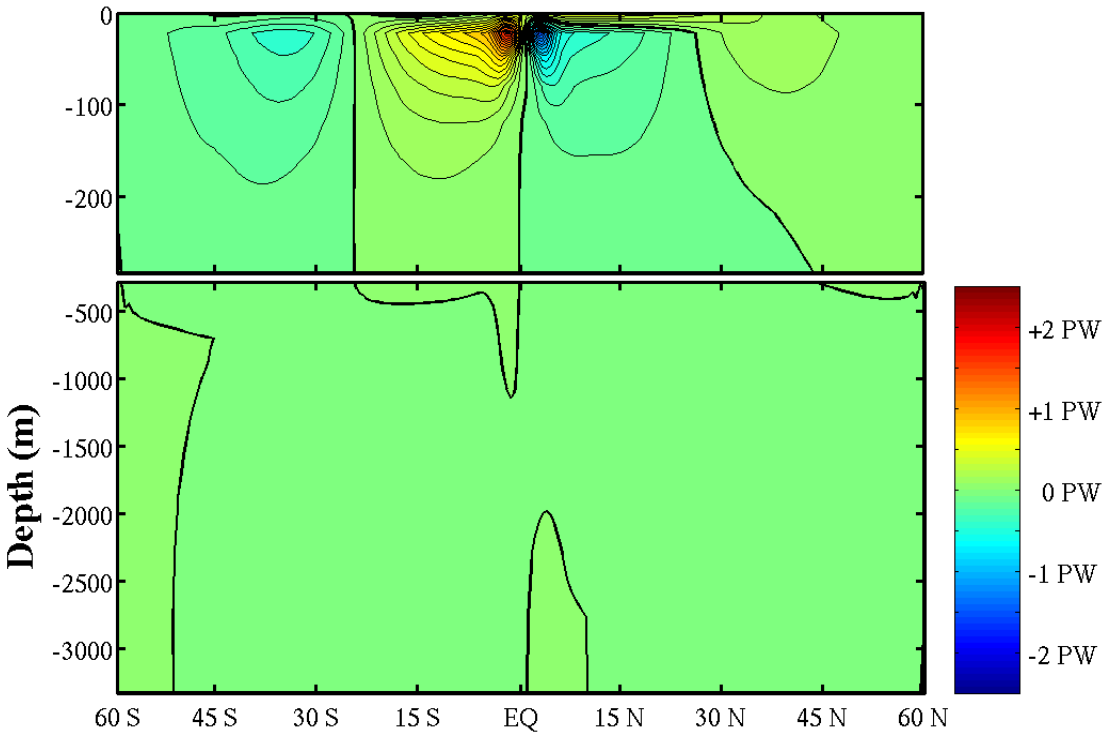

FIGURE 62. Meridional Heat Transport for Ratio 4:1 and B = -5 (Case D)

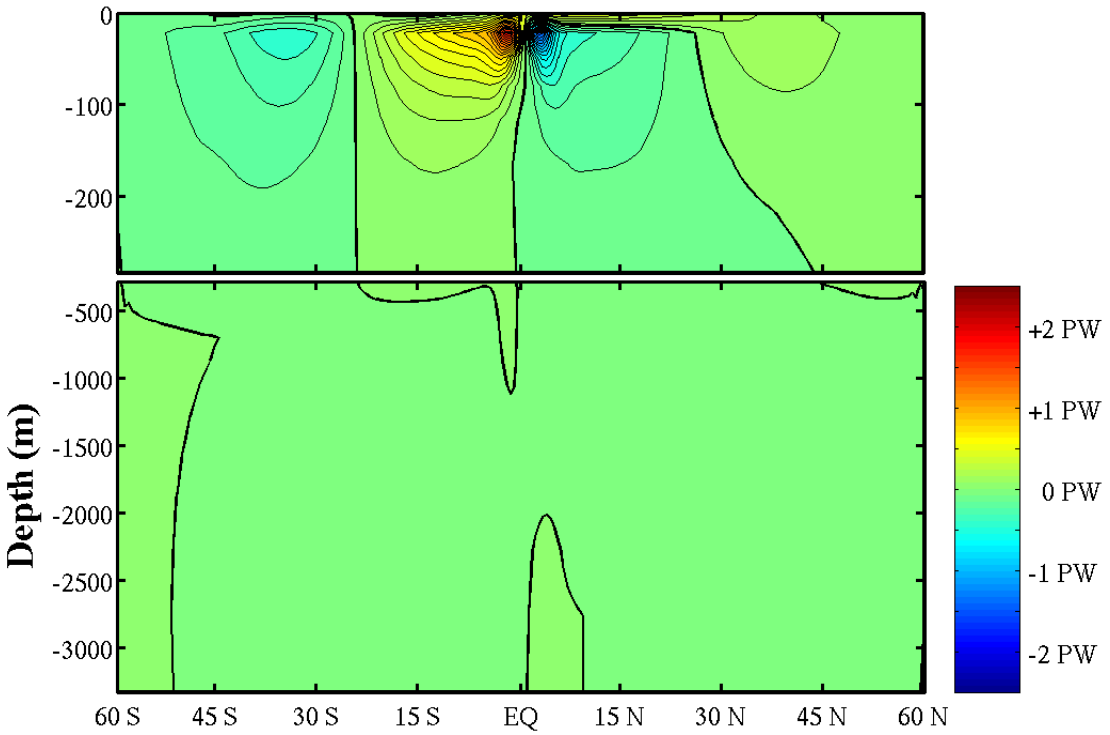

FIGURE 63. As FIGURE 62 except B = -7.5 (Case O)

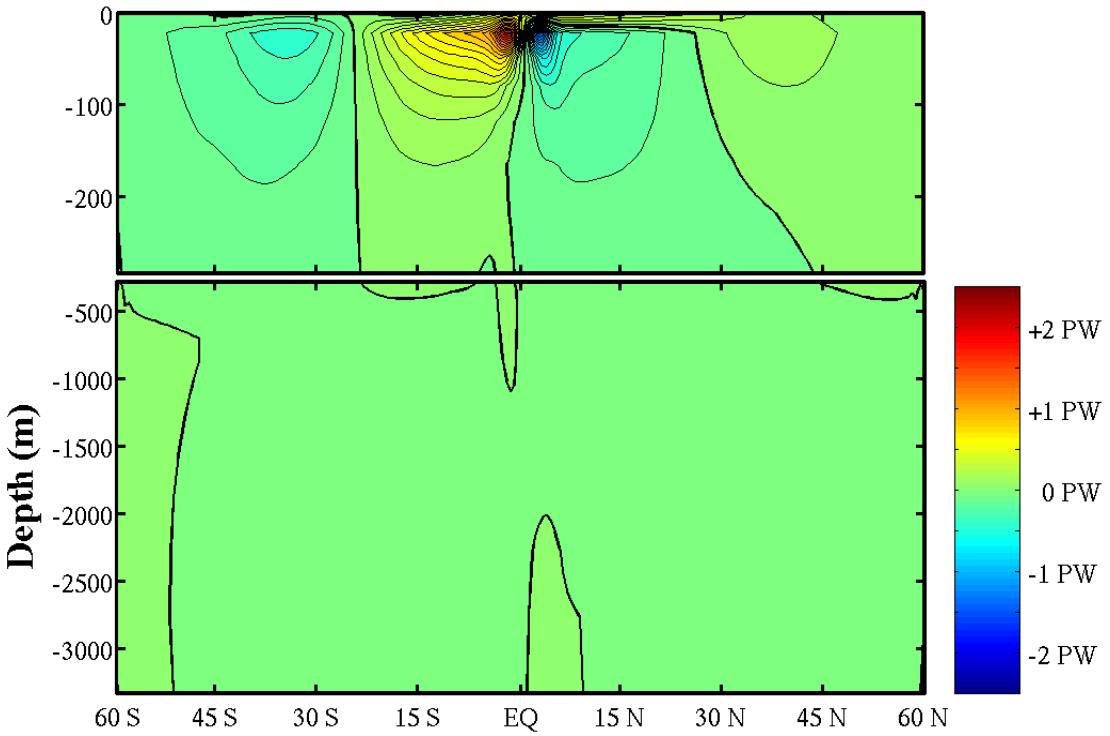

FIGURE 64. As FIGURE 62 except B = -10 (Case P)

C. TOTAL MERIDIONAL HEAT TRANSPORT

1. Differences in Wind Stress Forcing

In each of the following figures, the sea surface temperature forcing is constant, while the curves represent the zonally and vertically integrated heat transport across the latitude shown. Positive (negative) values of heat transport indicate northward (southward) transport. Power is given in terawatts and the wind stress peak amplitude ratio (south-to-north) is used to label each curve. Meridional heat transport for the case of both wind stress and temperature forcing symmetry is represented with a dashed line and is included in all plots in this section.

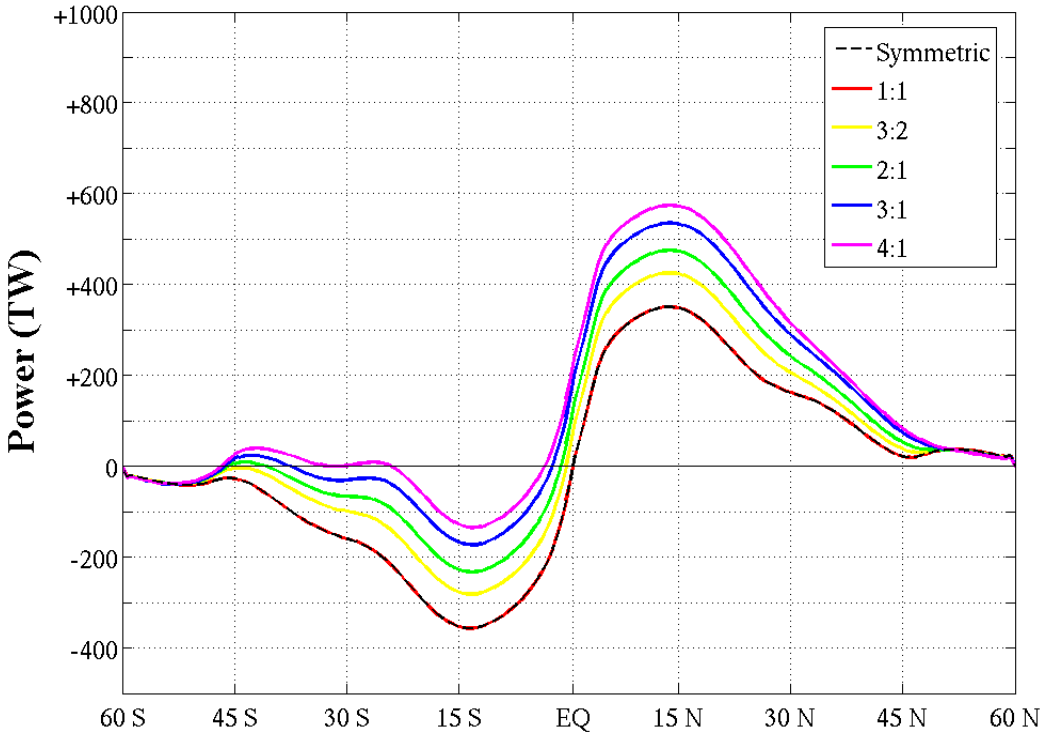

FIGURE 65. Total Meridional Heat Transport (Symmetric Temperature Forcing)

In this figure, the temperature forcing coefficient (B) for each of these four cases is zero making the sea surface temperature forcing symmetric about the equator. The following three figures show the meridional heat transport for cases where temperature forcing is asymmetric. The temperature forcing coefficient is annotated.

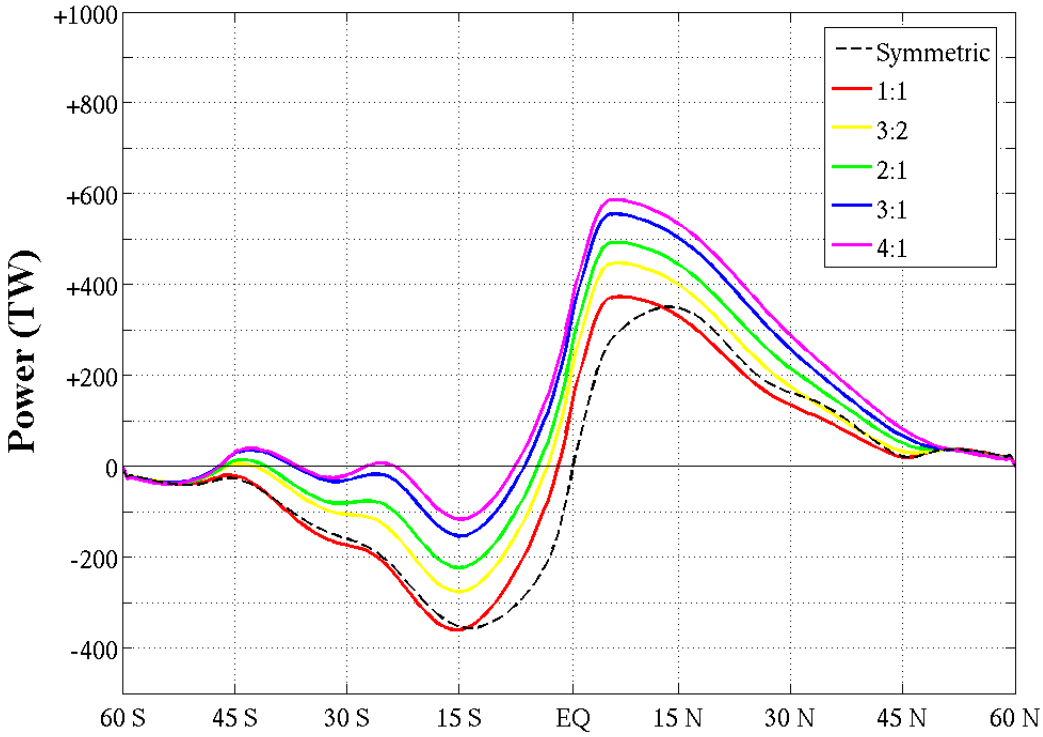

FIGURE 66. As FIGURE 65 except B = -5

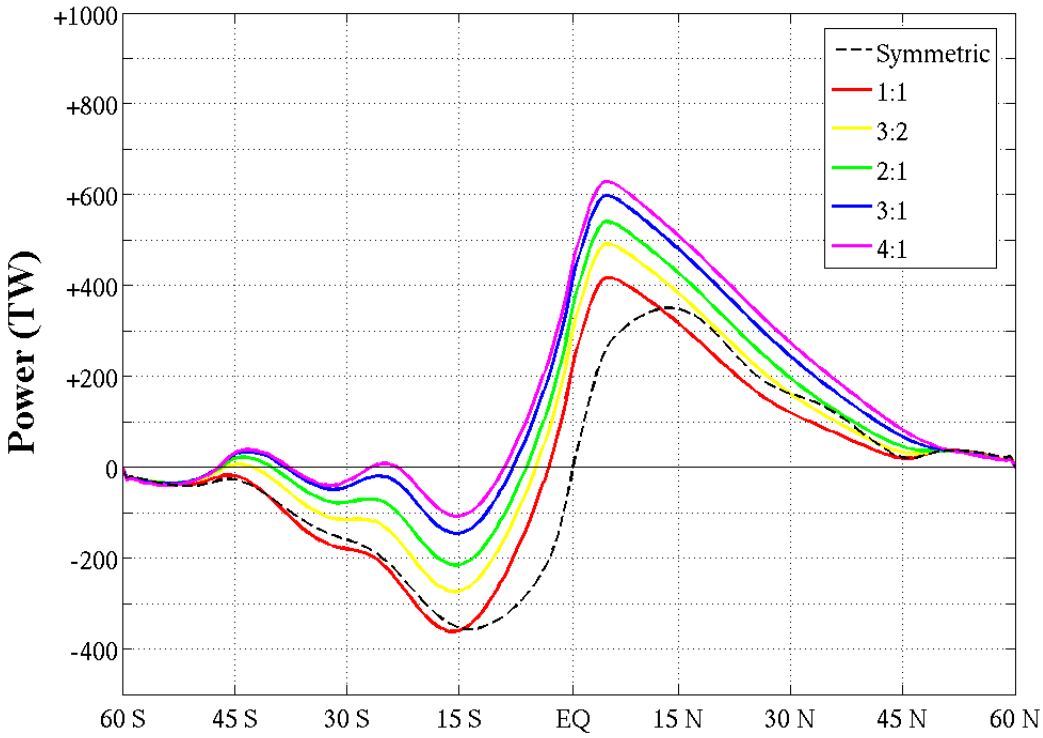

FIGURE 67. As FIGURE 65 except B = -7.5

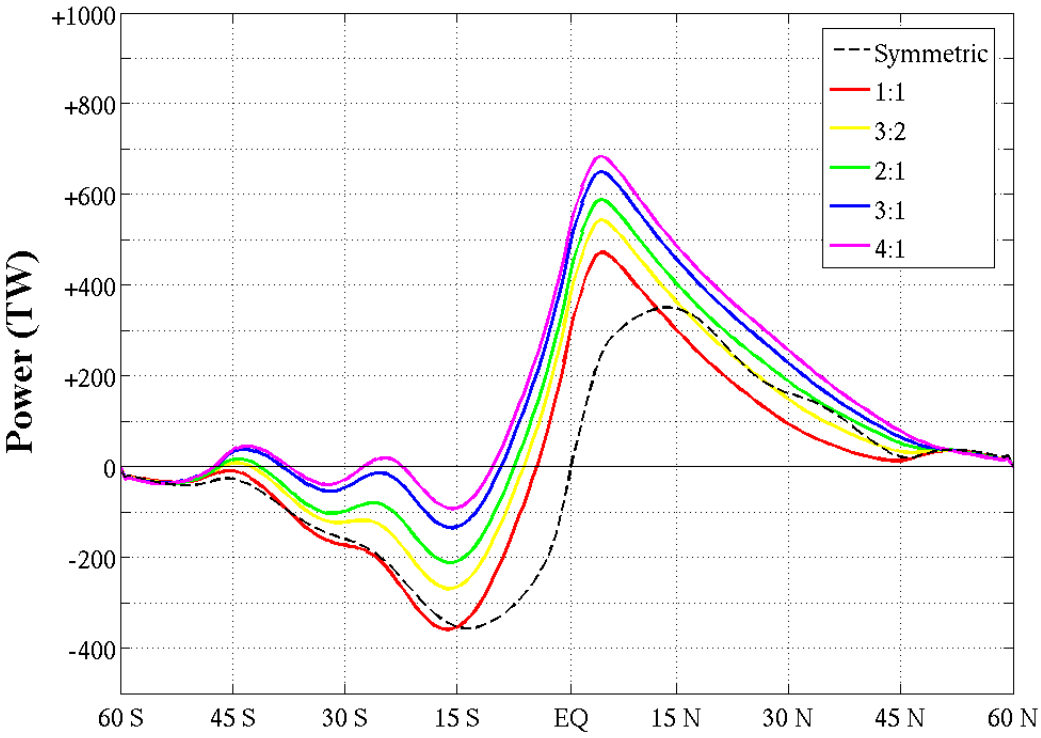

FIGURE 68. As FIGURE 65 except B = -10

2. Differences in Sea Surface Temperature Forcing

In each of the following figures, the wind stress forcing is constant. The curves represent the zonally and vertically integrated heat transport across the latitude shown. Positive (negative) values of heat transport indicate northward (southward) transport. Power is given in terawatts and the temperature forcing coefficient used in Equation (5) is used to label each curve. As mentioned before, the dashed line shows the meridional heat transport in the dual-symmetric case.

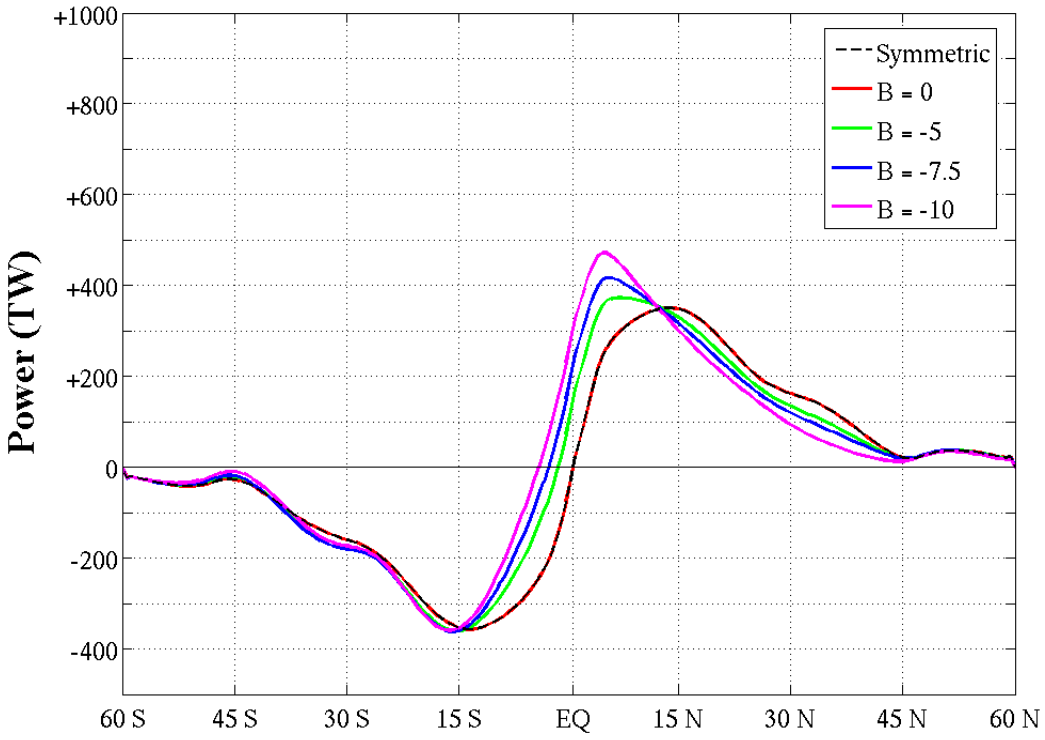

FIGURE 69. Total Meridional Heat Transport (Symmetric Wind Stress Forcing)

In this figure, the wind stress forcing coefficient (A) for each of these four cases is zero making the sea surface temperature forcing symmetric about the equator. The following three figures show the meridional heat transport for cases where wind stress forcing is asymmetric. The wind stress peak amplitude ratio is given with each figure.

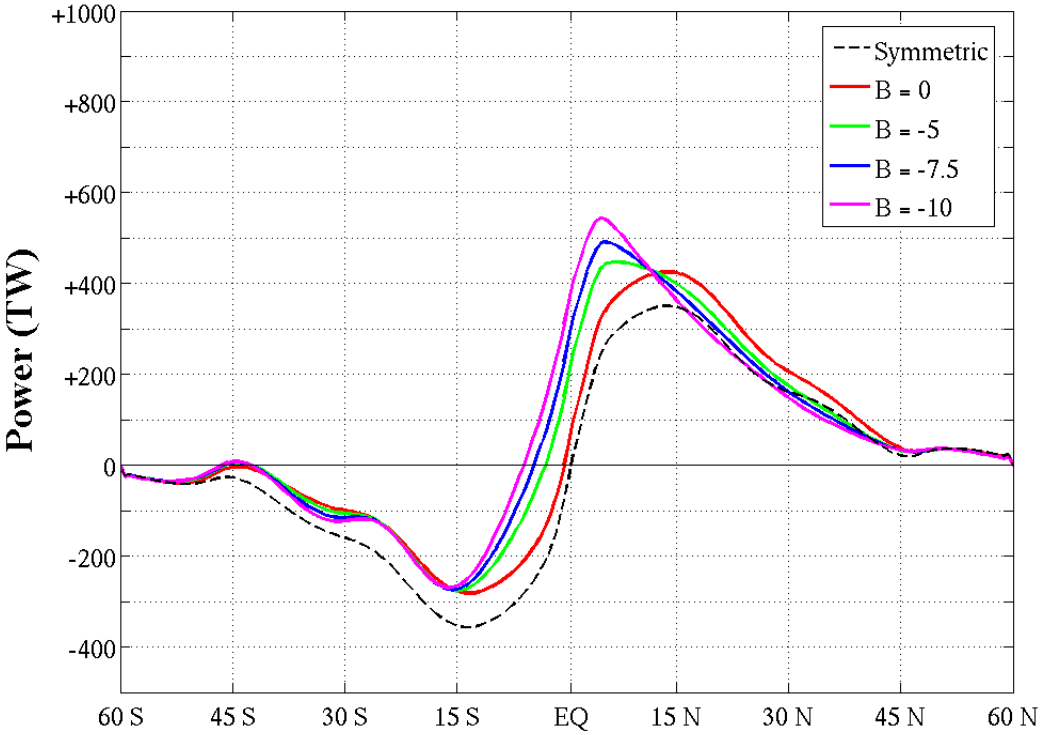

FIGURE 70. As FIGURE 69 except A = 3:2

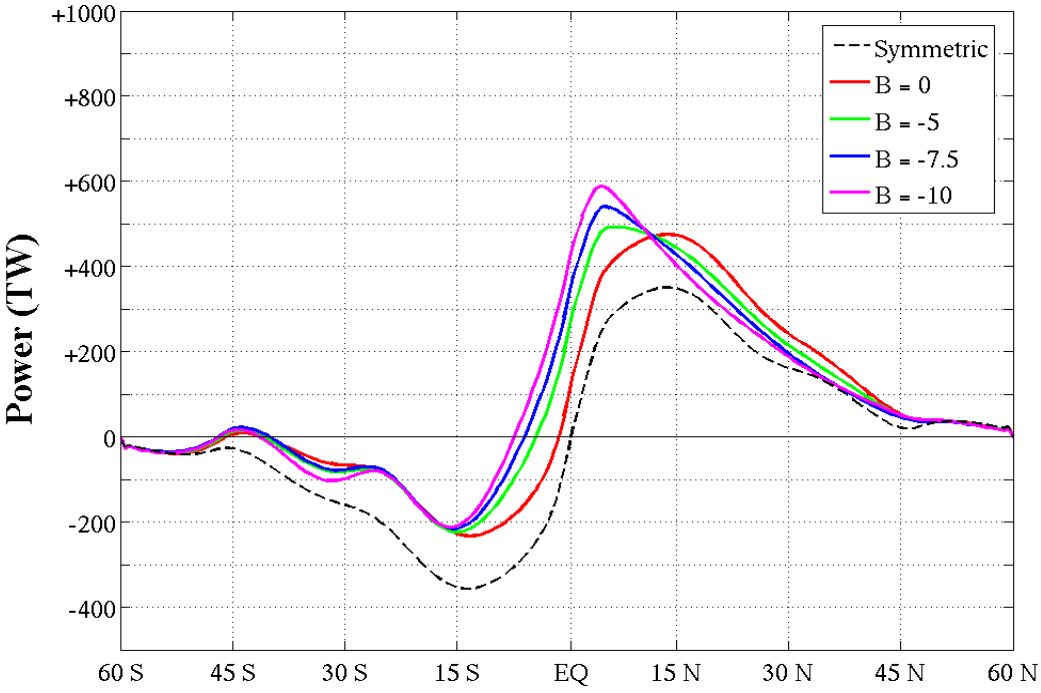

FIGURE 71. As FIGURE 69 except A = 2:1

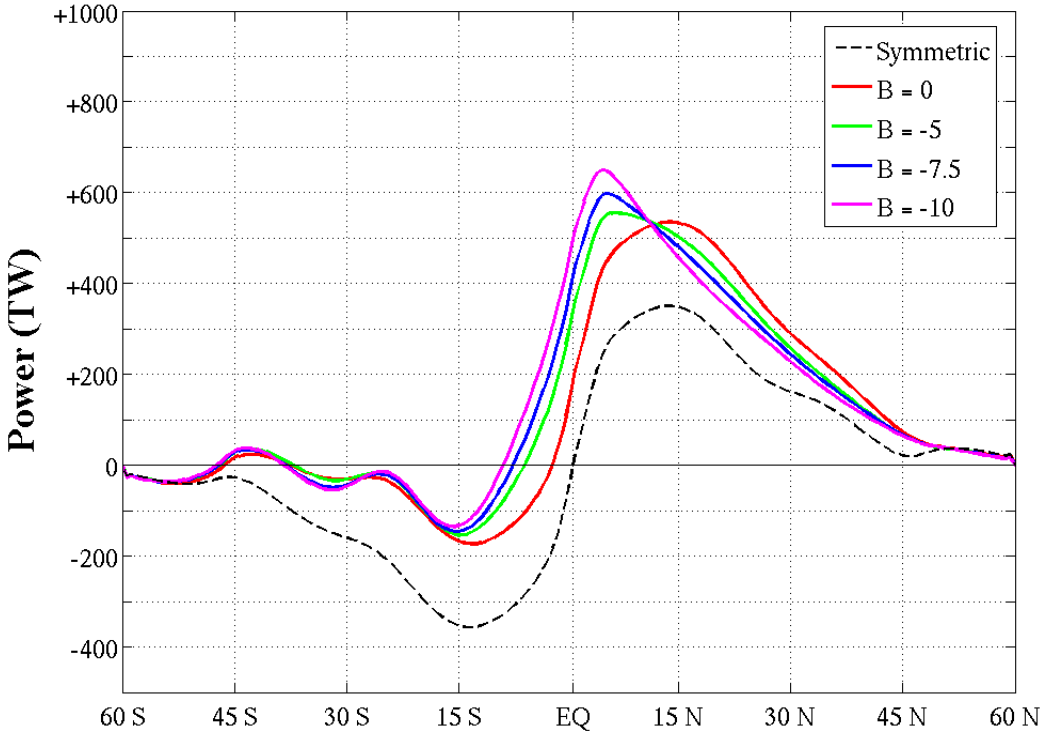

FIGURE 72. As FIGURE 69 except A = 3:1

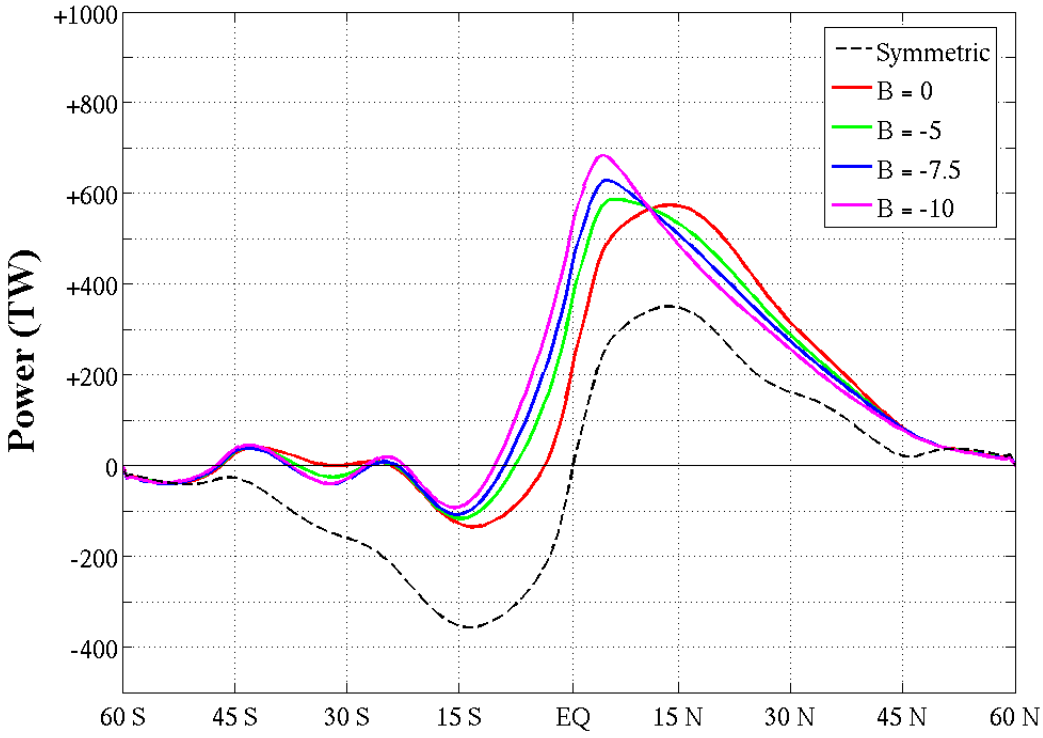

FIGURE 73. As FIGURE 69 except A = 4:1

D. NET SURFACE HEAT FLUX

All figures in this section show net heat flux at the surface. The zero contour is in bold and contour lines are spaced at 25 Wm^{-2} intervals. Positive (negative) values indicate flux into (out of) the ocean.

1. The Symmetric Case

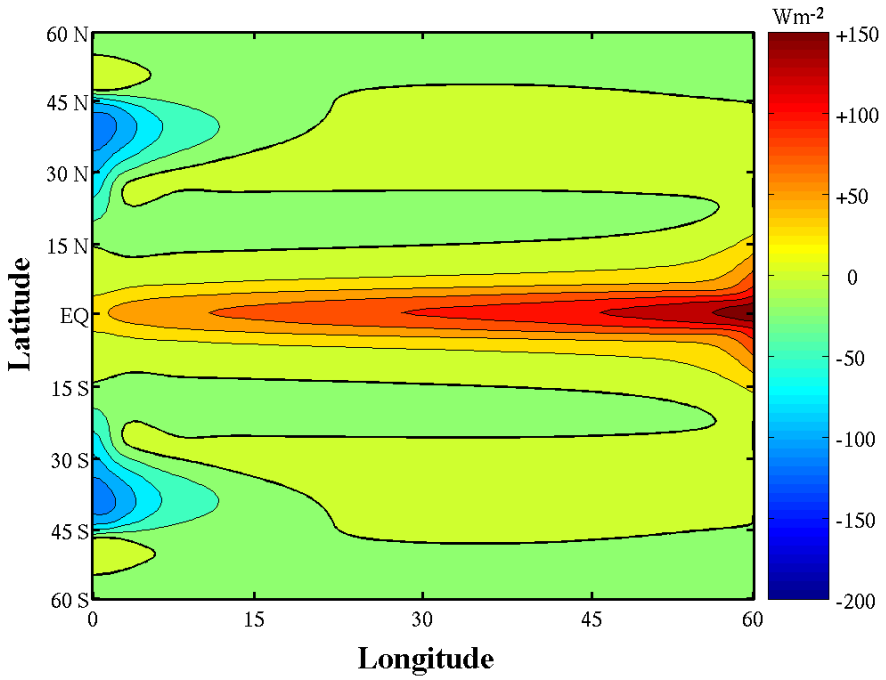

FIGURE 74. Net Surface Heat Flux for the Symmetric Case

2. Cases of Wind Stress Asymmetry

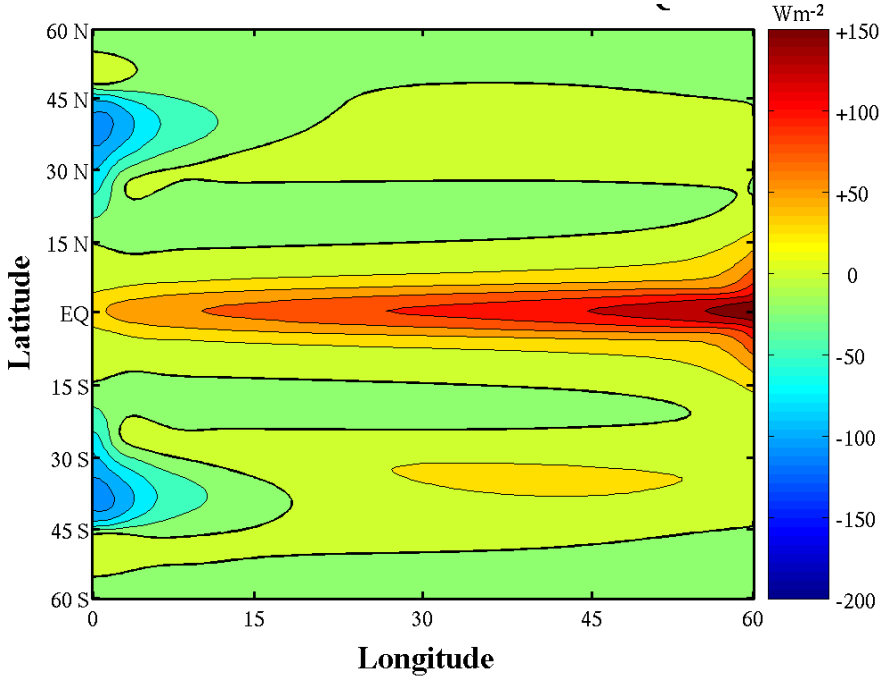

FIGURE 75. Net Surface Heat Flux for Ratio 3:2 (Case Q)

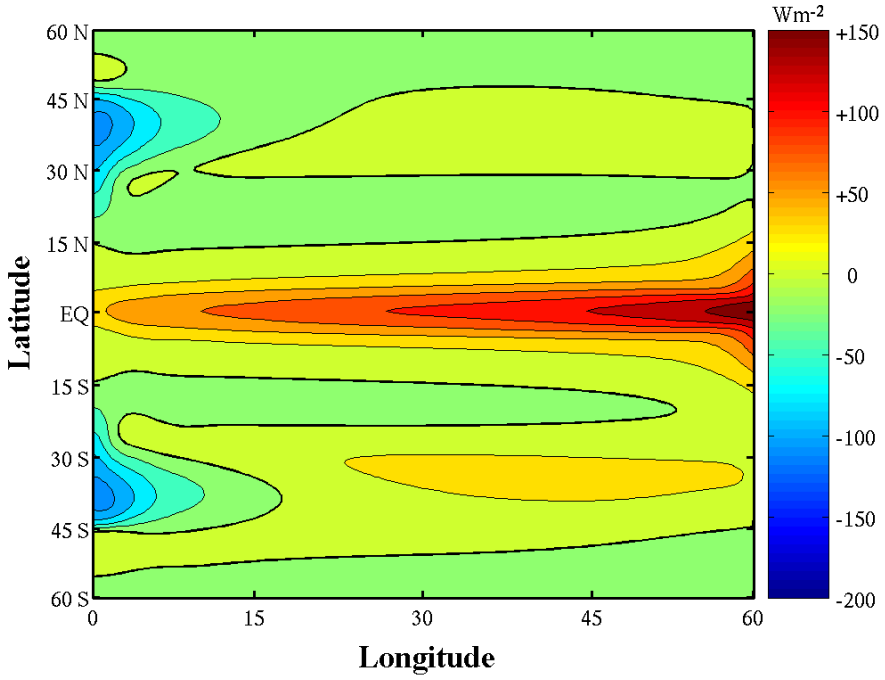

FIGURE 76. Net Surface Heat Flux for Ratio 2:1 (Case I)

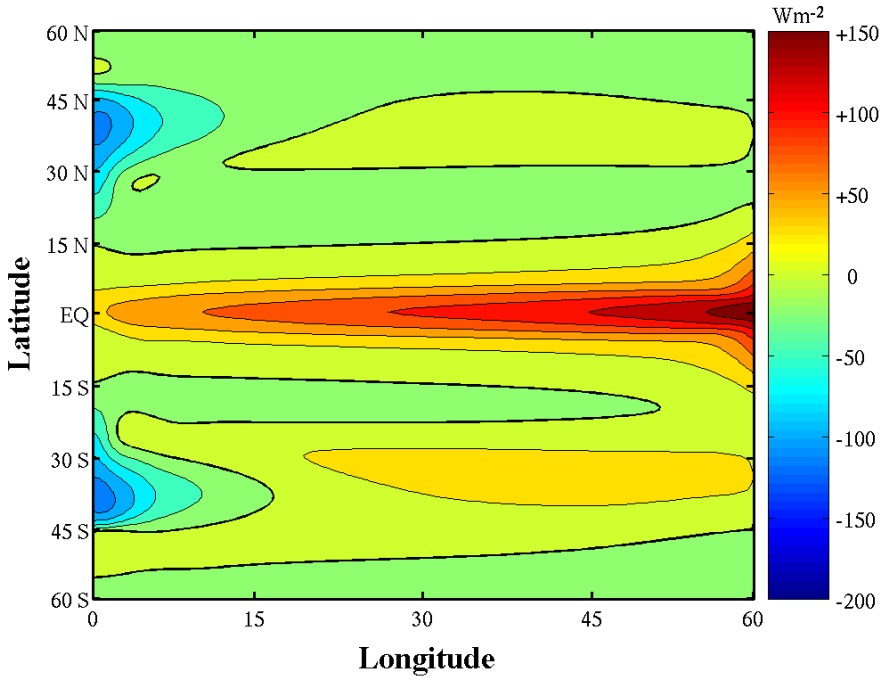

FIGURE 77. Net Surface Heat Flux for Ratio 3:1 (Case J)

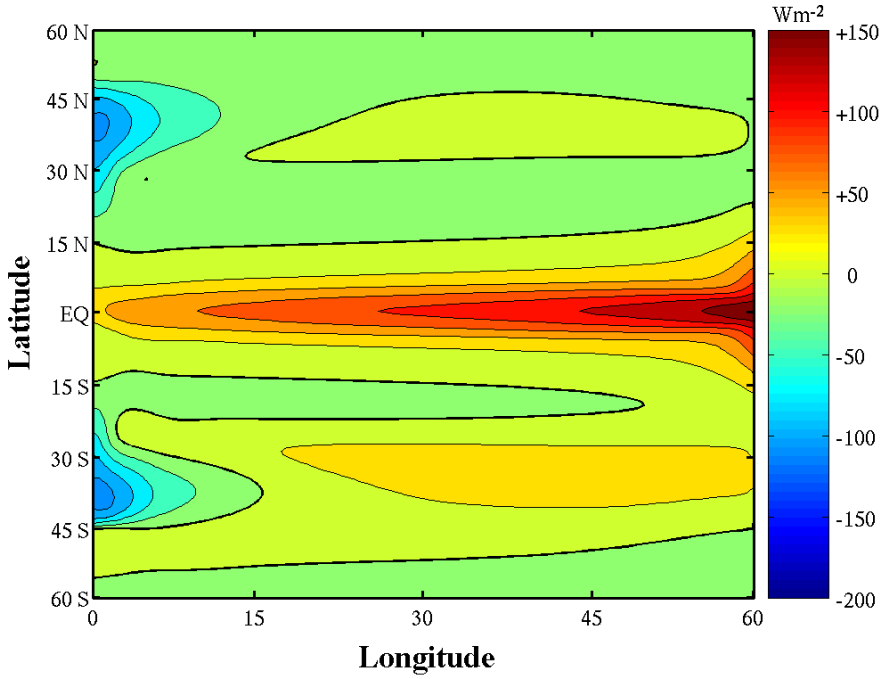

FIGURE 78. Net Surface Heat Flux for Ratio 4:1 (Case B)

3. Cases of Temperature Forcing Asymmetry

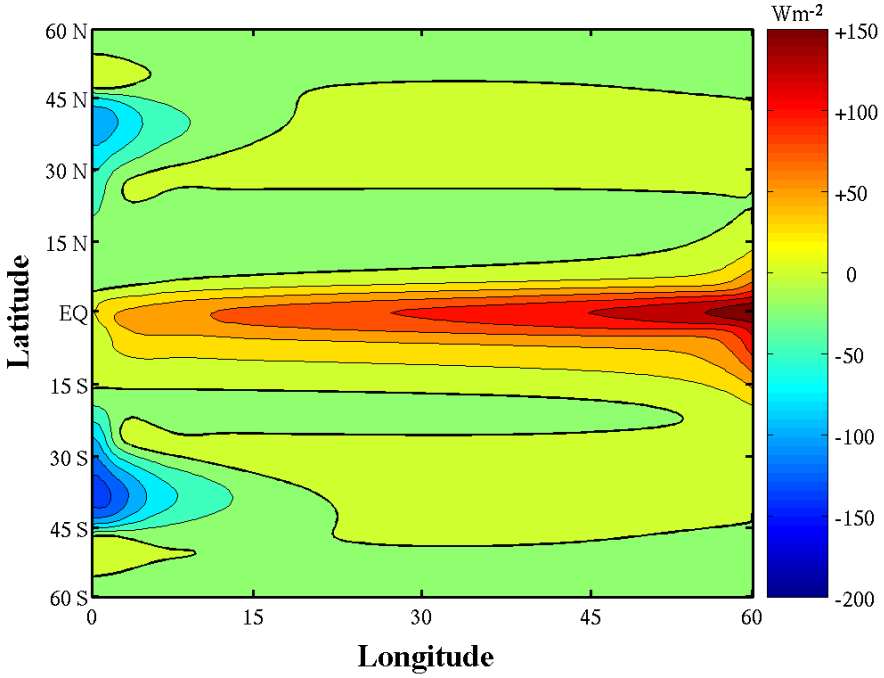

FIGURE 79. Net Surface Heat Flux for B = -5 (Case C)

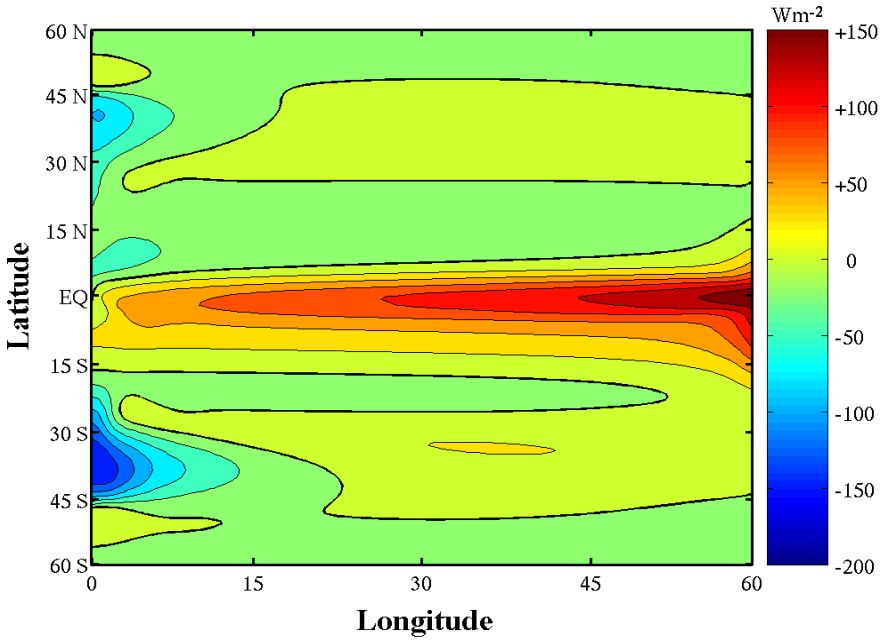

FIGURE 80. Net Surface Heat Flux for B = -7.5 (Case K)

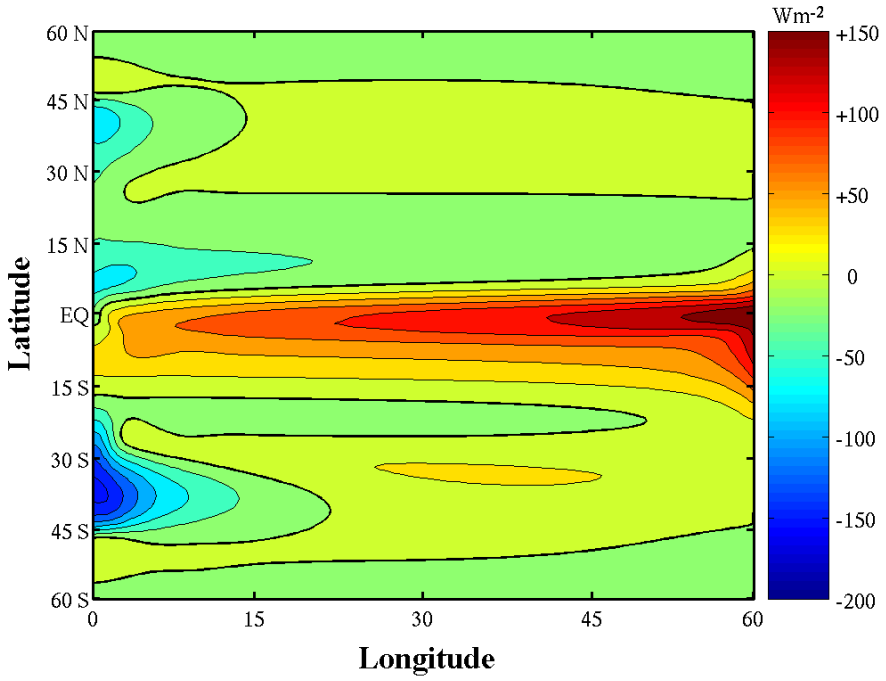

FIGURE 81. Net Surface Heat Flux for B = -10 (Case L)

4. Cases of Wind Stress and Temperature Forcing Asymmetry

The following figures are labeled with the wind stress amplitude ratio and the value of the coefficient B. The specific case is also listed. These figures are grouped by wind stress peak amplitude ratio and then in order of lower to higher temperature forcing.

a. Dual-Asymmetric Cases for Wind Stress Ratio 3:2

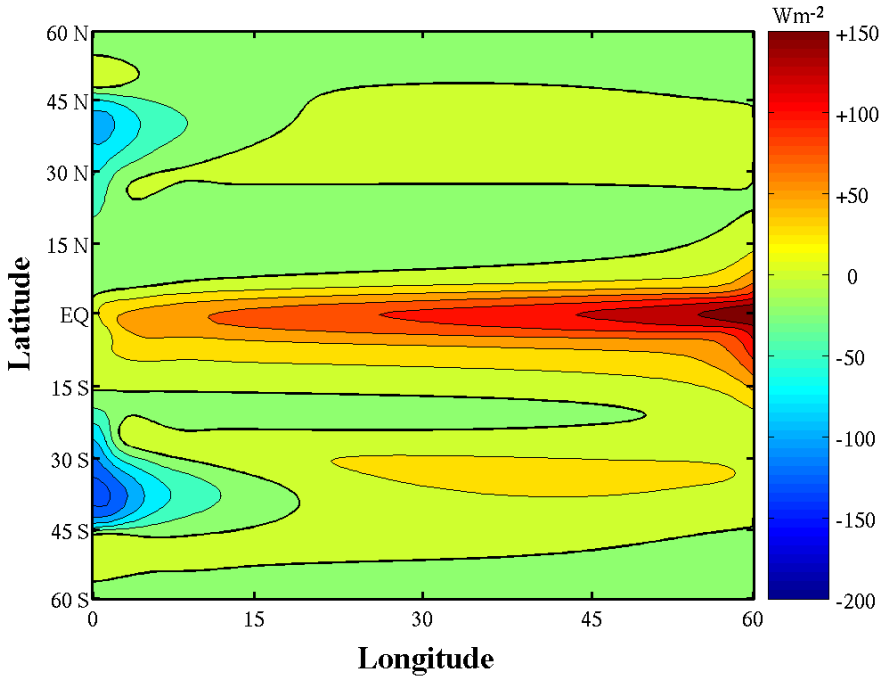

FIGURE 82. Net Surface Heat Flux for Ratio 3:2 and B = -5 (Case R)

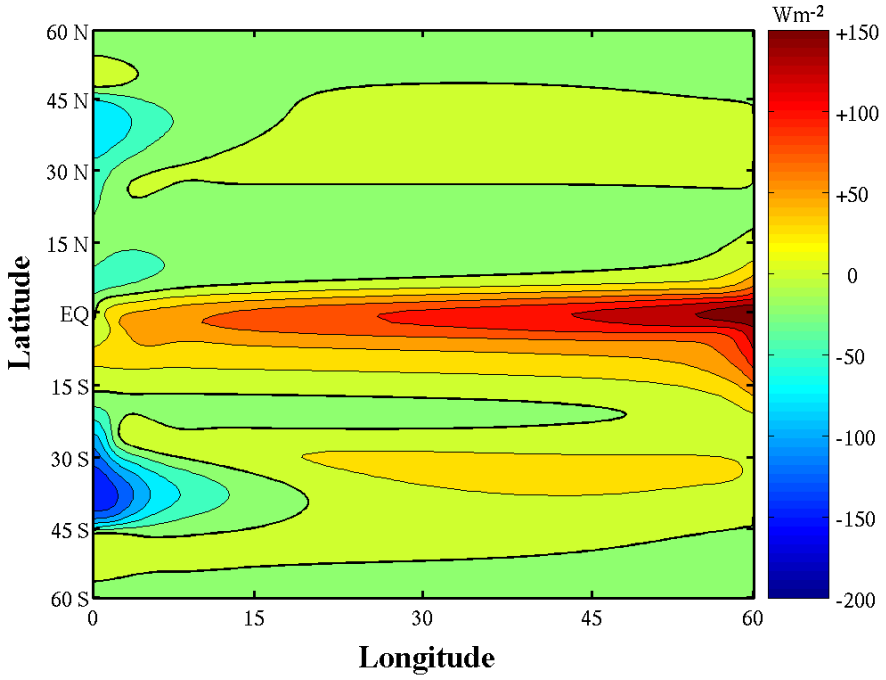

FIGURE 83. As FIGURE 85 except B = -7.5 (Case S)

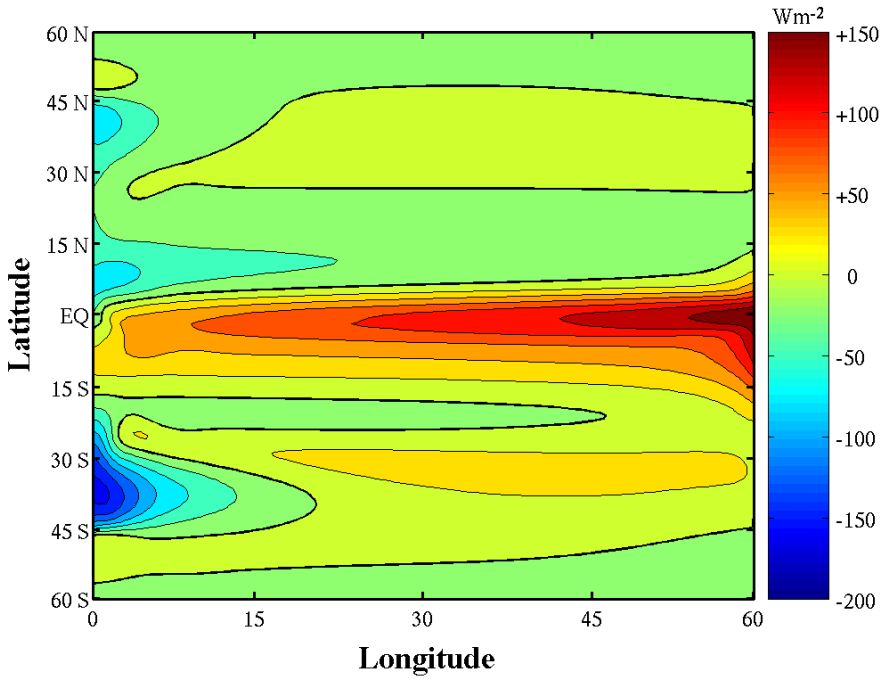

FIGURE 84. As FIGURE 85 except B = -10 (Case T)

b. Dual-Asymmetric Cases for Wind Stress Ratio 2:1

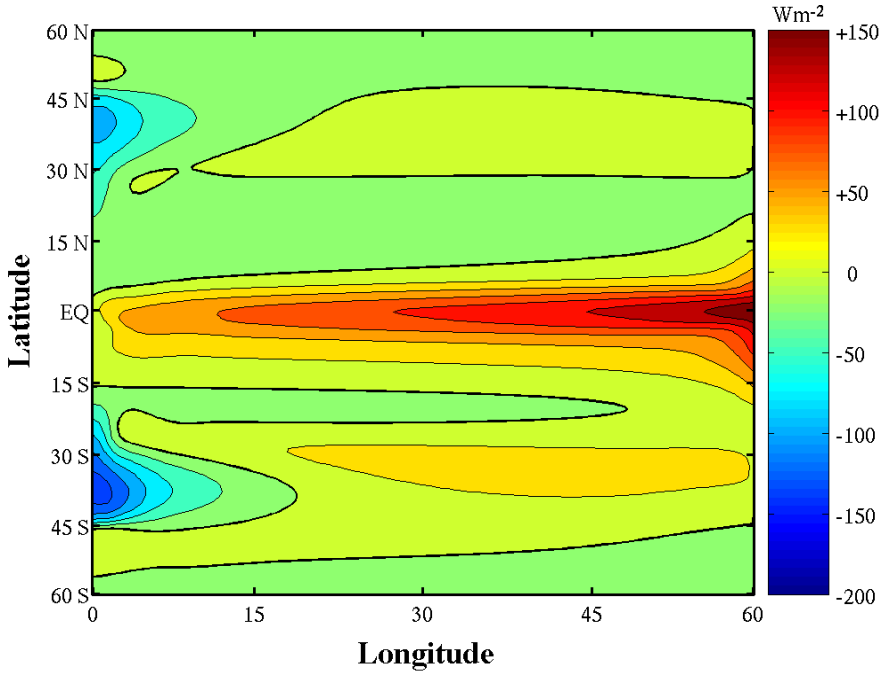

FIGURE 85. Net Surface Heat Flux for Ratio 2:1 and B = -5 (Case M)

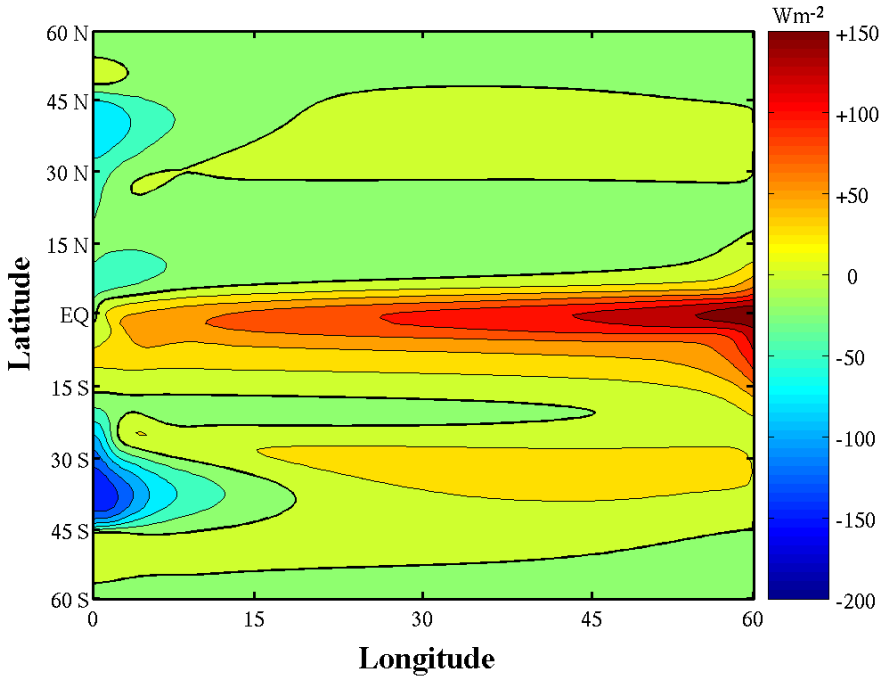

FIGURE 86. As FIGURE 85 except B = -7.5 (Case E)

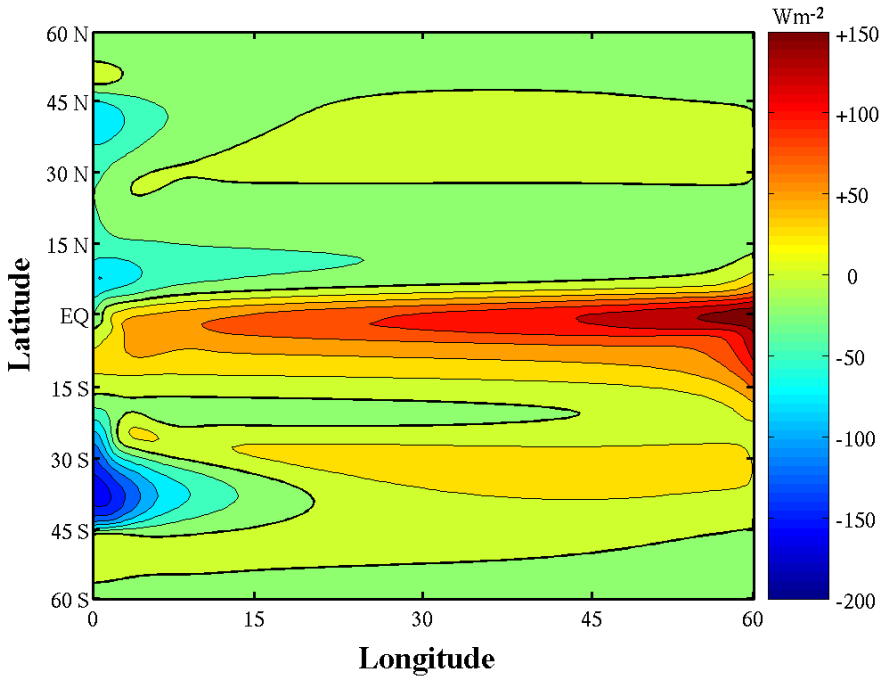

FIGURE 87. As FIGURE 85 except B = -10 (Case G)

c. Dual-Asymmetric Cases for Wind Stress Ratio of 3:1

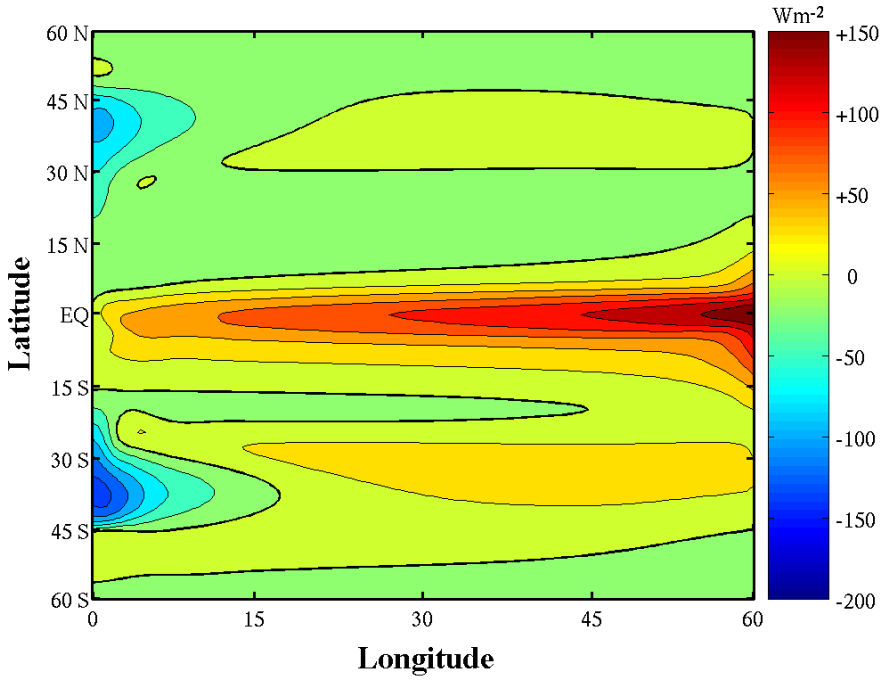

FIGURE 88. Net Surface Heat Flux for Ratio 3:1 and B = -5 (Case N)

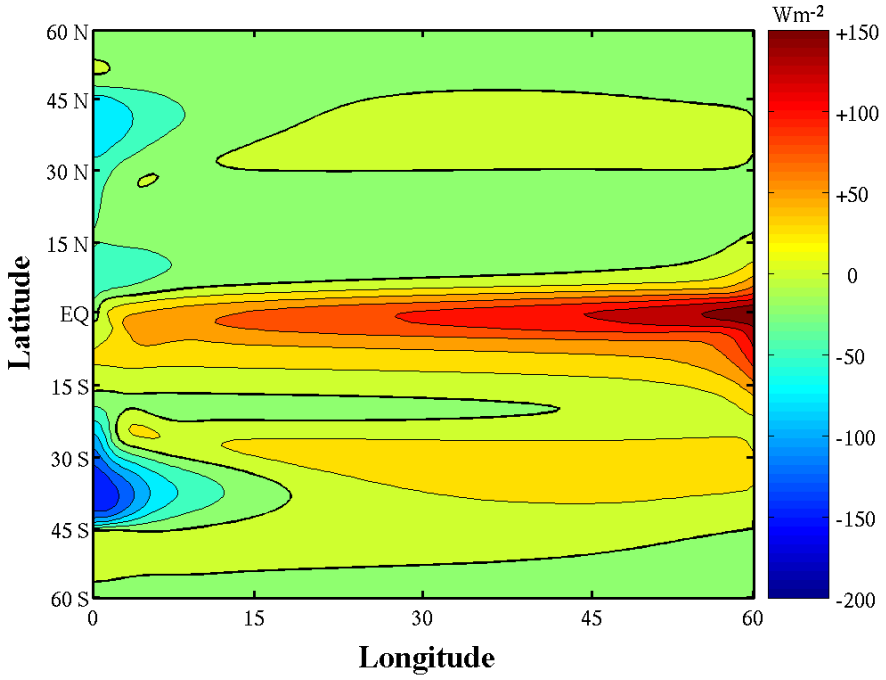

FIGURE 89. As FIGURE 88 except B = -7.5 (Case F)

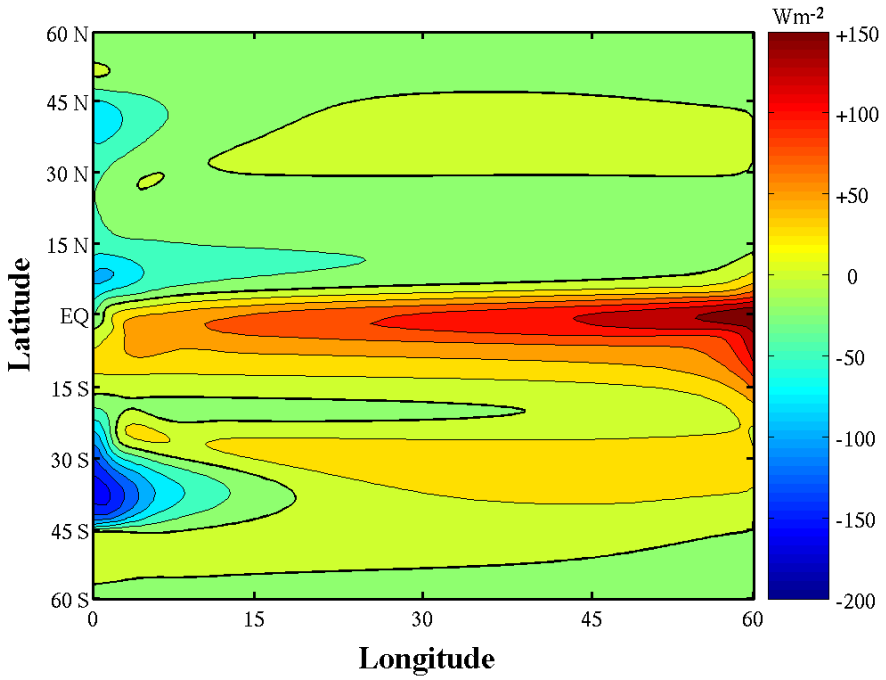

FIGURE 90. As FIGURE 88 except B = -10 (Case H)

d. Dual-Asymmetric Cases for Wind Stress Ratio of 4:1

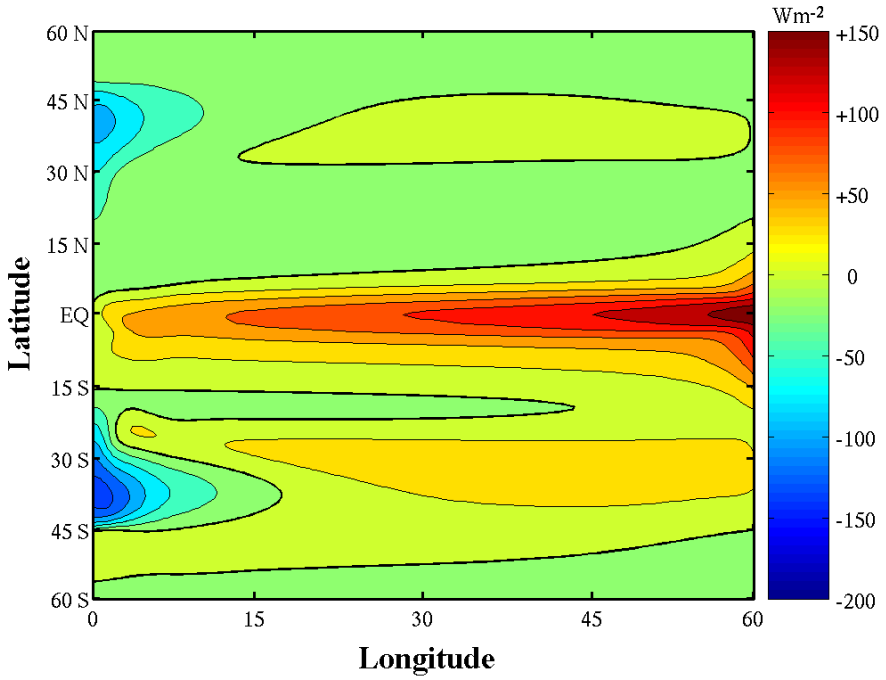

FIGURE 91. Net Surface Heat Flux for Ratio 4:1 and B = -5 (Case D)

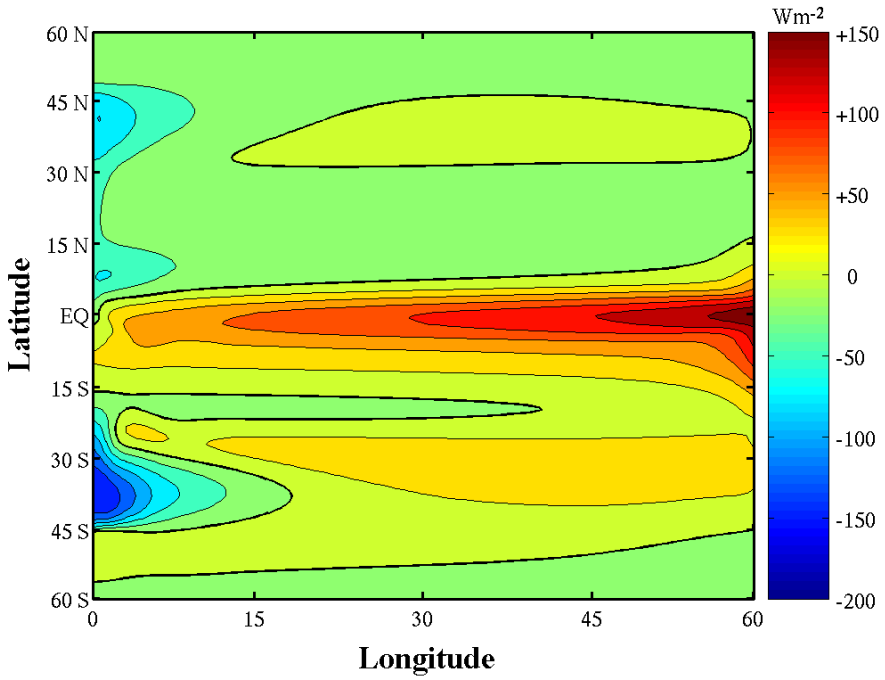

FIGURE 92. As FIGURE 91 except B = -7.5 (Case O)

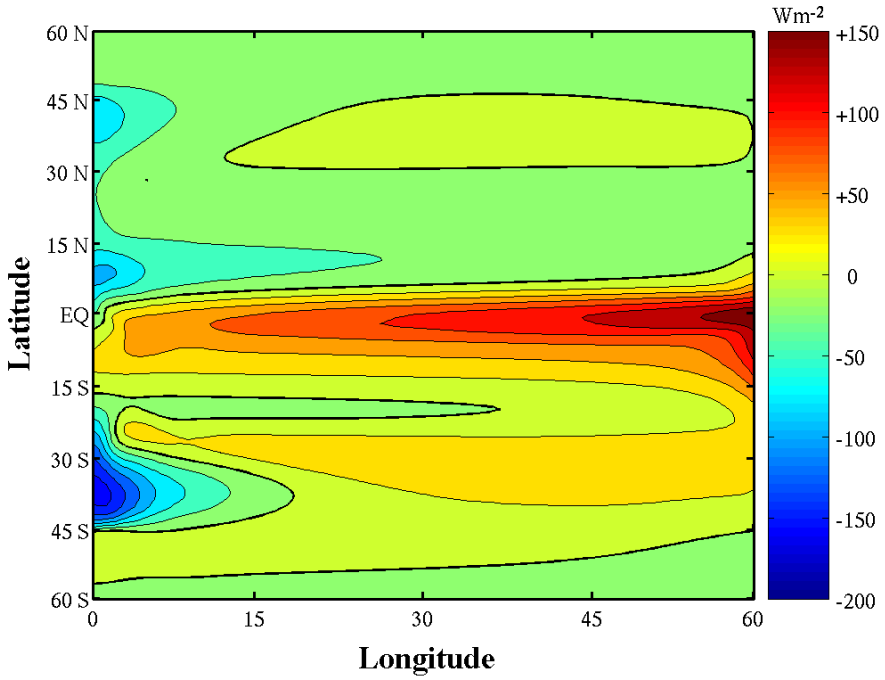

FIGURE 93. As FIGURE 91 except B = -10 (Case P)

E. INTERHEMISPHERIC MERIDIONAL OVERTURNING CIRCULATION AND HEAT TRANSPORT

1. Interhemispheric Volumetric Transport Solutions

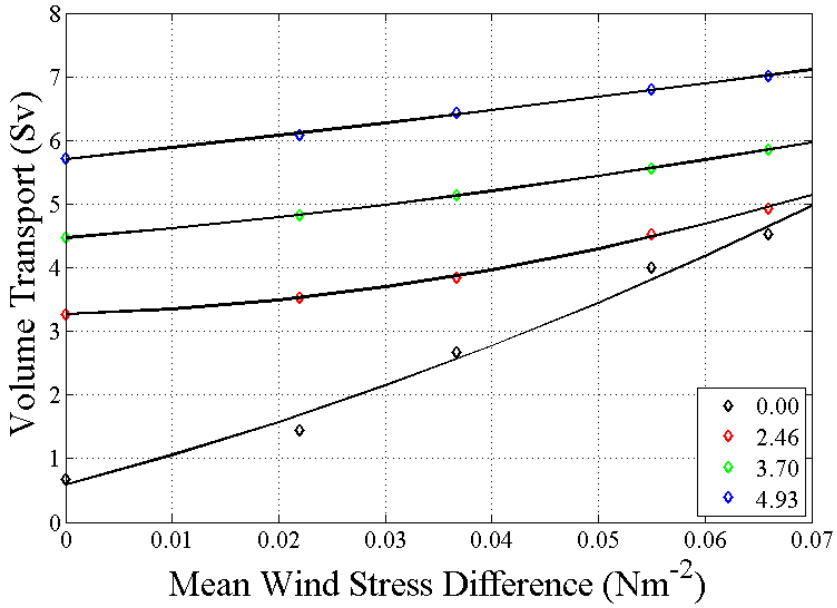

FIGURE 94. Volumetric Transport Solutions for Constant Temperature Forcing

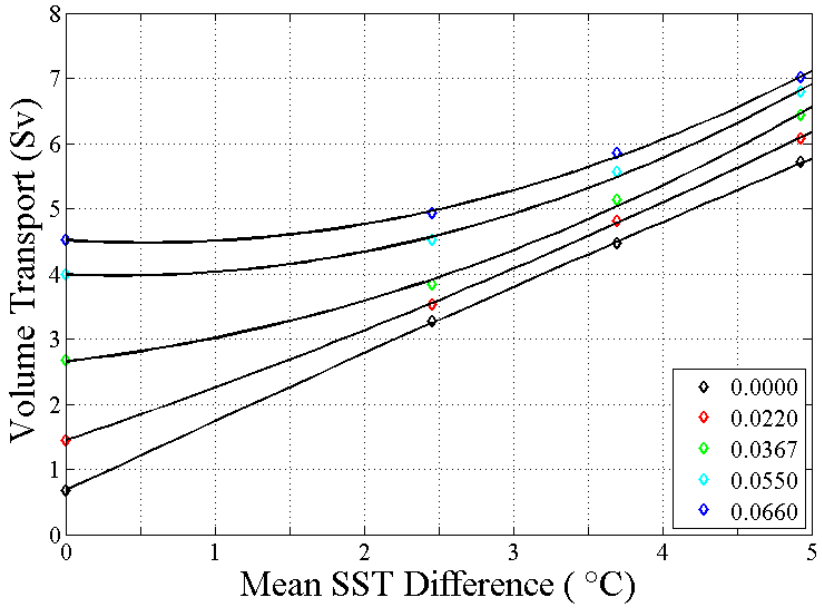

FIGURE 95. Volumetric Transport Solutions for Constant Wind Stress Forcing

2. Interhemispheric Heat Transport Solutions

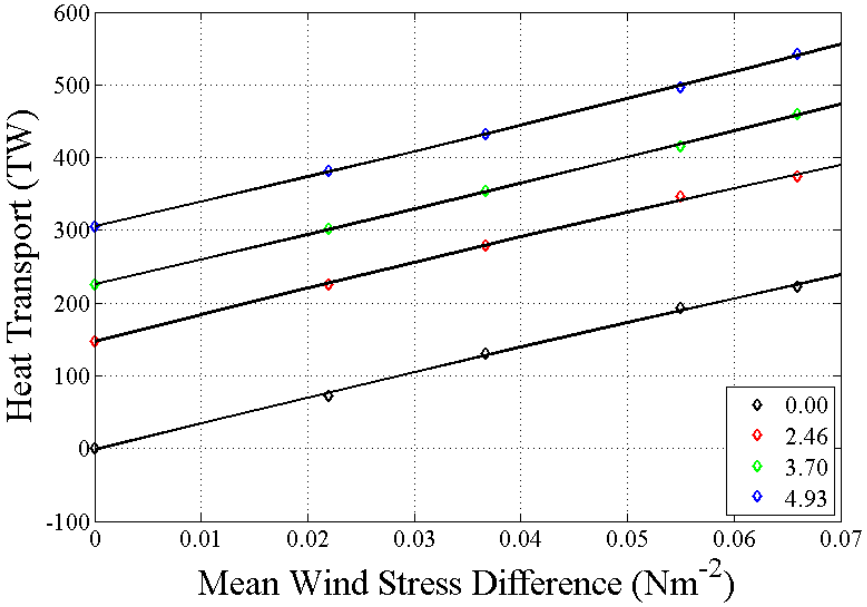

FIGURE 96. Heat Transport Solutions for Constant Temperature Forcing

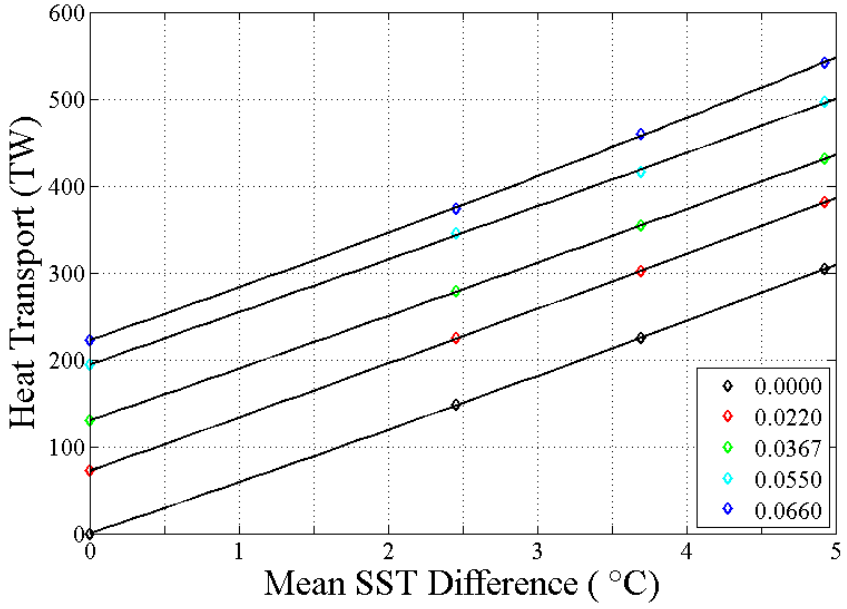

FIGURE 97. Heat Transport Solutions for Constant Wind Stress Forcing

3. Interhemispheric Total Transports

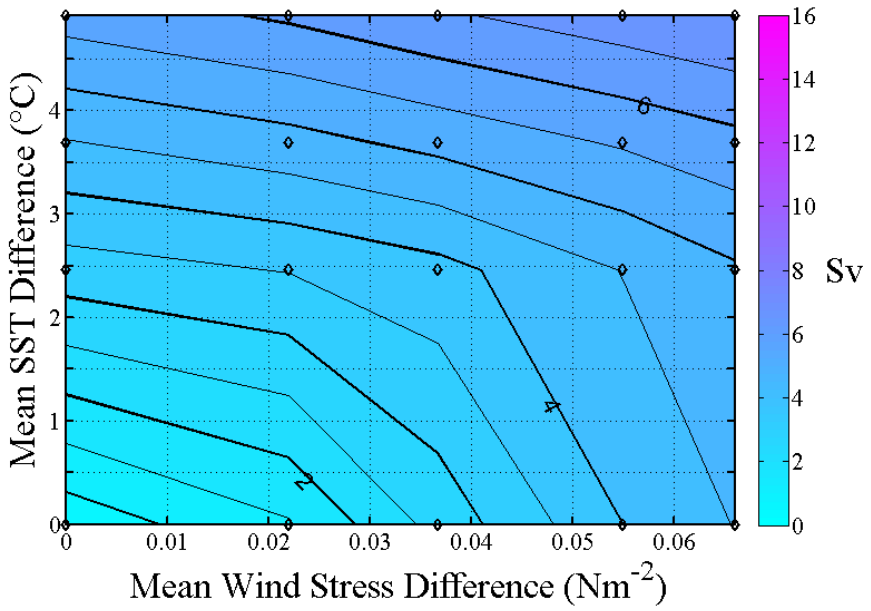

FIGURE 98. Volumetric Transport Solution for Dual Forcing

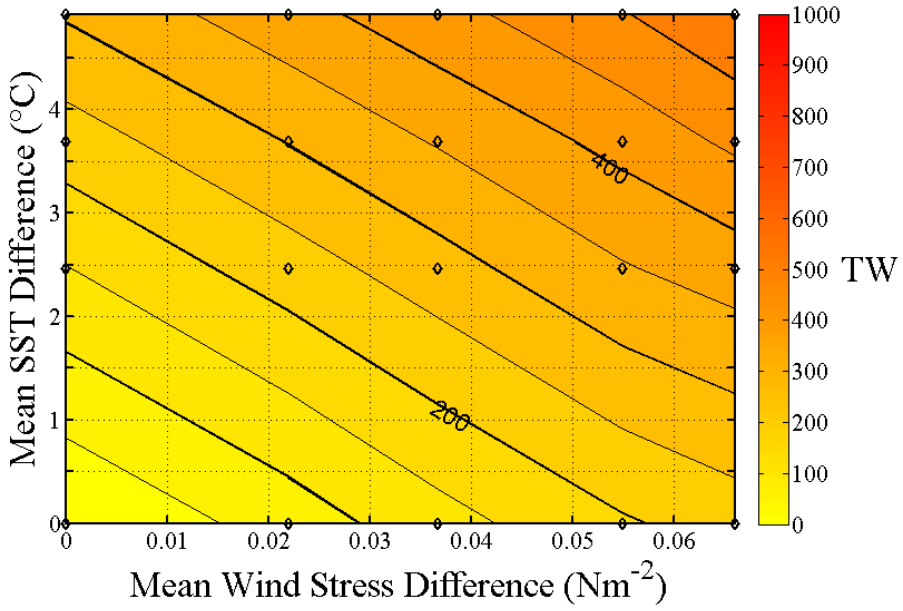

FIGURE 99. Heat Transport Solution for Dual Forcing

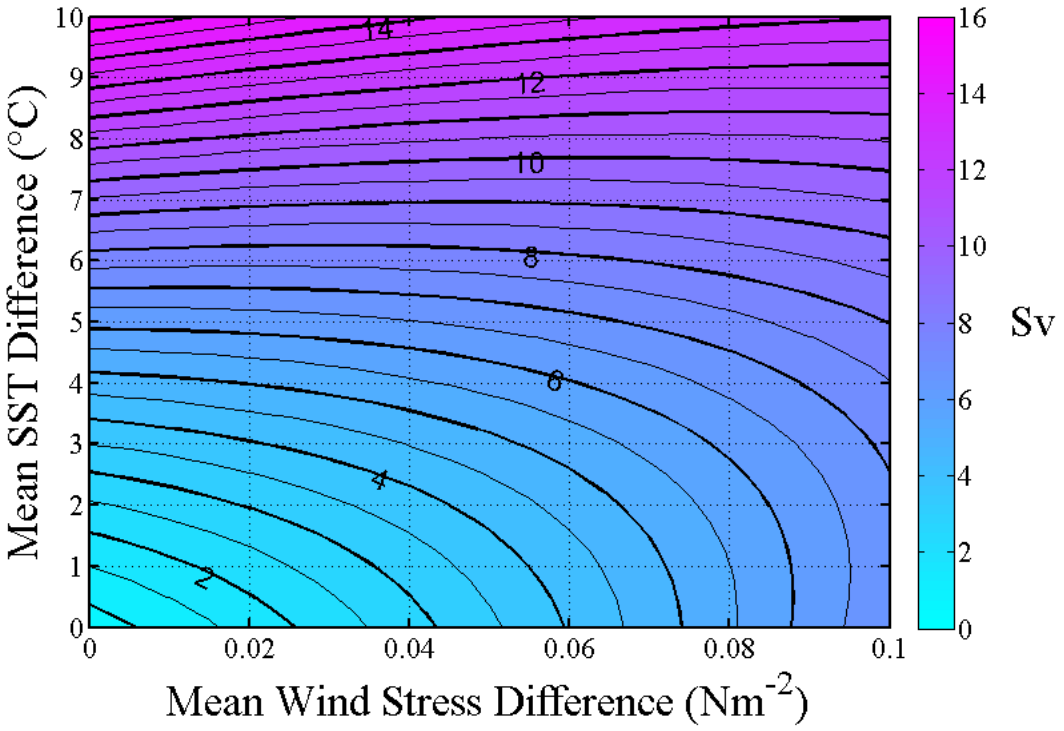

FIGURE 100. Volumetric Transport Solutions

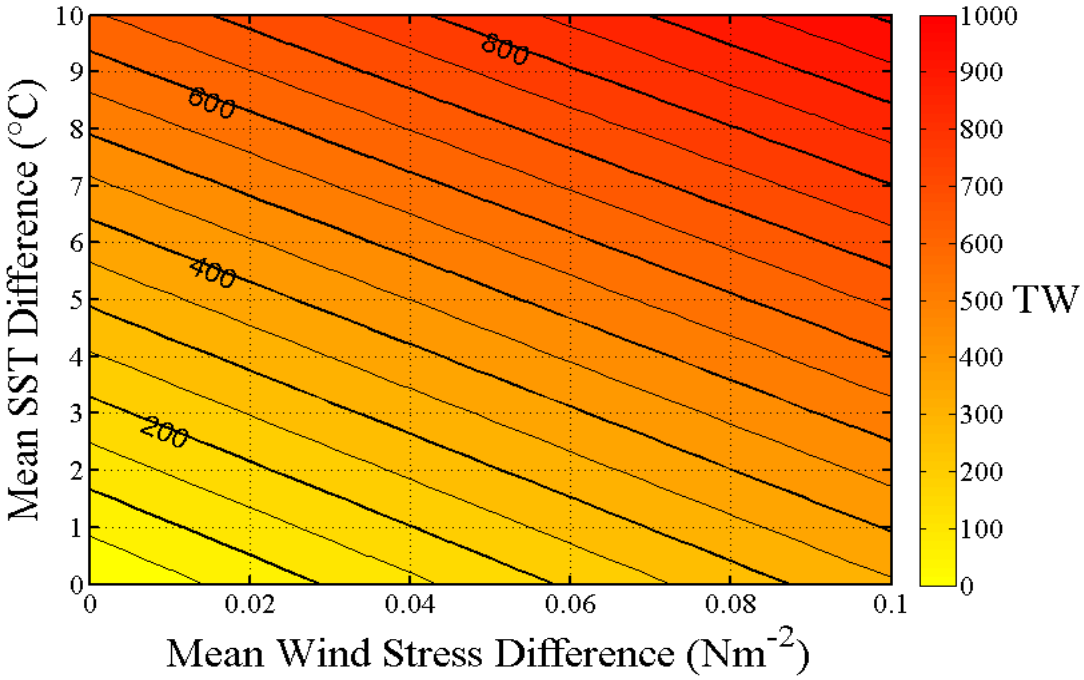

FIGURE 101. Heat Transport Solutions

THIS PAGE INTENTIONALLY LEFT BLANK

LIST OF REFERENCES

Adcroft, A., et al. (2008), *The MITgcm User Manual*. MIT Department of EAPS, Cambridge, MA.

Boccaletti, G., R. Ferrari, A. Adcroft, D. Ferreira, and J. Marshall (2005), The vertical structure of ocean heat transport. *Geophys. Res. Lett.*, **32**, L10603.

Bryan, F. (1986), High-latitude salinity effects and interhemispheric thermohaline circulations. *Nature*, **323**, 301-304.

Bunker, A. F. (1988), Surface energy fluxes of the South Atlantic ocean. *Monthly Weather Review*, **116**, 809-823.

Gent, P. R. and J. C. McWilliams (1990), Isopycnal mixing in ocean circulation models. *J. Phys. Oceanogr.*, **20**, 150-155

Hirschi, J., and J. Marotzke (2007), Reconstructing the meridional overturning circulation from boundary densities and the zonal wind stress. *J. Phys. Oceanogr.*, **37**, 743-763.

Hsiung, J., R. E. Newell, and T. Houghby (1989), The annual cycle of heat storage and ocean meridional heat transport. *J. Roy. Meteor. Soc.*, **115**, 1-28.

Kamenkovich, I., J. Marotzke, P. H. Stone (2000), Factors affecting heat transport in an ocean general circulation model. *J. Phys. Oceanogr.*, **30**, 175-194.

Klinger, B. A., S. Drijfhout, J. Marotzke, and J. R. Scott (2004), Remote wind-driven overturning in the absence of the Drake Passage effect. *J. Phys. Oceanogr.*, **34**, 1036-1049.

Kuhlbrodt, T., A. Griesel, M. Montoya, A. Levermann, M. Hofmann, and S. Rahmstorf (2004), On the driving processes of the Atlantic meridional overturning circulation. *Rev. Geophys.*, **45**, 2004RG000166.

Luyten, J. R., J. Pedlosky, and H. Stommel (1983), The ventilated thermocline, *J. Phys. Oceanogr.*, **13**, 292-309.

Marotzke, J. (1997), Boundary mixing and the dynamics of three-dimensional thermohaline circulations. *J. Phys. Oceanogr.*, **27**, 1713-1728.

Marotzke, J., and B.A. Klinger (2000), The dynamics of equatorially asymmetric thermohaline circulations. *J. Phys. Oceanogr.*, **30**, 955-970.

Marotzke, J., and P.H. Stone (1995), Atmospheric transports, the thermohaline circulation, and flux adjustment in a simple coupled model. *J. Phys. Oceanogr.*, **25**, 1350-1364.

Marotzke, J., and J. Willebrand (1991), Multiple equilibria of the global thermohaline circulation. *J. Phys. Oceanogr.*, **21**, 1372-1385.

Marshall, J., and T. Radko (2003), Residual-mean solutions for the Antarctic Circumpolar Current and its associated overturning circulation. *J. Phys. Oceanogr.*, **33**, 2341-2354.

Marshall, J., and T. Radko (2004), A model of the upper branch of the meridional overturning of the southern ocean. *Prog. Oceanogr.*, **70**, 331-345.

Munk, W.H. (1966), Abyssal recipes. *Deep Sea Research.*, **13**, 707-730.

Murphy, D. (2007), *To follow the water: exploring the sea to discover climate*, Basic Books, 278pp.

Park, S., C. Deser, and M. A. Alexander (2005), Estimation of the surface heat flux response to sea surface temperature anomalies over the global oceans. *J. Climate*, **18**, 4582-4599.

Pickard, G. L., and W. J. Emery (2003), *Descriptive Physical Oceanography*, Fifth Edition, Butterworth-Heinemann, 320pp.

Radko, T. (2005), Analytical solutions for the ACC and its overturning circulation. *J. Mar. Res.*, **63**, 1041-1055.

Radko, T. (2007), A mechanism for establishment and maintenance of the meridional overturning in the upper ocean. *J. Mar. Res.*, **65**, 85-116.

Radko, T., and J. Marshall (2004), The leaky thermocline. *J. Phys. Oceanogr.*, **34**, 1648--1662.

Radko, T., and J. Marshall (2006), The Antarctic circumpolar current in three dimensions. *J. Phys. Oceanogr.*, **36**, 651-669.

Rahmstorf, S. (1995), Multiple convection patterns and thermohaline flow in an idealized OGCM. *J. Climate*, **8**, 3028-3039.

Rahmstorf, S. (2002), Ocean circulation and climate during the past 120,000 years. *Nature*, **419**, 207-214.

Rahmstorf, S., and M. H. England (1997), Influence of southern hemisphere winds on north Atlantic deep water flow. *J. Phys. Oceanogr.*, **27**, 2040-2054.

Rahmstorf, S., and A. Ganopolski (1999), Simple theoretical model may explain apparent climate instability. *J. Climate*, **12**, 1349-1352.

Rahmstorf, S., and J. Willebrand (1995), The role of temperature feedback in stabilizing the thermohaline circulation. *J. Phys. Oceanogr.*, **25**, 787-805.

Rooth, C. (1982), Hydrology and ocean circulation. *Prog. Oceanogr.*, **11**, 131-149.

Scott, J. R., and J. Marotzke (2002), The location of diapycnal mixing and the meridional overturning circulation. *J. Phys. Oceanogr.*, **32**, 3578-3595.

Scott, J. R., J. Marotzke, P. H. Stone (1999), Interhemispheric thermohaline circulation in a coupled box model. *J. Phys. Oceanogr.*, **29**, 351-365.

Stammer, D., C. Wunsch, R. Giering, C. Eckert, P. Heimbach, J. Marotzke, A. Adcroft, C. N. Hill, and J. Marshall (2003), Volume, heat, and freshwater transports of the global ocean circulation 1993-2000, estimated from a general circulation model constrained by World Ocean Circulation Experiment (WOCE) data. *J. Geophys. Res.*, **108(C1)**, doi: 10.1029/2001JC001115.

Stommel, H., and A.B. Arons (1960a), On the abyssal circulation of the world ocean – I: Stationary planetary flow pattern on a sphere. *Deep Sea Research.*, **6**, 140-154.

Stommel, H., and A.B. Arons (1960b), On the abyssal circulation of the world ocean – II: An idealized model of the circulation pattern and amplitude in oceanic basins. *Deep Sea Research.*, **6**, 217-233.

Stommel, H. (1961), Thermohaline convection with two stable regimes of flow. *Tellus*, **13**, 224-230.

Timmermann, A., and H. Goosse (2004), Is the wind stress forcing essential for the meridional overturning circulation? *Geophys. Res. Lett.*, **31**, L04303.

von Storch, J.-S., H. Sasaki, and J. Marotzke (2007), Wind-generated power input to the deep ocean: an estimate using a 1/10° general circulation model. *J. Phys. Oceanogr.*, **37**, 657-672.

Weaver, A.J., J. Marotzke, P.F. Cummins, and E.S. Sarachik (1993), Stability and variability of the thermohaline circulation. *J. Phys. Oceanogr.*, **23**, 39-60.

Wunsch, C. (2005), The total meridional heat flux and its oceanic and atmospheric partition. *J. Climate*, **18**, 4374-4380.

Wyrtki, K. (1961), The thermohaline circulation in relation to the general circulation in the oceans, *Deep Sea Research.*, **8**, 39-64.

THIS PAGE INTENTIONALLY LEFT BLANK

INITIAL DISTRIBUTION LIST

1. Defense Technical Information Center
   Ft. Belvoir, Virginia

2. Dudley Knox Library
   Naval Postgraduate School
   Monterey, California

3. Timour Radko
   Department of Oceanography
   Naval Postgraduate School
   Monterey, California

4. Jeffrey Haferman
   Naval Postgraduate School
   Monterey, California

5. Mary L. Batteen
   Department of Oceanography
   Monterey, California